NASA Contractor Report 168016

LABYRINTH SEAL FORCES ON A WHIRLING ROTOR

D. V. Wright

Westinghouse R & D Center
Pittsburgh, Pennsylvania

January 1983

Prepared for

NATIONAL AERONAUTICS AND SPACE ADMINISTRATION
Lewis Research Center
Under Contract NAS 3-20825

TABLE OF CONTENTS

1. SUMMARY

The main objective of the program was to obtain accurate experimental data on the whirl force generated by labyrinth seals when the rotor whirls subsynchronously. These results are needed to guide development of a verified analytical method for predicting and avoiding whirl instability of shrouded turbines and other machines having labyrinth seals. Other objectives were to measure the whirling pressure field in the seal annulus and to compare present theoretical predictions of the seal forces with the measured forces. The objectives were accomplished.

The test rig described in Reference 1 was modified to include a novel active whirl damping and stiffness system which consists of electromagnetic shakers, motion transducers, and feedback amplifiers for adding controlled amounts of positive or negative damping, cross stiffness, and direct stiffness to the rotor system. Adjusting the feedback controls to obtain neutral whirl stability of the rotor system and applying the calibration constants to the control settings are all that is required to evaluate the whirl excitation constant (tangential force on the rotor in the whirl direction/whirl amplitude) and radial stiffness (dynamic centering force on the rotor/whirl amplitude) of a seal. The controls were adjusted to obtain a steady forward or backward whirl (in the rotational direction or opposite to it, respectively) circular orbit with a constant amplitude of 0.019 mm (0.75 mils) single peak.

Accurate and repeatable values were obtained for the whirl excitation constant and radial stiffness of diverging (S1), converging (S2), and straight (S3) two-strip seals (outlet clearance greater than, less than,

or equal to the inlet clearance, respectively) and the effects of pressure drop, back pressure, whirl direction, and whirl frequency were determined. The seals tested are shown in Figs. 2 and 5. Four back pressure P_3 values were used [from 103.42 kPa (15 psia) to 413.69 kPa (60 psia)] and the pressure drop P_1-P_3 was varied up to the maximum value possible [27.6 kPa (4 psi) at the highest back pressure and more than twice this value at the lowest back pressure] within the 0.026 kg/sec (45 SCFM) flow limitation of the air supply (through the test seal). Direct stiffness feedback was not used in most of the tests so that the whirl frequency varied as the seal stiffness varied. For example, when the pressure drop was increased to 45 kPa (6.527 psi) the whirl frequency increased by about 10% for the diverging seal, 22% for the straight seal, and 30% for the converging seal above the zero pressure drop values of 10.82Hz for backward whirl and 13.05Hz for forward whirl (0.36 and 0.435, respectively, of the 30Hz rotational frequency). Direct stiffness feedback was used in a few tests to vary the whirl frequency over wider ranges (7.75 to 19.6 Hz). All data are plotted and tabulated in this report.

The diverging and straight model seals are destabilizing (positive whirl excitation constant E) for backward whirl and the converging model seal is stabilizing (negative E) for backward whirl. All three seals are stabilizing for forward whirl. The backward whirl excitation constant of the straight seal is only about 25% as large as that of the diverging seal, which has an E value of about 9kN/m (51.4 lb/in) at the higher pressure drops. The whirl force is directly proportional to whirl amplitude and it increases with increasing pressure drop, but it is affected only moderately by back pressure and whirl frequency and is not affected significantly by seal offset.

The dynamic characteristics of the model seals should not be assumed to predict those of other seals directly unless they have about the same parameter values (including geometry, preswirl velocity V_1 (see Fig. 1), pressure and density conditions, rotor and seal roughnesses, rotor speed, and whirl frequency). The results given in this report are primarily useful for guiding development of a valid analytical whirl force prediction

method that can be used in the design of turbines, pumps, and compressors that will not whirl.

Dynamic pressure transducers were installed in the outer surface of the seal annulus at two diametrical points and the phasor difference between the two pressures was recorded after filtering the difference signal with a 30-Hz low pass filter to eliminate most of the random pressure fluctuations caused by turbulence. See Fig. 14. With zero static offset the perturbation pressure field [of the order of 0.138kPa (0.02 psi)] in the seal annulus is distributed sinusoidally around the circumference and it whirls in synchronism with the whirling rotor. The corresponding net dynamic pressure force on the rotor was determined for a few different pressure conditions and the whirl excitation constant and radial stiffness were then calculated from the tangential and radial components of this pressure force. These annulus pressure whirl excitation constant (E_{ap}) and radial stiffness (K_{sap}) values were found to differ from the values measured with the active whirl damping and stiffness system, which includes all seal forces on the rotor. The annulus pressure whirl excitation constant was usually somewhat (25 to 44%) larger than the directly measured E value for the diverging and converging seals, but roughly the same for the straight seal. In addition, the annulus pressure radial stiffnesses were substantially different from the directly measured K_s values. These differences may be due in part to errors in the annulus pressure results because of interference from the turbulent pressure fluctuations; however, the differences appear too large to be fully accounted for by this. Therefore, it is concluded that the seal forces are not caused solely by a whirling perturbation pressure field in the seal annulus with circumferential pressure gradients only; either radial and axial pressure gradients in the seal annulus or drag forces on the rotor are significant. Our present seal force theory neglects these effects.

Our existing computer program was used to calculate the seal whirl excitation constant and radial stiffness of the test seals for several different pressure drops and back pressures. This computer program calculates the whirling perturbation pressure field in the annulus by treating

the seal clearances as circumferential assemblages of variable-area orifices and it assumes circumferential pipe flow in the annulus with appropriate rotor and seal friction factors. It also considers the angular momentum of the inlet flow. However, it neglects Reynolds number effects in the annulus circumferential flow, neglects radial and axial pressure gradients in the annulus, and neglects drag forces on the rotor.

Agreement between the analytical and experimental results was poor. The theoretical backward whirl excitation constants are between 40 and 75% of the experimental values for the diverging seal and about 70% of the experimental values for the converging seal. They have the wrong sign and are only about 20% of the experimental values for the straight seal. Even worse, the theoretical forward whirl excitation constants for all three seals are less than 10% of the experimental values and have the wrong sign. In addition, the radial stiffnesses of all three seals for both whirl directions are completely erroneous; they are much too low or have the wrong sign. Thus, the present theory is invalid and needs to be improved.

2. INTRODUCTION

Self-excited rotor whirl has often caused unsatisfactory operation of turbines and other machines. Forces in the labyrinth seals, flow forces on the blades, and forces in the bearing oil films are of primary importance in turbine rotor stability. If the sum of the tangential forces acting on a whirling rotor in the whirl direction is greater than zero, the whirl amplitude will increase until either failure occurs or system nonlinearity causes equilibrium to be reached. Whirl at the fundamental bending natural frequency of the rotor typically becomes very large at loads slightly above the critical load at which instability initiates. Thus, turbines must be designed to avoid self-excited rotor whirl; if it occurs, design changes must usually be made to eliminate it before rated load can be achieved.

Present knowledge of labyrinth seal forces on a whirling rotor is inadequate. Analyses of seal forces resulting from the circumferentially varying flows and static pressure in the seal annulus have been made by many investigators, as described in References 1-3, but a complete experimentally verified theory has not yet been achieved. The analyses differ widely in their predictions. Test results obtained on operating turbines or compressors or on model air turbines do not provide accurate information on the forces of a single seal because forces from several seals and from the blading all act simultaneously. Accurate test results on individual single-cavity seals are needed to guide development of a valid method for calculating labyrinth seal whirl forces and to verify the method. The objective of this program is to obtain such test results.

In contrast to the poor state of knowledge on labyrinth seal whirl forces, blade whirl forces and bearing damping forces are understood reasonably well. Although improved information on them is also needed, they are much better understood than are labyrinth seal forces. When the

seal and blade whirl excitation constants (ratios of destabilizing whirl forces to whirl amplitude) of a rotor are known, as well as the bearing damping and stiffness and the rotor mass and stiffness, the stability of the rotor can be predicted by the method given in Reference 1. The basic data obtained on labyrinth seal forces in this program will be useful in the development of a valid seal force prediction method which will enable self-excited rotor whirl to be avoided in the design stage.

Identification of design modifications that will make labyrinth seals for a particular application as stabilizing as possible, or at least less destabilizing, is not part of the present program. To accomplish this will require the future development of an analytical seal force prediction method that includes all of the important phenomena and correctly accounts for the effects of all seal parameters. Additional test results may be needed to adequately verify this theory over the entire range of seal parameters and operating conditions of interest.

3. WHIRL EXCITATION CONSTANT AND RADIAL STIFFNESS

Figure 1 shows a diverging ($C_2 > C_1$) single-cavity labyrinth seal and a rotor that is whirling backward (opposite to the rotational direction) in a circular orbit with amplitude r and circular frequency Ω_b. The varying clearances modulate the local flows in and out of the seal and circumferentially in the seal annulus, and thereby cause the static pressure in the seal annulus to vary circumferentially and periodically. At each instant the varying component of the static pressure has an essentially sinusoidal distribution around the circumference and this pressure pattern rotates in synchronism with the rotor whirl. The net force F acting on the rotor due to the annulus pressure distribution has a tangential component $F_t = E_b r$ in the whirl direction and a radially inward component $F_r = K_{sb} r$, so that the seal force is destabilizing and stiffening in this case. E_b and K_{sb} are the whirl excitation constant and radial stiffness, respectively, of the seal for backward whirl. They are essentially independent of whirl amplitude. The whirl excitation constant in particular is quite different for forward and backward whirl, and the backward and forward whirl excitation constants and radial stiffnesses of converging ($C_2 < C_1$) and straight ($C_1 = C_2$) seals are all different, as will be shown later. It should be mentioned that other phenomena and forces, such as radial and axial pressure gradients in the seal annulus and shear forces on the rotor surface, may contribute to the total seal force on the whirling rotor in addition to the circumferentially varying pressure field described above.

If the rotor whirl orbit is circular and the seal has zero static offset, the magnitudes of the tangential and radial components of the net seal force are constant throughout the whirl orbit, so that E and K_s are constants. If the orbit is elliptical or if the seal has some static offset, then F_t and F_r vary during the whirl orbit; however, E and K_s can be defined as averages so that they are still constants.

Thus,

$$E = \frac{F_{tav}}{r} \tag{1}$$

and

$$K_s = \frac{F_{rav}}{r} \tag{2}$$

where F_{tav} = the average tangential force on the rotor in the whirl direction

F_{rav} = the average dynamic centering force on the rotor

and

r = the average radius of the whirl orbit.

A more precise way to express the dynamic characteristics of a seal is in terms of twelve direct and cross stiffness, damping, and mass coefficients, as is customary for bearings. In these terms, the seal forces acting on the rotor in the positive x and y directions are

$$F_x = -(K_{xx}x + K_{xy}y + B_{xx}\dot{x} + B_{xy}\dot{y} + D_{xx}\ddot{x} + D_{xy}\ddot{y}) \tag{3}$$

$$F_y = -(K_{yx}x + K_{yy}y + B_{yx}\dot{x} + B_{yy}\dot{y} + D_{yx}\ddot{x} + D_{yy}\ddot{y}) \tag{4}$$

If a circular orbit is assumed and the averages of the $E = F_t/r$ and $K_s = F_r/r$ values at $\Omega t = 0°$ and $90°$ are taken, the whirl excitation constant and radial stiffness are given by

$$E_f = (1/2)[(K_{xy} - K_{yx}) - (B_{xx} + B_{yy})\Omega - (D_{xy} - D_{yx})\Omega^2] \tag{5}$$

$$K_{sf} = (1/2)[(K_{xx} + K_{yy}) + (B_{xy} - B_{yx})\Omega - (D_{xx} + D_{yy})\Omega^2] \tag{6}$$

for forward whirl, and

$$E_b = (1/2)\left[(K_{yx} - K_{xy}) - (B_{xx} + B_{yy})\Omega - (D_{yx} - D_{xy})\Omega^2\right] \qquad (7)$$

$$K_{sb} = (1/2)\left[(K_{xx} + K_{yy}) + (B_{yx} - B_{xy})\Omega - (D_{xx} + D_{yy})\Omega^2\right] \qquad (8)$$

for backward whirl.

No attempt was made in this investigation to evaluate the twelve coefficients described above. The orbit of the test rig rotor is always essentially circular because of the strong gyroscopic coupling. Consequently, the simple concepts of whirl excitation constant and radial stiffness defined by Eqs. 1 and 2 are used to express all seal force results.

4. TEST EQUIPMENT AND PROCEDURES

4.1 Test Rig

The test rig used in this investigation of the whirl excitation constants and radial stiffnesses of labyrinth seals is shown schematically in Fig. 2, and a photograph of the test rig, air supply and discharge system, and instrumentation is shown in Fig. 3. An early version of the test rig was described in Reference 1. During this investigation, the test rig was modified to include an active whirl damping and stiffness system, which greatly improved the accuracy of the overall system. This active system is described in Section 4.2.

The rotor is rigidly supported by preloaded ball bearings in a housing that is elastically pivoted by means of three bar springs. Since the shaft is relatively stiff, the rotor system is essentially a single-degree-of-freedom system for either rocking vibration about the pivot in a plane or conical whirling of the rotor system with a nodal point at the pivot. Pushrods, which are longitudinally stiff and laterally very flexible, connect the rotor system in the x and y directions to spring-guided platforms, which in turn are connected to electromagnetic shakers. Other pushrods transmit the x and y rotor motions to the displacement and velocity transducers shown. The tuning springs and adjustable dampers shown in Fig. 2 were not used in this investigation. Instead, the displacement and velocity transducer signals are connected to feedback amplifiers that drive the electromagnetic shakers. The resulting active whirl damping and stiffness system can add controlled amounts of positive or negative damping, cross stiffness, and direct stiffness to the rotor system. It applies forces to the whirling rotor system which can be adjusted to just counteract the rotor forces generated by the seal (and the damping forces of the test rig) and

thereby achieve neutral stability of the system and a steady constant-amplitude forward or backward whirl orbit. After this neutral stability condition is obtained for a given back pressure and pressure drop across the seal, calibration constants are applied to the feedback control settings to determine the whirl excitation constant and radial stiffness of the seal referred to the guided platforms.

Six uniformly spaced inlet pipes bring air into a 360-degree manifold having top and bottom faces of perforated metal and fine-weave nylon taffeta cloth to provide uniform inlet flow distribution and low turbulence. The leakage air flow through the test (top) seal of up to 0.026 kg/s (45 SCFM) leaves the model through two outlet pipes and then goes through a throttling valve, a flow meter (Ellison, No. 730 Annubar, 100 SCFM for air at 15 psia) and a muffler. A somewhat smaller amount of air leaks through the dummy seal at the thrust balance disk. Since this dummy seal is located at the elastic pivot, which is the nodal point of the system, the dummy seal has negligible exciting effect on the system. The dummy seal leakage air flows out of the model through two paths; one path through a discharge line from the lower plenum to a throttling valve and the muffler downstream from the flowmeter, and the second path through the pushrod clearances in the housing wall. Additional air is supplied to the lower plenum through a separate inlet line so that the pressure in the lower plenum can be kept equal to P_3 to minimize the net thrust on the rotor.

A small damper is mounted on each of the four guided platforms to prevent high-frequency instability of the system when large amounts of feedback are used. As shown in Figs. 2 and 4, each damper consists of a 93.4-gram mass supported by two flat "springs" made from Lord LD400 viscoelastic damping material. Since the fixed-base natural frequency of the spring-supported mass of the damper in the pushrod direction is about 500 Hz, these devices provide substantial damping at all frequencies above about 400 Hz. They act as pure masses at the low whirl frequencies of interest.

The clearances and other geometry of the diverging (S1), converging (S2), and straight (S3) seals tested are shown in Fig. 5. The seal bores were accurately circular; the inside diameter of each strip differed by less than 0.015 mm (0.6 mils) in any direction, and the seals were wedged during installation to reduce this error by a factor of two or more. The disk diameter differed by less than 0.005 mm (0.2 mils) in any direction. The seal strips are spaced 12.70 mm apart; however, the effective length a of the seal is 12.918 mm. This corresponds to the ratio of the annulus cross sectional area (with chamfer) to the seal radial depth b.

The snubber shown in Fig. 5 was used to prevent excessive whirl amplitude of the rotor system and the catastrophic dry friction whirl that occurs if the rotor inadvertently contacts the seal strips while it is rotating. This occurred twice during early tests, so the snubber clearance was reduced to the small value shown to prevent it from happening again.

4.2 Active Whirl Damping and Stiffness System

The active whirl damping and stiffness system is shown schematically in Fig. 6. Its operation and calibration will be described in detail because it can also be useful in other investigations. If the rotor is whirling in a circular orbit in the forward (rotational) direction and the X and Y amplifier switches are set positive as shown, a positive X displacement (to the right) causes a rotor force in the negative X direction and a positive Y displacement (upward) causes a rotor force in the negative Y direction. Thus, both forces correspond to positive spring forces so they raise the whirl frequency of the system and the magnitudes of the active stiffnesses are directly proportional to the settings of the K_{XX} and K_{YY} potentiometers. If the X and Y amplifier switches were set negative, the forces would correspond to negative spring forces and they would lower the whirl frequency. Similarly, if the $\dot{X}$ and $\dot{Y}$ amplifier switches were set positive, positive

$\dot{X}$ and $\dot{Y}$ velocities would cause rotor forces in the negative X and Y directions. These forces correspond to positive viscous damping forces (the sum of which is a tangential force that acts oppositely to the whirl direction), so they would absorb energy from the whirl and cause its amplitude to decay. The magnitudes of the active damping constants are directly proportional to the settings of the B_{XX} and B_{YY} potentiometers. If the $\dot{X}$ and $\dot{Y}$ amplifiers were set negative, the rotor forces would correspond to negative damping forces. If these forces exceeded the positive damping forces of the system (such as from the seal if it is stabilizing and from the hysteresis of the shaker springs and pivot springs), the rotor system would whirl at its natural frequency with increasing amplitude.

Both the active direct stiffnesses and active dampers described above behave the same for either direction of whirl; however, this is not true for the cross stiffnesses to be described next. For forward whirl the X displacement leads the Y displacement by 90 degrees. If the XY amplifier switch is set positive and the YX amplifier switch set negative, then the Y force is a maximum in the positive Y direction when the X displacement is a positive maximum and the X force is a maximum in the negative X direction when the Y displacement is a positive maximum. Therefore, both of these forces are in the whirl direction so they are destabilizing; they put energy into the vibration and increase its amplitude. They correspond to a positive forward whirl excitation constant, as indicated by the first two terms on the righthand side of Eq. 5. The magnitudes of these two cross stiffness forces, $K_{XY}Y$ and $K_{YX}X$ (where K_{YX} is negative in this case) are proportional to the settings of the K_{XY} and K_{YX} potentiometers. Conversely, if the XY amplifier switch were set negative and the YX amplifier switch set positive, the cross stiffness forces would be stabilizing (positive damping) and they would correspond to a negative forward whirl excitation constant.

In backward whirl the Y displacement leads the X displacement by 90 degrees. If the YX amplifier switch were set negative and the XY amplifier switch set positive, then the X force would be a maximum in the

negative X direction when the Y displacement is positive maximum and the Y force would be a maximum in the positive Y direction when the X displacement is positive maximum. Therefore, both of these forces would be opposite to the whirl direction, so they would be stabilizing and correspond to a negative backward whirl excitation constant, as indicated by the first two terms on the righthand side of Eq. 7 when K_{YX} is negative and K_{XY} is positive as in this case. Conversely, if the XY amplifier switch were set negative and the YX amplifier switch set positive, the cross stiffness forces would be destabilizing and correspond to a positive backward whirl excitation constant. In summary, positive K_{XY} and negative K_{YX} are destabilizing for forward whirl (as denoted by DSF in Fig. 6) and stabilizing for backward whirl, and vice versa.

Although for the circular orbits being used the channels could be combined [e.g., $K_d = \pm (1/2)\ (K_{XX} + K_{YY})$, $B = \pm (1/2)\ (B_{XX} + B_{YY})$, and $K_c = \pm (1/2)\ (K_{XY} - K_{YX})$], they are kept separate for calibration and checking purposes, and the following operating procedures are followed. The YX amplifier switch is always set negative when the XY amplifier switch is set positive, and vice versa; and the K_{YX} and K_{XY} potentiometer settings are always made equal. The $\dot{X}$ amplifier switch is always set positive when the $\dot{Y}$ amplifier switch is set positive, and vice versa; and the B_{XX} and B_{YY} potentiometer settings are always made equal. Finally, the X amplifier switch is always set positive when the Y amplifier switch is set positive, and vice versa; and the K_{XX} and K_{YY} potentiometer settings are always made equal.

Cross stiffness K_c and direct damping B channels are both needed even though either can destabilize or stabilize the rotor system.* Cross damping, direct mass, and cross mass channels are not needed in the present measuring system so they are omitted. For example, if the backward whirl excitation constant of a seal is positive and large and the forward whirl excitation constant of the seal is negative and smaller (as is the case for the diverging seal tested) neutral forward whirl stability cannot be achieved with either the K_c channels or the B channels alone. To do this requires that DSF K_c (destabilizing for

*In a given whirl direction.

forward whirl, K_{XY} positive and K_{YX} negative) and positive B both be increased until the rotor system is stable against backward whirl with some stability margin and is neutrally stable for forward whirl. Increasing DSF K_c alone would destabilize the rotor system for forward whirl before stabilizing it against backward whirl.

Although the active whirl damping and stiffness system described in this report was developed for measuring seal forces, it can be used for other purposes as well. One application would be in studies of rotor system dynamics in which the active system (with cross damping added) could be used to simulate a bearing or seal with any desired dynamic stiffness and damping characteristics. Another application would be for stabilizing small high-speed machines that experience self-excited rotor whirl because of destabilizing blade and seal forces in conjunction with inadequate bearing damping. Larger shakers could be used as needed and perhaps only positive B channels would be needed.

The control unit of the active whirl damping and stiffness system is shown in Fig. 7. Its overall voltage gains (G_{KYY}, G_{KXY}, etc.) are given in the title for each ten-turn gain potentiometer set at its maximum position of 1000. For example, when a voltage is applied to input terminal Y and potentiometers K_{YY} and K_{XY} are both set at 1000, the voltage at output terminal Y is 1.0116 times the input voltage and the voltage at output terminal X is 0.3364 times the input voltage. Similarly, when a voltage is applied to input terminal X and potentiometers K_{XX} and K_{YX} are both set at 1000, the voltage at output terminal X is 1.0093 times the input voltage and the voltage at output terminal Y is 0.3372 times the input voltage. Also, when a voltage is applied to input terminals $\dot{X}$ and $\dot{Y}$ and potentiometers B_{XX} and B_{YY} are both set at 1000, the voltage at output terminal X is 22.22 times the input voltage and the voltage at output terminal Y is 25.32 times the input voltage. The input units (displacement and velocity transducers and instrumentation) and output units (power amplifiers and electromagnetic shakers) are shown in Fig. 8 along with their individual calibration constants.

The gains shown in Fig. 7 were selected to obtain the full scale ranges shown in the box on the lower right in Fig. 7. These full scale ranges were chosen to cover the whirl excitation constant and radial stiffness ranges of the three seals tested. The full scale ranges are

$$B_{XX} = (.4542\ \frac{\text{volt-sec}}{\text{in}})(22.22)(10.27)(\frac{\text{amp}}{52.2\ \text{volt}})(.8627\ \frac{\text{lb}}{\text{amp}}) = 1.713\ \frac{\text{lb-sec}}{\text{in}} = 300\ \frac{\text{N-s}}{\text{m}} \quad (9)$$

$$B_{YY} = \frac{(.3995)(25.32)(10.15)(.8642)}{51.8} = 1.713\ \frac{\text{lb-sec}}{\text{in}} = 300\ \frac{\text{N-s}}{\text{m}} \quad (10)$$

$$K_{XX} = (2000\ \frac{\text{volt}}{\text{in}})(1.0093)(10.27)(\frac{\text{amp}}{52.2\ \text{volt}})(.8627\ \frac{\text{lb}}{\text{amp}}) = 342.6\ \frac{\text{lb}}{\text{in}} = 60{,}000\ \frac{\text{N}}{\text{m}} \quad (11)$$

$$K_{YY} = \frac{(2000)(1.0116)(10.15)(.8642)}{51.8} = 342.6\ \frac{\text{lb}}{\text{in}} = 60{,}000\ \frac{\text{N}}{\text{m}} \quad (12)$$

$$K_{XY} = \frac{K_{XX}}{3} = 114.2\ \frac{\text{lb}}{\text{in}} = 20{,}000\ \frac{\text{N}}{\text{m}} \text{ and } K_{YX} = \frac{K_{YY}}{3} = 114.2\ \frac{\text{lb}}{\text{in}} = 20{,}000\ \frac{\text{N}}{\text{m}} \quad (13)$$

since $$G_{KXY} = \frac{G_{KXX}}{3} = .3364 \text{ and } G_{KYX} = \frac{G_{KYY}}{3} = .3372$$

The exact shaker force sensitivities were determined by performing bump tests on the rotor system with various B_{XX} and B_{YY} potentiometer settings and measuring the log decrement δ of the resulting logarithmically decaying vibration. Thus, the actual velocity damping being provided by the active whirl damping and stiffness system is

$$B = 2 f_n M_p (\delta - \delta_o) \tag{14}$$

where f_n = natural frequency of the rotor system

M_p = modal mass of the rotor system referred to the platforms

δ = log decrement with the B dials at a particular setting

δ_o = log decrement with the B dials set at zero.

Then the shaker sensitivities required to satisfy Eqs. 9 and 10 were calculated. Next, it was verified that the overall sensitivities of the direct stiffness channels were the same by using the negative B's to cause self-excited vibration of the system in both the X and Y directions, one direction at a time, when the direct stiffness dials were both set at 700 (0.7 of full scale) and observing that the new higher natural frequencies f_X and f_Y were identical. Finally, the K_c dials were set at full scale DSF and the positive B values required for neutral stability (with the non-rotating rotor whirling in a forward circular orbit) were determined. The cross stiffness dial settings K_c corresponding to given direct damping dial settings B at a given vibration frequency f are

$$K_c = \left(\frac{1000}{114.2}\right)\left(\frac{1.713}{1000}\right) B\omega = \frac{Bf}{10.61} \tag{15}$$

Or more precisely, $K_c - K_{ct} = Bf/10.61$ where K_{ct} is the tare cross stiffness dial setting(s) required to cause neutral stability when B=0.

The C_p capacitors at the X and Y inputs in Fig. 7 were used to trim the (very small) phase shifts of the X and Y channels so that the damping of the system in the X and Y directions was unchanged when the K_{XX} and K_{YY} values were changed from +400 to -400. The whirl damping of the rotor system was then essentially unchanged when the K_{XX} and K_{YY} potentiometers were changed from 0 to 700, even though the natural frequency of the system increased from 11.90 Hz to 14.83 Hz. The C_s capacitors in the $\dot{X}$ and $\dot{Y}$ amplifier feedback loops were used to roll off

the high-frequency gains of these amplifiers to prevent high-frequency instability of the rotor system when the B dials were at large settings.

The modal mass M_p of the non-rotating rotor system (which is used in Eq. 14) was measured to be 13.29 kg (29.3 lbm) by using the following procedure. With the B_{YY} dial set at +1000 and all K dials set at 0, the negative B_{XX} dial was increased from 0 until a self-excited vibration of 0.019 mm (0.75 mils) single peak built up in the X direction at the system natural frequency f_n = 11.90 Hz. A small mass ΔM was then attached to the X shaker platform and the new natural frequency f_a was measured. If the modal stiffness of the rotor system were unaffected by the mass addition, then $f_a = f_n \sqrt{M/(M+\Delta M)}$ so that the modal mass of the system referred to the platform would be

$$M_p = \frac{\Delta M}{\left(\frac{f_n}{f_a}\right)^2 - 1} \tag{16}$$

This process was repeated using additional ΔM values and the resulting values of M_p calculated from Eq. 16 were plotted against ΔM. Extrapolating this curve to $\Delta M = 0$ then gave the correct value for the system modal mass referred to the platform. The same values of f_n and M_p were obtained when the above procedure was repeated in the Y direction.

4.3 Modal Characteristics of Test Rig

Although the distances from the elastic pivot to the seal midplane and to the pushrods are equal, shaft flexibility causes the platform motion X_p and the disk motion X_d at the seal to be somewhat different, and their ratio varies when the seal and platform stiffnesses are changed. Consequently, the modal mass M_{dm} of the rotor system referred to the disk is different from the modal mass M_{pm} referred to the platform. Since the kinetic energy is the same

$$M_{dm} = M_{pm}\left(\frac{X_p}{X_d}\right)^2 \tag{17}$$

The modal stiffness K_{dm} referred to the disk is similarly related to the modal stiffness K_{pm} referred to the platform

$$K_{dm} = K_{pm}\left(\frac{X_p}{X_d}\right)^2 \tag{18}$$

since

$$K_m = M_m \omega_n^2 \tag{19}$$

The damping energy per cycle, $\pi K_c X^2 = \pi B \omega X^2$, referred to the disk and to the platform is the same. Therefore, the cross stiffness K_{dc} referred to the disk is related to the cross stiffness K_{pc} referred to the platform by the following equation:

$$K_{dc} = K_{pc}\left(\frac{X_p}{X_d}\right)^2 \tag{20}$$

and the velocity damping values are similarly related.

$$B_d = B_p\left(\frac{X_p}{X_d}\right)^2 \tag{21}$$

The active whirl damping and stiffness system applies known amounts of velocity damping, cross stiffness, and direct stiffness to the guided platforms. Since the platform damping and cross stiffness must be referred to the disk in order to evaluate the whirl excitation constant of the seal, the squared amplitude ratio $(X_p/X_d)^2$ of the test rig had to be evaluated over the seal and platform stiffness ranges of

interest. Although the radial stiffness of the seal could have been evaluated by using negative direct stiffness values at the platforms to hold the whirl frequency constant over the ranges of seal operating conditions, this was not done. It was more accurate and convenient to keep the platform direct stiffness zero and to let the seal stiffness change the whirl frequency somewhat. Consequently, it was necessary to generate a curve of seal stiffness versus vibration frequency for zero added platform stiffness. This section gives the modal characteristics of the test rig and the curves needed to reduce the seal test results.

The modal characteristics of the rotor system with the rotor at zero speed were measured with various springs added to the platforms and the disk, and with various large masses added to the disk. For each condition, measurements were made of the system natural frequency, the ratio of platform motion to disk motion, and the input modal masses at the platform and the disk. These were measured by adding three different small masses one at a time at the point being measured, using Eq. 16, and then extrapolating the resulting calculated modal masses back to zero added mass. The modal mass and displacement ratio values were then adjusted as needed to satisfy Eq. 17. The zero-speed results shown in Figs. 9-12 and Tables 1 and 2 were obtained; interpolated points are included. Note that the disk motion was $1/\sqrt{.67} = 1.22$ times the platform motion when the stiffest platform spring was used, but only $1/\sqrt{.904} = 1.05$ times the platform motion when no added platform stiffness was used.

The forward and backward whirl natural frequencies and platform modal masses of the rotor system were then measured with the rotor at operating speed (30 Hz) and with various springs added to the platforms. It should be recognized that gyroscopic moments at the top and bottom disks cause the modal mass to increase and the modal stiffness to decrease for backward whirl and to change oppositely for forward whirl. If the shaft were rigid, the modal inertia would be

$$I_m = I \mp \frac{I_o \omega}{2\Omega} \tag{22}$$

and the corresponding modal stiffness would be

$$K_m = K \pm \frac{I_o \omega \Omega}{2} \tag{23}$$

where the upper and lower signs apply to forward and backward whirl, respectively. I_o is the polar moment of inertia of the rotor, ω is the circular rotational frequency, and Ω is the circular whirl frequency. See Reference 4. The measured results of these tests are shown in Figs. 9-12 and Tables 1 and 2, along with some points that were deduced from the measured data and other considerations. Some approximations were made, such as assuming that the $(X_p/X_d)^2$ vs f curve for zero platform stiffness and varying seal (disk) stiffness in Fig. 9 is the same for forward and backward whirl as it is for zero speed (because of Eqs. 22 and 23 and the fact that the measured zero-speed curves for disk stiffness and added disk mass are essentially straight-line extensions of each other), and assuming that the curve is a straight line although it actually curves somewhat. The equation of this line for zero platform stiffness is

$$\left(\frac{X_p}{X_d}\right)^2 = .748 + .0131\ f \tag{24}$$

In addition, some points were adjusted to make the curves in the various graphs smooth and mutually consistent.

Mass-spring representations of the test rig for backward whirl, forward whirl, and zero speed were derived to provide improved understanding of the modal characteristic curve trends and help in deducing points that could not be measured directly. The two-mass representation shown in Fig. 13 was used. A Hooke-Jeeves pattern search optimization procedure was used to determine the six representation constants that result in the best match between the modal characteristics of the representation and of the actual system as specified by nine measured

quantities given in Table 1. These quantities are the fundamental natural frequency, $(X_p/X_d)^2$, and M_{pm} for each of the three spring conditions: $K_p = K_s = 0$, $K_s = 0$ and K_p of the .125 in. spring, and $K_p = 0$ and K_s of the .098 in. spring. The resulting representation constants are given in Table 3. The backward whirl representation matched its specified measured quantities very closely and the forward whirl and zero speed representations gave reasonably good matches. Since the actual system has distributed stiffness and mass instead of being lumped as assumed in these representations, the matching for other disk and platform stiffnesses may not be as good. However, it is believed that the idealized system shown in Fig. 13 is close enough dynamically to the actual system to give reasonably accurate predictions of the test rig modal characteristics over the seal and platform stiffness ranges of interest.

4.4 Data Acquisition and Reduction

The platform destabilizing cross stiffness K_c dial values required to cause instability of the rotor system with the top seal omitted but with the snubber installed and accurately centered are given in Table 4. Thus, the net whirl damping of the system without a top seal is positive for both backward and forward whirl. This damping is caused by air forces in the snubber clearance, air forces on the top and bottom faces of the disks, air forces in the dummy seal (which should have negligible effect because they act at the pivot), and very small mechanical losses in the shaker springs, pivot springs, bearings, and other system components. Consequently, when tests were run (using the test method and pressure ranges described in Section 1) with a top seal installed, the values given in Table 4 were added to the equivalent platform stabilizing K_c dial readings since the tare values given in Table 4 are also stabilizing. Although these correction values directly apply to the zero platform stiffness and zero seal stiffness case only, they were used for all other cases as well. It is believed that the resulting

errors are relatively small and less than those caused by imperfect centering of the snubber. Positive damping B dial readings were converted to stabilizing cross stiffness dial readings by means of Eq. 15 and added to the actual stabilizing K_c dial readings (which are negative if they are destabilizing). This sum is then added to the appropriate dial correction value from Table 4 to obtain the net equivalent stabilizing K_c dial value, which is the K_c value given in the data sheets, Tables 5-31. A positive (stabilizing) equivalent K_c value corresponds to a positive (destabilizing) whirl excitation constant (since they are equal at neutral stability); it is multiplied by the scale constant and referred to the seal location by means of the following equation

$$E = (.1142)(\text{dial } K_c)\left(\frac{X_p}{X_d}\right)^2 \text{ lb/in} \qquad (25)$$

(or $E = 20\ (\text{dial } K_c)(X_p/X_d)^2$ N/m), which is used to calculate the values tabulated. Equation 24 or Fig. 9 is used to evaluate $(X_p/X_d)^2$. The radial stiffness K_s of the seal is determined from Fig. 12 using the measured whirl frequency.

The foregoing procedure for determining E will now be illustrated using test results for the S1 diverging seal at P_3 = 15 psia and $P_1 - P_3$ = 3 psi. For backward whirl, Table 5, B dial = 416 and actual K_c dial = 0 so the total corrected K_c dial value tabulated = [(416)(10.50)/10.61] + 50 = 461.7 and E = (.1142)(461.7)(.8856) = 46.69 lb/in. For forward whirl, Table 9, B dial = 144 and DSF K_c dial = 400 so the corrected K_c dial value tabulated = [(144)(12.88)/10.61] - 400 + 17 = - 208 and E = (.1142)(- 208)(.9167) = - 21.77 lb/in. The B dials were not needed for the S2 converging seal or the S3 straight seal; only the K_c dials were used in those tests.

Data obtained in tests run to determine the effect of whirl frequency on the whirl excitation constants of the seals are given in Tables 27-31. Platform direct stiffness dial settings of 0, 500, 1000,

and - 500 were used, which correspond to platform stiffnesses of 0, 171.3, 342.6, and - 171.3 lb/in, respectively (or 0, 30, 60, and - 30 kN/m), shown in the K_p column of the tables. The corrected K_c dial values and E values tabulated were calculated the same way as in the other tables except that $(X_p/X_d)^2$ could not be calculated from Eq. 24 when K_p was non zero. Instead, $(X_p/X_d)^2$ was determined from Fig. 9 by drawing a line parallel to the appropriate (backward or forward whirl) variable-platform-stiffness line from the point on the zero-platform-stiffness line corresponding to the measured whirl frequency when $K_p = 0$ to the whirl frequency measured for the platform stiffness being used. This is illustrated in Fig. 9 for the S1 diverging seal with backward whirl, P_3 = 15 psia, $P_1 - P_3$ = 3 psi, and direct platform stiffnesses of 171.3 lb/in. The dashed line goes from the point (10.50, .8856) to $(X_p/X_d)^2$ = .829 at f = 12.61 Hz.

4.5 Seal Annulus Pressure Measurements

Dynamic pressure transducers were installed in the outer surface of the seal annulus at two diametrical points and the phasor difference between the two pressures was recorded after filtering the difference signal with a 30-Hz low pass filter to eliminate most of the random pressure fluctuations caused by turbulence. See Fig. 14. The measured sinusoidal pressure differences and their phase angles relative to the Y displacement are given in Table 32 for each seal at a few selected pressure conditions. The phase angle α values were obtained by analyzing photographs of oscilloscope traces and then correcting the phase angles for the phase lag of the filter. The whirl amplitude at the seal is also given; it corresponds to 0.019 mm (0.75 mils) single peak at the platforms.

If the static offset of a seal were zero, then from symmetry and the fact that the individual pressures are sinusoidal at whirl frequency, P_{21} would be equal to and in phase with $-P_{22}$, and the circumferential pressure distribution in the seal annulus would be sinusoidal.

For this case, the instantaneous force acting on the rotor in the direction from maximum positive pressure to maximum negative pressure is

$$F = 4\left(\frac{\Delta P}{2}\right) Ra \int_0^{\pi/2} \sin^2\beta d\beta = \frac{\pi Ra\Delta P}{2} \qquad (26)$$

where β is the angle from the perpendicular to the direction of the total force, ΔP is the maximum pressure difference at diametrical points in the seal, R is the rotor radius, and a is the seal axial length. This force whirls in the same direction as the rotor and has a constant amplitude. As can be seen from Fig. 15, the whirl excitation constant and radial stiffness of the seal are given by

$$E = \mp \left(\frac{\pi Ra}{2}\right) \frac{(P_{21}-P_{22})}{r} \cos(45 \pm \alpha) \qquad (27)$$

$$K_s = -\left(\frac{\pi Ra}{2}\right) \frac{(P_{21}-P_{22})}{r} \sin(45 \pm \alpha) \qquad (28)$$

where the upper sign applies for forward whirl and the lower sign applies for backward whirl. These equations were used to calculate the E and K_s values given in Table 32.

The effect of static offset on the annulus pressures of all three seals was measured. Light rubber bands hooked onto the platforms were used to displace the rotor a small amount toward each of the pressure transducers and in the perpendicular directions. The largest effect was observed for the S1 diverging seal during backward whirl. These results are given in Table 33.

5. TEST RESULTS AND DISCUSSION

5.1 Measured Seal Forces

Measured backward and forward whirl excitation constants, radial stiffnesses, whirl frequencies, and mass flow rates are shown in Figs. 16-23 for the S1 diverging seal, in Figs. 24-30 for the S2 converging seal, and in Figs. 31-36 for the S3 straight seal. All of the results were obtained with platform motions of 0.019 mm (0.75 mils) single peak; however, whirl amplitude had little effect (usually less than 2%) on the whirl excitation constants for amplitudes up to 0.025 mm. To achieve this insensitivity to whirl amplitude required careful centering of the snubber; its static offset had to be held well below 0.012 mm.

The curves are discussed and compared in the fifth paragraph of Section 1 and in Conclusions 5-14 of Section 6. The fact that the whirl excitation constants of the diverging and straight seals tend to be approximately independent of back pressure at low pressure drops but not at high pressure drops suggests that there are different flow regimes or dominant mechanisms at low and high pressure drops. The dips and peaks also indicate that transitions or other unusual phenomena occur in labyrinth seals. Whether or not the dips and peaks are affected by static offset should be investigated.

Whirl frequency affects the whirl excitation constants of the diverging and straight seals only moderately, but it affects those of the converging seal significantly. See Tables 27-31. It has very little effect on the diverging seal with backward whirl. The forward and backward whirl excitation constants of the converging seal are approximately proportional to whirl frequency over a 1.5 to 1 range.

The measured whirl excitation constant data given in this report are believed to be accurate within 3% $\pm$ 0.1 kN/m (0.57 lb/in) and to be

repeatable much closer than that except close to sudden slope changes or peaks and dips. The sources of error include (a) inaccuracies in calibrating the active whirl damping and stiffness system, (b) gain drift of the displacement transducer signal conditioners (their gains were checked and readjusted frequently to keep this error relatively small), (c) inaccuracies in determining the modal characteristics of the test rig, (d) imperfect setting of the dials when adjusting for neutral whirl stability, (e) inaccuracies of the mercury manometer used to measure the pressure drop across the seal and of the Bourdon tube gages used to measure the back pressure, (f) imperfect centering of the snubber and small variations of its whirl excitation constants with whirl frequency, which were neglected, (g) temperature variations, and (h) imperfect geometry and centering of the test seals. The seal bore out-of-roundness could have caused more error than is given above. The measured radial stiffnesses are thought to be accurate within 3% $\pm$ 0.6 kN/m (3.4 lb/in).

5.2 Measured Annulus Pressures

Some whirl excitation constants and radial stiffnesses calculated from the measured annulus pressures are given in Table 32 for all three test seals. These calculations (which used Eqs. 27 and 28) assume that the seal annulus pressure is distributed sinusoidally. This is true only if the static offset is zero; it was small in these tests [0.0137 mm (0.54 mils) for the diverging seal, as discussed a little later] but not zero. The total pressure difference at diametrical points in the annulus is not affected significantly by static offset, as shown in Table 33. Furthermore, measurements with the active whirl damping and stiffness system showed that the seal forces were essentially unaffected by small static offset. Consequently, it is concluded that the amount by which the annulus pressure distribution becomes nonsinusoidal due to static offset is not sufficient to affect the net seal forces significantly.

The annulus pressure whirl excitation constant and radial stiffness values given in Table 32 differ from the values measured with

the active whirl damping and stiffness system, which includes all seal forces on the rotor whether they are understood or not. The annulus pressure whirl excitation constant was usually somewhat (25 to 44%) larger than the directly measured E value for the diverging and converging seals, but roughly the same for the straight seal. In addition, the annulus pressure radial stiffnesses were substantially different from the directly measured K_s values. The annulus pressure K_s value was 23 to 60% as large as the directly measured K_s value for the converging and straight seals, but the annulus pressure K_s value was either much too large or had the wrong sign in the case of the diverging seal. These differences may be due in part to errors in the annulus pressure results because of interference from the turbulent pressure fluctuations; however, the differences appear too large to be fully accounted for by this. Other phenomena must be contributing to the seal forces.

The effect of static offset on annulus pressures P_{21} and $-P_{22}$ in the diverging seal can be seen from Table 33 and the vector diagrams shown in Fig. 37. They show that small static offsets change the amplitudes and phases of P_{21} and $-P_{22}$ by large amounts, though they do not change $P_{21}-P_{22}$ significantly.* Static offset has substantially less effect on the annulus pressures of the converging and straight seals.

If the seal were geometrically perfect and the static offset were zero, P_{21} and $-P_{22}$ would both go to the triangular points denoted by $(P_{21}-P_{22})/2$ in Figs. 37a and 37b. It is evident that the rotor would have to be offset in a direction about midway between the directions of offsets 2 and 3 in order to make the true static offset zero. The magnitudes and angles of the offsets required to bring (one at a time) P_{21} and $-P_{22}$ to the triangular points for both backward and forward whirl were calculated. The average of these four required offsets showed that the rotor would have to be displaced 0.0137 mm (0.539 mils) in the $\theta = 0.21°$ direction to make the true offset zero. The four required offsets were nearly the same, which indicates that the accuracy of the pressure measurements was not degraded excessively by the turbulent pressure fluctuations superimposed on the whirl frequency component of

*It is interesting to note that rotating the offset vector clockwise causes the pressure effect vectors [e.g., $(\vec{P}_{21})_2 - (\vec{P}_{21})_1$] to rotate counterclockwise for both backward and forward whirl.

the annulus pressures. The calculated average required offset is shown by the triangular point in Fig. 37c.

5.3 Theoretical Seal Forces

As described in the last two paragraphs of Section 1, the forces of the test seals were calculated with an existing computer program that had been thought to be approximately valid; however, the theoretical results do not agree with the test results. The theoretical forward whirl results and the radial stiffnesses are completely invalid. The only theoretical results that agree at all with the test results are the backward whirl excitation constants of the diverging and converging seals, and even those are considerably smaller than the measured values. See Figs. 38 and 39. Since the theory attempts to calculate the whirling perturbation pressure field in the seal annulus, and the annulus pressure measurements showed that this pressure field at least approximately predicts the backward and forward whirl excitation constants, even though it does not predict the radial stiffnesses at all well, it is not understood why the theoretical results are so poor. Evidently some major factors are omitted or are wrong in the present theory. It is recommended that analyses be made to identify the sources of the errors in the theory, and that a valid theory be developed that closely predicts the test results given in this report.

6. CONCLUSIONS

(1) Accurate measured values were obtained for the forces generated by single-cavity labyrinth seals when the rotor whirls subsynchronously. These results will aid development of a valid analytical seal force prediction method that can be used in the design of turbines, pumps, and compressors to avoid self-excited rotor whirl.

(2) Labyrinth seal forces on a whirling rotor can be measured accurately and repeatably with the test rig and active whirl damping and stiffness system described in this report.

(3) The measured whirl excitation constants given in this report are believed to be accurate within 3% $\pm$ 0.1 kN/m (0.57 lb/in) and to be repeatable much closer than that except close to sudden slope changes or peaks and dips. The measured radial stiffnesses are thought to be accurate within 3% $\pm$ 0.6 kN/m (3.4 lb/in).

(4) Although the converging model seal is stabilizing for both forward and backward whirl and the diverging and straight model seals are destabilizing for backward whirl, this may not be true for other seals having different parameters. Consequently, it is not justified at this time to conclude that converging seals are always the best ones to use to avoid self-excited whirl of machines.

(5) The whirl excitation constant of all three seals for both whirl directions has the general trend of increasing proportionally to the square root of the pressure drop. However, the curves deviate from their trend lines in the following ways: (a) the curves for the lower back pressures tend to level out at high pressure drops, (b) the curves tend to be below their trend lines at the lower pressure drops and to have a pronounced dip at a pressure drop in the range of 4 kPa (0.58 psi) to 9 kPa (1.3 psi), and (c) some of the curves also have a pronounced peak above their trend lines at an intermediate or low pressure drop, as

shown in Fig. 16, for example. The pressure drops at which the dips and peaks occur vary with back pressure.

(6) The whirl excitation constant of the diverging and straight seals tends to be approximately independent of back pressure at low pressure drops and to increase with back pressure at high pressure drops. Back pressure has more effect on the whirl excitation constant of the converging seal at low pressure drops.

(7) The complicated behavior described in Conclusions 5 and 6 suggests that very complex phenomena act in labyrinth seals. Different regimes or mechanisms may be dominant at low and high pressure drops, and transitions, wave effects, or resonances may occur, perhaps involving spiraling flows in the seal annulus as discussed in References 2 and 3.

(8) The backward whirl excitation constant E_b of the diverging seal is positive and large, so this seal is strongly destabilizing for backward whirl. $E_b \simeq 9$ kN/m (51.4 lb/in) at the higher pressure drops. E_b of the straight seal is also positive but it is only about 25% as large as the E_b of the diverging seal. E_b of the converging seal is negative and large.

(9) The forward whirl excitation constant E_f of all three seals is negative and large. E_f is largest for the converging seal, about 82% as much for the straight seal, and about 65% as much for the diverging seal.

(10) Forward self-excited whirl is much more likely to occur than backward self-excited whirl in turbines with oil film bearings and non-overhung rotors. Turbine blade forces are destabilizing for forward whirl (and stabilizing for backward whirl) when the rotor is not overhung, and oil film bearings have much smaller damping for forward whirl than for backward whirl. Consequently, labyrinth seals for such machines should be designed to have as large a negative forward whirl excitation constant as possible to provide the most stabilization of the machine.

(11) Whereas the backward and forward whirl excitation constants of a seal are quite different, the radial stiffnesses are nearly the same for both whirl directions.

(12) The radial stiffness of the converging seal is large and positive for both backward and forward whirl. $K_{sb} \tilde{=} 25$ kN/m (143 lb/in) when $P_1-P_3 = 20$ kPa (2.9 psi). It is directly proportional to pressure drop up to 12 kPa (1.74 psi) and then continues to increase with increasing pressure drop at a slightly smaller rate. It is nearly independent of back pressure. K_{sf} is about 92% as large as K_{sb} at high pressure drops.

(13) The radial stiffness of the straight seal for both whirl directions is positive and about 65% as large as the radial stiffness of the converging seal. It also tends to be directly proportional to pressure drop, but with somewhat decreased slope at low pressure drops in the case of K_{sb}. It also is approximately independent of back pressure, except that it decreases somewhat at the lower back pressures.

(14) The radial stiffness of the diverging seal for both whirl directions is positive at the higher back pressures and only about 30% as large as the radial stiffness of the converging seal. It tends to be proportional to pressure drop for P_1-P_3 greater than 12 kPa (1.74 psi); at lower pressure drops it is slightly negative. At the lowest back pressure, $P_3 = 103.42$ kPa (15 psia), the radial stiffness is negative at low and intermediate pressure drops and K_{sb} goes to a negative maximum of -3.7 kN/m (-21 lb/in) at $P_1-P_3 = 20.7$ kPa (3 psi). This behavior is very different from that of the other two seals.

(15) The whirl force is directly proportional to whirl amplitude and it is not affected significantly by static offset of the seal.

(16) Whirl frequency affects the whirl excitation constants of the diverging and straight seals only moderately, but it affects those of the converging seal significantly. The whirl excitation constants of the converging seal are approximately proportional to whirl frequency over a 1.5 to 1 range.

(17) Seal whirl excitation constants calculated from alternating pressures measured in the seal annulus differ somewhat from the values measured with the active whirl damping and stiffness system, which includes all seal forces on the rotor. In addition, annulus pressure radial stiffnesses differ substantially from the directly measured values. Consequently, either radial and axial pressure gradients in the seal annulus or drag forces on the rotor are significant; the seal forces are not caused solely by a whirling perturbation pressure field in the seal annulus with circumferential pressure gradients only.

(18) Static offset strongly affects the alternating pressures at diametrical points in the annulus of the diverging seal; however, static offset has little effect on the phasor difference between the two pressures, and therefore has little effect on the net annulus pressure force on the rotor. See Table 33. Static offset moderately affects the individual alternating pressures in the converging and straight seals, but again it has little effect on the phasor difference between the two pressures.

(19) The poor agreement obtained between analytical seal force predictions and the experimental results shows that present theory is invalid; it needs to be improved.

(20) Theory indicates that preswirl velocity (V_1 in Fig. 1) and rotor roughness (such as would be caused by different blade shroud heights) both strongly affect the seal forces on a whirling rotor. To establish whether or not this is true, tests should be run with antiswirl vanes installed as shown in Fig. 40 and with a stepped rotor as shown in Fig. 41. With no antiswirl vanes, the preswirl velocity is approximately equal to one-half of the rotor surface speed.

7. REFERENCES

1. Wright, D. V., "Air Model Tests of Labyrinth Seal Forces On a Whirling Rotor," Journal of Engineering for Power, Trans. ASME, Series A, Vol. 100, No. 14, Oct. 1978, pp. 533-543.

2. Benckert, H. and Wachter, J., "Flow Induced Spring Coefficients of Labyrinth Seals for Application in Rotor Dynamics," pp. 189-212 of NASA Lewis Conference Publication 2133, Rotordynamic Instability Problems in High-Performance Turbomachinery, 1980.

3. Iwatsubo, T., "Evaluation of Instability Forces of Labyrinth Seals in Turbines or Compressors," pp. 139-167 of NASA Lewis Conference Publication 2133, Rotordynamic Instability Problems in High-Performance Turbomachinery, 1980.

4. DenHartog, J. P., Mechanical Vibrations, 4th ed., McGraw-Hill, New York, 1956, pp. 258-259.

Dwg. 7739A33

TABLE 1—MODAL CHARACTERISTICS OF SEAL WHIRL MODEL. B DENOTES BACKWARD WHIRL (OPPOSITE TO THE 30 RPS ROTATION), F DENOTES FORWARD WHIRL, AND ZS DENOTES ZERO SPEED

Spring Thickness, Inches		Whirl	f	$(X_p/X_d)^2$	M_{pm}	K_{dm}
Platform	Disk	Direction	Hz		lbm	lb/in
0	0	B	10.82	.890	32.8	349.4
.073	0	B	13.13	.829	34.1	498.3
.098	0	B	15.44	.762	35.8	665.0
.125	0	B	18.85	.654	39.3	933.7
0	0	F	13.05	.919	26.3	420.9
.073	0	F	15.27	.858	28.0	572.7
.098	0	F	17.66	.792	30.2	762.8
.125	0	F	21.15	.686	34.5	1082.7
0	0	ZS	11.90	.904	29.3	383.6
.073	0	ZS	14.15	.843	31.1	536.8
.098	0	ZS	16.50	.776	33.2	717.1
.125	0	ZS	20.00	.670	37.0	1013.9
0	.073	ZS	13.60	.926	28.7	502.7
0	.098	ZS	16.40	.963	28.3	749.4
.073	.073	ZS	15.83	.866	30.6	679.0
.098	.073	ZS	18.00	.797	32.6	860.7
.125	.073	ZS	21.20	.687	36.4	1149.4
.125	.098	ZS	23.25	.715	35.1	1387.4
0	.073	B	12.52	.912	32.2	470.7
0	.098	B	15.32	.949	31.7	721.9
0	.073	F	14.75	.941	25.8	540.1
0	.098	F	17.55	.978	25.5	785.5

Dwg. 7739A34

TABLE 2—SEAL STIFFNESS REQUIRED FOR VARIOUS SEAL WHIRL MODEL NATURAL FREQUENCIES WHEN THE PLATFORM STIFFNESS IS ZERO

Backward Whirl		Forward Whirl		Zero Speed	
f Hz	K_s lb/in	f Hz	K_s lb/in	f Hz	K_s lb/in
10.50	−21.0	12.87	−11.5	11.90	0
10.82	0	13.05	0	12.50	39.8
11.00	11.8	13.50	30.4	13.00	73.8
11.50	45.5	14.00	64.5	13.60	115.6
12.00	79.2	14.50	99.0	14.00	146.0
12.52	117.2	14.75	115.9	14.50	187.2
13.00	154.9	15.00	135.8	15.00	228.2
13.50	196.4	15.50	176.1	15.50	271.1
14.00	238.5	16.00	217.0	16.00	314.4
14.50	282.5	16.50	259.8	16.40	351.1
15.00	327.5	17.00	302.7		
15.32	356.4	17.55	350.5		

Dwg. 7739A35

TABLE 3—TEST RIG MASS-SPRING REPRESENTATION CONSTANTS. SEE FIG. 13. B DENOTES BACKWARD WHIRL, F FORWARD WHIRL, AND ZS ZERO SPEED

Whirl Direction	M_d lbm	M_p lbm	K_r lb/in	K_o lb/in	K_p lb/in	K_s lb/in
B	18.1462	12.2436	3523.27	378.862	879.630	349.722
F	15.4536	9.6011	4102.55	436.232	893.327	368.476
ZS	16.8605	10.6962	3823.58	405.922	894.328	360.749

TABLE 4—CROSS STIFFNESS DIAL CORRECTION. ADD THE APPROPRIATE TABULATED VALUE TO THE MEASURED STABILIZING K_c DIAL VALUE TO OBTAIN THE CORRECTED K_c DIAL VALUE

	Backward Whirl	Forward Whirl
P_3, psia	K_c, Dial	K_c, Dial
15	50	17
30	54	22
45	59	28
60	68	35

TABLE 5—DYNAMIC CHARACTERISTICS OF S1 DIVERGING SEAL FOR BACKWARD WHIRL AND 15 PSIA DOWNSTREAM PRESSURE

$P_1 - P_3$ psi	f Hz	K_c Dial	$\dot{m}$ SCFM	$(X_p/X_d)^2$	E lb/in	K_s lb/in
0.0	10.79	+5.0	0.0	.8893	+0.5	−1.9
0.1	10.78	+67.3	1.76	.8892	+6.8	−2.7
0.2	10.77	92.6	3.4	.8891	9.4	−3.3
0.4	10.75	107.8	6.0	.8888	10.9	−4.6
0.6	10.72	127.8	7.4	.8884	13.0	−6.5
0.8	10.69	144.7	8.5	.8880	14.7	−8.5
1.0	10.66	195.7	9.5	.8876	19.8	−10.4
1.2	10.64	250.6	10.5	.8874	25.4	−11.8
1.5	10.60	319.7	12.0	.8869	32.4	−14.3
1.75	10.58	374.1	13.3	.8866	37.9	−15.7
2.0	10.56	411.3	14.5	.8863	41.6	−17.0
2.5	10.52	442.6	16.9	.8858	44.8	−19.7
3.0	10.50	461.7	19.1	.8856	46.7	−21.0
3.5	10.56	478.0	21.1	.8863	48.4	−17.0
4.0	10.67	487.4	23.0	.8878	49.4	−9.8
4.5	10.77	495.6	24.5	.8891	50.3	−3.3
5.0	10.89	501.6	26.0	.8907	51.0	+4.5
6.0	11.10	509.3	28.7	.8934	52.0	+18.1
7.0	11.30	523.9	31.2	.8960	53.6	+31.6
8.0	11.50	528.0	33.2	.8987	54.2	+45.5
9.0	11.70	530.8	34.5	.9013	54.6	+59.5

Dwg. 7739A38

TABLE 6—DYNAMIC CHARACTERISTICS OF S1 DIVERGING SEAL FOR BACKWARD WHIRL AND 30 PSIA DOWNSTREAM PRESSURE

$P_1 - P_3$ psi	f Hz	K_c Dial	$\dot{m}$ SCFM	$(X_p/X_d)^2$	E lb/in	K_s lb/in
0.02	10.80	+7.0	0.0	.8895	+0.7	−1.3
0.1	10.79	+44.3	1.76	.8893	+4.5	−1.9
0.2	10.77	102.7	3.52	.8891	10.4	−3.3
0.5	10.72	167.2	8.4	.8884	17.0	−6.5
0.7	10.69	193.0	10.6	.8880	19.6	−8.5
1.0	10.65	274.8	13.4	.8875	27.9	−11.1
1.2	10.64	334.8	15.1	.8874	33.9	−11.8
1.5	10.65	379.2	17.5	.8875	38.4	−11.1
1.7	10.70	396.9	19.3	.8882	40.3	−7.9
2.0	10.77	418.4	21.5	.8891	42.5	−3.3
2.5	11.00	435.5	24.8	.8921	44.4	+11.8
3.0	11.18	443.9	27.6	.8945	45.3	+23.4
3.5	11.35	446.6	30.0	.8967	45.7	+35.1
4.0	11.48	452.2	32.2	.8984	46.4	+44.1
4.5	11.60	458.5	34.2	.9000	47.1	+52.5
5.0	11.70	475.2	36.0	.9013	48.9	+59.5
5.5	11.80	494.4	37.8	.9026	51.0	+66.3
6.0	11.90	522.8	39.5	.9039	54.0	+72.8
7.0	12.10	567.2	42.8	.9065	58.7	+86.5

Dwg. 7739A39

TABLE 7—DYNAMIC CHARACTERISTICS OF S1 DIVERGING SEAL FOR BACKWARD WHIRL AND 45 PSIA DOWNSTREAM PRESSURE

$P_1 - P_3$ psi	f Hz	K_c Dial	$\dot{m}$ SCFM	$(X_p/X_d)^2$	E lb/in	K_s lb/in
0.08	10.83	+ 9.0	0.0	.8899	+ 0.9	+ 0.6
0.12	10.82	+ 2.0	2.11	.8897	+ 0.2	0.0
0.2	10.80	109.9	3.52	.8895	+11.2	− 1.3
0.35	10.75	140.1	6.16	.8888	+14.2	− 4.6
0.5	10.73	188.4	8.8	.8886	19.1	− 5.9
0.7	10.70	208.3	12.0	.8882	21.1	− 7.9
0.85	10.71	225.6	14.4	.8883	22.9	− 7.2
1.0	10.72	266.1	16.5	.8884	27.0	− 6.5
1.25	10.73	301.7	19.5	.8886	30.6	− 5.9
1.5	10.76	332.8	22.5	.8890	33.8	− 4.0
2.0	10.88	371.8	27.5	.8905	37.8	+ 4.0
2.5	11.01	406.6	31.0	.8922	41.4	+12.4
3.0	11.14	437.0	34.0	.8939	44.6	+20.8
3.5	11.26	467.6	36.8	.8955	47.8	+29.0
4.0	11.38	498.8	39.5	.8971	51.1	+37.2
4.5	11.50	535.9	41.8	.8987	55.0	+45.5
5.0	11.60	567.4	44.0	.9000	58.3	+52.5

Dwg. 7739A40

TABLE 8—DYNAMIC CHARACTERISTICS OF S1 DIVERGING SEAL FOR BACKWARD WHIRL AND 60 PSIA DOWNSTREAM PRESSURE

$P_1 - P_3$ psi	f Hz	K_c Dial	$\dot{m}$ SCFM	$(X_p/X_d)^2$	E lb/in	K_s lb/in
0.15	10.81	+ 8.0	0.0	.8896	+ 0.8	− 0.6
0.18	10.80	+ 8.7	3.17	.8895	+ 0.9	− 1.3
0.3	10.73	112.5	5.28	.8886	+11.4	− 5.9
0.4	10.64	138.2	7.04	.8874	14.0	−11.8
0.5	10.60	187.9	8.8	.8869	19.0	−14.3
0.7	10.66	228.8	12.2	.8876	23.2	−10.4
0.85	10.69	224.2	14.7	.8880	22.7	− 8.5
1.0	10.72	221.6	17.2	.8884	22.5	− 6.5
1.2	10.76	235.3	20.3	.8890	23.9	− 4.0
1.5	10.81	271.8	24.7	.8896	27.6	− 0.6
2.0	10.90	338.2	30.4	.8908	34.4	+ 5.2
2.5	11.00	394.6	35.0	.8921	40.2	+11.8
3.0	11.10	465.5	39.0	.8934	47.5	+18.1
3.5	11.20	521.9	42.2	.8947	53.3	+24.9
4.0	11.30	579.2	45.0	.8960	59.3	+31.7

Dwg. 7739A32

TABLE 9—DYNAMIC CHARACTERISTICS OF S1 DIVERGING SEAL FOR FORWARD WHIRL AND 15 PSIA DOWNSTREAM PRESSURE

$P_1 - P_3$ psi	f Hz	K_c Dial	$(X_p/X_d)^2$	E lb/in	K_s lb/in
0.0	13.04	+2.0	.9188	+0.2	−0.5
0.05	13.04	−7.0	.9188	−0.7	−0.5
0.1	13.04	−36.2	.9188	−3.8	−0.5
0.2	13.03	−41.7	.9187	−4.4	−1.2
0.4	13.02	−34.2	.9186	−3.6	−1.8
0.6	13.02	−31.0	.9186	−3.3	−1.8
0.8	13.01	−37.8	.9184	−4.0	−2.5
1.0	13.00	−5.3	.9183	−0.6	−3.1
1.1	12.99	+11.0	.9182	+1.2	−3.8
1.2	12.98	+18.2	.9180	+1.9	−4.4
1.3	12.96	−12.1	.9178	−1.3	−5.7
1.4	12.95	−48.2	.9176	−5.1	−6.3
1.5	12.94	−88.0	.9175	−9.2	−7.0
1.8	12.90	−165.8	.9170	−17.4	−9.6
2.0	12.88	−200.2	.9167	−21.0	−10.9
2.2	12.88	−214.7	.9167	−22.5	−10.9
2.4	12.87	−212.3	.9166	−22.2	−11.5
2.5	12.87	−206.3	.9166	−21.6	−11.5
2.6	12.87	−206.3	.9166	−21.6	−11.5
3.0	12.88	−208.0	.9167	−21.8	−10.9
3.5	12.92	−210.2	.9173	−22.0	−8.2
4.0	13.00	−209.6	.9183	−22.0	−3.1
4.5	13.10	−212.6	.9196	−22.3	+3.4
5.0	13.20	−220.6	.9209	−23.2	+10.0
6.0	13.42	−233.4	.9238	−24.6	+24.9
7.0	13.63	−234.3	.9266	−24.8	+39.3
8.0	13.83	−223.6	.9292	−23.7	+53.1
9.0	14.00	−221.9	.9314	−23.6	+64.5

Dwg. 7739A31

TABLE 10—DYNAMIC CHARACTERISTICS OF S1 DIVERGING SEAL FOR FORWARD WHIRL AND 30 PSIA DOWNSTREAM PRESSURE

$P_1 - P_3$ psi	f Hz	K_c Dial	$(X_p/X_d)^2$	E lb/in	K_s lb/in
0.02	13.10	+ 2.0	.9196	+ 0.2	+ 3.4
0.05	13.10	+ 5.6	.9196	+ 0.6	+ 3.4
0.1	13.10	− 13.4	.9196	− 1.4	+ 3.4
0.15	13.10	− 32.4	.9196	− 3.4	+ 3.4
0.2	13.09	− 58.3	.9195	− 6.1	+ 2.9
0.35	13.08	− 59.5	.9193	− 6.2	+ 2.1
0.4	13.08	− 60.3	.9193	− 6.3	+ 2.1
0.45	13.07	− 48.0	.9192	− 5.0	+ 1.4
0.5	13.07	− 43.9	.9192	− 4.6	+ 1.4
0.6	13.06	− 29.6	.9191	− 3.1	+ 0.8
0.7	13.06	− 16.1	.9191	− 1.7	+ 0.8
0.8	13.05	− 11.1	.9190	− 1.2	0.0
0.9	13.05	− 27.1	.9190	− 2.8	0.0
1.0	13.05	− 63.6	.9190	− 6.7	0.0
1.2	13.07	−130.4	.9192	−13.7	+1.4
1.4	13.10				+3.4
1.5	13.13	−193.6	.9200	− 20.3	+5.4
1.7	13.19	−209.3	.9208	− 22.0	+9.3
2.0	13.30	−225.2	.9222	− 23.7	16.7
2.5	13.47	−244.8	.9245	− 25.8	28.3
3.0	13.62	−275.8	.9264	− 29.2	38.6
3.5	13.75	−291.1	.9281	− 30.9	47.5
4.0	13.88	−299.3	.9298	− 31.8	56.5
4.5	14.00	−302.6	.9314	− 32.2	64.5
5.0	14.11	−315.0	.9328	− 33.6	72.3
5.5	14.21	−320.1	.9342	− 34.1	77.8
6.0	14.30	−323.0	.9353	− 34.5	85.0

Dwg. 7739A41

TABLE 11—DYNAMIC CHARACTERISTICS OF S1 DIVERGING SEAL FOR FORWARD WHIRL AND 45 PSIA DOWNSTREAM PRESSURE

$P_1 - P_3$ psi	f Hz	K_c Dial	$(X_p/X_d)^2$	E lb/in	K_s lb/in
0.08	13.06	+3.0	.9191	+0.3	+0.8
0.1	13.06	+1.5	.9191	+0.2	+0.8
0.2	13.05	−27.5	.9190	−2.9	0.0
0.3	13.03	−60.8	.9187	−6.4	−1.2
0.4	13.01	−63.3	.9184	−6.6	−2.5
0.5	13.00	−57.1	.9183	−6.0	−3.1
0.6	13.01	−48.0	.9184	−5.0	−2.5
0.7	13.02	−44.3	.9186	−4.6	−1.9
0.8	13.03	−46.7	.9187	−4.9	−1.2
0.9	13.04	−62.7	.9188	−6.6	−0.5
1.0	13.07	−86.2	.9192	−9.0	+1.4
1.2	13.15	−136.1	.9203	−14.3	+6.8
1.5	13.26	−190.8	.9217	−20.1	+14.0
2.0	13.45	−252.1	.9242	−26.6	+26.9
2.5	13.61	−281.9	.9263	−29.8	+37.9
3.0	13.75	−316.0	.9281	−33.5	47.5
3.5	13.88	−343.4	.9298	−36.5	56.5
4.0	13.99	−356.0	.9313	−37.9	63.9
4.5	14.08	−372.6	.9324	−39.7	68.7
5.0	14.15	−378.9	.9334	−40.4	74.5

Dwg. 7739A42

TABLE 12—DYNAMIC CHARACTERISTICS OF S1 DIVERGING SEAL FOR FORWARD WHIRL AND 60 PSIA DOWNSTREAM PRESSURE

$P_1 - P_3$ psi	f Hz	K_c Dial	$(X_p/X_d)^2$	E lb/in	K_s lb/in
0.15	13.00	+5.0	.9183	+0.5	−3.1
0.18	12.99	+9.5	.9182	+1.0	−3.8
0.4	12.95	−55.1	.9176	−5.8	−6.3
0.45	12.95	−63.3	.9176	−6.6	−6.3
0.5	12.96	−66.9	.9178	−7.0	−5.7
0.6	12.98	−66.9	.9180	−7.0	−4.4
0.7	13.00	−66.9	.9183	−7.0	−3.1
0.8	13.02	−73.1	.9186	−7.7	−1.9
1.0	13.07	−104.0	.9192	−10.9	+1.4
1.2	13.14	−129.1	.9201	−13.6	+6.1
1.5	13.25	−192.5	.9216	−20.3	+13.3
2.0	13.45	−257.9	.9242	−27.2	+26.9
2.5	13.61	−298.2	.9263	−31.5	+37.9
3.0	13.75	−336.5	.9281	−35.7	+47.5
3.5	13.86	−354.4	.9289	−37.6	+55.1
4.0	13.95	−377.4	.9307	−40.1	+61.3

Dwg. 7739A43

TABLE 13—DYNAMIC CHARACTERISTICS OF S2 CONVERGING SEAL FOR BACKWARD WHIRL AND 15 PSIA DOWNSTREAM PRESSURE

$P_1 - P_3$ psi	f Hz	K_c Dial	$\dot{m}$ SCFM	$(X_p/X_d)^2$	E lb/in	K_s lb/in
0.0	10.87	−10	0.0	.8904	−1.0	+3.3
0.3	11.10	−78	3.8	.8934	−8.0	+18.1
0.7	11.39	−140	6.3	.8972	−14.3	+37.9
0.85	11.51	−155	7.0	.8988	−15.9	+46.4
1.0	11.61	−168	7.7	.9001	−17.3	53.8
1.1	11.68	−159	8.2	.9010	−16.4	58.6
1.2	11.75	−148	8.6	.9019	−15.2	63.2
1.5	11.97	−146	9.9	.9048	−15.1	77.7
2.0	12.31	−145	12.0	.9093	−15.1	102.3
2.5	12.62	−150	14.1	.9133	−15.6	125.6
3.0	12.90	−175	16.1	.9170	−18.3	147.0
3.5	13.16	−202	18.0	.9204	−21.2	167.8
4.0	13.41	−230	19.9	.9237	−24.3	189.6
5.0	13.87	−280	23.5	.9297	−29.7	227.3
6.0	14.27	−345	26.5	.9349	−36.8	263.8
7.0	14.65	−420	28.8	.9399	−45.1	295.5
8.0	14.95	−468	30.6	.9438	−50.4	323.0
9.0	15.18	−520	32.3	.9469	−56.2	344.0
10.0	15.35	−550	33.8	.9491	−59.6	359.5
11.0	15.50	−580	35.2	.9511	−63.0	374.0

Dwg. 7739A44

TABLE 14—DYNAMIC CHARACTERISTICS OF S2 CONVERGING SEAL FOR BACKWARD WHIRL AND 30 PSIA DOWNSTREAM PRESSURE

$P_1 - P_3$ psi	f Hz	K_c Dial	$\dot{m}$ SCFM	$(X_p/X_d)^2$	E lb/in	K_s lb/in
0.3	11.10	−134	4.3	.8934	−13.7	+18.1
0.6	11.30	−183	7.6	.8960	−18.7	+31.7
0.7	11.37	−213	8.7	.8969	−21.8	+36.5
0.85	11.47	−183	10.1	.8983	−18.8	+43.6
1.0	11.55	−181	11.4	.8993	−18.6	48.2
1.5	11.95	−199	15.7	.9045	−20.6	76.2
2.0	12.34	−251	19.7	.9097	−26.1	104.2
2.5	12.60	−296	23.0	.9131	−30.9	124.6
3.0	12.85	−361	25.8	.9163	−37.8	143.8
4.0	13.35	−461	30.0	.9229	−48.6	184.9
5.0	13.81	−573	33.2	.9289	−60.8	222.5
6.0	14.23	−636	36.0	.9344	−67.9	258.3
7.0	14.60	−691	38.6	.9393	−74.1	291.0
8.0	14.90	−749	41.1	.9432	−80.7	318.0
9.0			43.5			

Dwg. 7739A45

TABLE 15—DYNAMIC CHARACTERISTICS OF S2 CONVERGING SEAL FOR BACKWARD WHIRL AND 45 PSIA DOWNSTREAM PRESSURE

$P_1 - P_3$ psi	f Hz	K_c Dial	$\dot{m}$ SCFM	$(X_p/X_d)^2$	E lb/in	K_s lb/in
0.3	11.04	− 181	5.0	.8926	− 18.5	+ 14.3
0.5	11.18	− 226	7.6	.8945	− 23.1	+ 23.4
0.7	11.32	− 246	10.2	.8963	− 25.2	+ 33.0
0.85	11.43	− 243	12.2	.8977	− 24.9	+ 40.6
1.0	11.54	− 244	14.0	.8992	− 25.1	48.4
1.2	11.69	− 259	16.3	.9011	− 26.7	58.3
1.5	11.89	− 316	19.5	.9038	− 32.6	72.5
2.0	12.22	− 401	24.4	.9081	− 41.6	95.2
3.0	12.78	− 506	31.0	.9154	− 52.9	137.5
4.0	13.29	− 601	35.6	.9221	− 63.3	179.1
5.0	13.75	− 696	39.7	.9281	− 73.8	217.8
6.0	14.14	− 791	43.3	.9332	− 84.3	252.0

Dwg. 7739A46

TABLE 16--DYNAMIC CHARACTERISTICS OF S2 CONVERGING SEAL FOR FORWARD WHIRL AND 15 PSIA DOWNSTREAM PRESSURE

$P_1 - P_3$ psi	f Hz	K_c Dial	$(X_p/X_d)^2$	E lb/in	K_s lb/in
0.0	13.00	− 1	.9183	−0.1	−3.1
0.2	13.16	− 56	.9204	−5.9	+7.4
0.25	13.22	− 68	.9212	−7.2	+11.2
0.3	13.25	− 73	.9216	−7.7	+13.2
0.5	13.42	− 95	.9238	−10.0	+24.9
0.7	13.59	− 91	.9260	− 9.6	36.5
0.9	13.75	− 81	.9281	− 8.6	47.5
1.0	13.82	− 76	.9290	− 8.1	52.2
1.2	13.97	− 85	.9310	− 9.0	62.6
1.35	14.10	−116	.9327	−12.4	70.4
1.5	14.19	−174	.9339	− 18.6	76.4
1.75	14.37	−203	.9362	− 21.7	89.0
2.0	14.53	−215	.9383	− 23.0	100.3
2.5	14.81	−243	.9420	− 26.1	121.2
3.0	15.07	−275	.9454	− 29.7	142.2
3.5	15.30	−303	.9484	− 32.8	160.0
4.0	15.52	−323	.9513	− 35.1	178.2
4.5	15.72	−351	.9539	− 38.2	194.7
5.0	15.92	−368	.9566	− 40.2	210.2
5.5	16.10	−395	.9589	− 43.3	225.5
6.0	16.29	−415	.9614	− 45.6	241.5
7.0	16.65	−453	.9661	− 50.0	272.8
8.0	16.96	−493	.9702	− 54.6	299.6
9.0	17.25	−528	.9740	− 58.7	325.0

Dwg. 7739A47

TABLE 17—DYNAMIC CHARACTERISTICS OF S2 CONVERGING SEAL FOR FORWARD WHIRL AND 30 PSIA DOWNSTREAM PRESSURE

$P_1 - P_3$ psi	f Hz	K_c Dial	$(X_p/X_d)^2$	E lb/in	K_s lb/in
0.2	13.20	−68	.9209	−7.2	+10.0
0.5	13.41	−113	.9237	−11.9	+24.1
0.75	13.58	−121	.9259	−12.8	+36.0
0.9	13.68	−155	.9272	−16.4	+42.8
1.0	13.75	−173	.9281	−18.3	+47.5
1.25	14.00	−203	.9314	−21.6	64.5
1.5	14.20	−235	.9340	−25.1	77.4
2.0	14.55	−288	.9386	−30.9	102.6
2.5	14.78	−338	.9416	−36.3	118.8
3.0	15.00	−378	.9445	−40.8	135.7
3.5	15.20	−396	.9471	−42.8	152.3
4.0	15.40	−420	.9497	−45.6	167.8
4.5	15.61	−450	.9525	−48.9	185.4
5.0	15.80	−477	.9550	−52.0	200.2
5.5	16.00	−498	.9576	−54.5	217.5
6.0	16.20	−528	.9602	−57.9	234.5
7.0	16.58	−576	.9652	−63.5	266.6
8.0	16.92	−618	.9697	−68.4	296.3
9.0	17.20	−673	.9733	−74.8	320.1

Dwg. 7739A48

TABLE 18—DYNAMIC CHARACTERISTICS OF S2 CONVERGING SEAL FOR FORWARD WHIRL AND 45 PSIA DOWNSTREAM PRESSURE

$P_1 - P_3$ psi	f Hz	K_c Dial	$(X_p/X_d)^2$	E lb/in	K_s lb/in
0.3	13.20	−97	.9209	−10.2	+10.0
0.5	13.35	−132	.9229	−13.9	+20.0
0.8	13.55	−158	.9255	−16.7	+33.9
1.0	13.70	−200	.9275	−21.2	44.1
1.5	14.07	−260	.9323	−27.7	68.3
2.0	14.37	−329	.9362	−35.2	88.7
2.5	14.60	−392	.9393	−42.0	105.0
3.0	14.84	−447	.9424	−48.1	124.4
4.0	15.29	−522	.9483	−56.5	159.1
5.0	15.70	−587	.9537	−63.9	192.1
6.0	16.10	−637	.9589	−69.8	225.6

TABLE 19—DYNAMIC CHARACTERISTICS OF S3 STRAIGHT SEAL FOR BACKWARD WHIRL AND 15 PSIA DOWNSTREAM PRESSURE

$P_1 - P_3$ psi	f Hz	K_c Dial	$\dot{m}$ SCFM	$(X_p/X_d)^2$	E lb/in	K_s lb/in
0.0	10.85	−12	0.0	.8901	− 1.2	+ 2.0
0.2	10.92	+ 1	3.6	.8910	+ 0.1	+ 6.4
0.5	11.02	− 4	6.9	.8924	− 0.4	+13.0
0.6	11.05	−14	7.6	.8928	− 1.4	+15.0
0.7	11.08	−15	8.2	.8931	− 1.5	16.9
0.85	11.13	− 5	9.2	.8938	− 0.5	20.1
0.9	11.15	+ 4	9.5	.8941	+ 0.4	21.5
1.0	11.18	+26	10.0	.8945	+ 2.7	23.4
1.1	11.22	+45	10.6	.8950	+ 4.6	26.1
1.2	11.25	+53	11.2	.8954	+ 5.4	28.3
1.3	11.28	55	11.7	.8958	5.6	30.2
1.4	11.32	64	12.3	.8963	6.6	33.0
1.5	11.35	78	12.8	.8967	8.0	35.1
1.6	11.39	95	13.3	.8972	9.7	37.9
1.75	11.43	103	14.1	.8977	10.6	40.6
2.0	11.52	107	15.3	.8989	11.0	47.2
2.5	11.69	108	17.7	.9011	11.1	58.3
3.0	11.87	116	20.0	.9035	12.0	70.0
3.5	12.05	118	22.0	.9059	12.2	83.2
4.0	12.24	123	24.0	.9083	12.8	96.9
4.3	12.35	120	25.0	.9098	12.5	104.9
4.5	12.42	117	25.7	.9107	12.2	109.8
4.7	12.49	115	26.3	.9116	12.0	115.0
5.0	12.61	108	27.2	.9132	11.3	124.9
5.25	12.70	105	27.8	.9144	11.0	131.4
5.50	12.79	105	28.5	.9155	11.0	137.9
5.75	12.87	102	29.1	.9166	10.7	145.0
6.0	12.96	98	29.7	.9178	10.3	152.6
6.5	13.13	95	30.9	.9200	10.0	166.8
7.0	13.29	92	32.1	.9221	9.7	179.0
8.0	13.58	91	34.4	.9259	9.6	203.6
9.0	13.82	95	36.7	.9290	10.1	223.3
10.0	14.00	80	38.8	.9314	8.5	238.5

Dwg. 7739A49

TABLE 20—DYNAMIC CHARACTERISTICS OF S3 STRAIGHT SEAL FOR BACKWARD WHIRL AND 30 PSIA DOWNSTREAM PRESSURE

$P_1 - P_3$ psi	f Hz	K_c Dial	$\dot{m}$ SCFM	$(X_p/X_d)^2$	E lb/in	K_s lb/in
0.02	10.85	−14	0.37	.8901	−1.4	+2.0
0.3	10.91	− 1	5.6	.8909	−0.1	+6.0
0.5	10.96	− 8	8.8	.8916	−0.8	+9.1
0.7	11.02	− 6	11.3	.8924	−0.6	+13.0
0.85	11.07	+ 5	13.0	.8930	+0.5	16.3
1.0	11.13	+32	14.6	.8938	+3.3	20.1
1.2	11.21	+58	16.6	.8949	+5.9	25.5
1.35	11.27	+71	18.1	.8956	+7.3	29.6
1.5	11.34	76	19.5	.8966	7.8	34.3
1.75	11.44	94	21.5	.8979	9.6	41.3
2.0	11.55	104	23.5	.8993	10.7	49.0
2.55	11.78	114	27.0	.9023	11.7	64.5
3.0	11.97	114	29.3	.9048	11.8	77.4
3.5	12.18	109	31.5	.9076	11.3	92.3
4.0	12.39	109	33.5	.9103	11.3	107.0
4.5	12.60	106	35.3	.9131	11.1	124.2
5.0	12.82	105	37.2	.9159	11.0	141.0
6.0	13.22	104	40.7	.9212	10.9	174.6
7.0	13.60	109	44.0	.9262	11.5	205.0

Dwg. 7739A50

TABLE 21—DYNAMIC CHARACTERISTICS OF S3 STRAIGHT SEAL FOR BACKWARD WHIRL AND 45 PSIA DOWNSTREAM PRESSURE

$P_1 - P_3$ psi	f Hz	K_c Dial	$\dot{m}$ SCFM	$(X_p/X_d)^2$	E lb/in	K_s lb/in
0.09	10.82	−11	+ 1.9	.8897	−1.1	+0.0
0.5	10.92	−16	9.3	.8911	−1.6	+6.5
0.75	10.99	−21	13.5	.8920	−2.1	+11.1
1.0	11.08	+ 1	17.0	.8931	+0.1	+16.9
1.25	11.17	+21	20.0	.8943	+2.1	22.8
1.5	11.28	+39	23.0	.8958	+4.0	30.2
2.0	11.50	+63	27.9	.8987	+6.5	45.5
2.5	11.72	71	31.5	.9015	+7.3	61.0
3.0	11.94	69	34.6	.9044	7.1	75.8
3.5	12.16	67	37.4	.9073	6.9	90.4
4.0	12.36	70	40.0	.9100	7.3	105.8
5.0	12.72	81	44.8	.9146	8.5	133.8
5.8	12.95	79	48.0	.9176	8.3	151.8

Dwg. 7739A51

TABLE 22—DYNAMIC CHARACTERISTICS OF S3 STRAIGHT SEAL FOR BACKWARD WHIRL AND 60 PSIA DOWNSTREAM PRESSURE

$P_1 - P_3$ psi	f Hz	K_c Dial	$\dot{m}$ SCFM	$(X_p/X_d)^2$	E lb/in	K_s lb/in
0.15	10.83	− 7	2.8	.8899	− 0.7	+ 0.6
0.5	10.92	− 27	9.3	.8911	− 2.7	+ 6.4
0.75	10.99	− 39	13.8	.8920	− 4.0	+11.1
1.0	11.08	− 42	18.0	.8931	− 4.3	+16.9
1.25	11.17	− 34	21.7	.8943	− 3.5	22.8
1.4	11.23	− 12	23.8	.8951	− 1.2	26.8
1.5	11.28	− 7	25.2	.8958	− 0.7	30.1
1.8	11.41	+ 8	28.9	.8975	+ 0.8	39.3
2.0	11.50	+ 33	31.2	.8987	+ 3.4	45.5
2.5	11.70	+ 38	36.0	.9013	+ 3.9	59.5
3.0	11.90	+ 43	39.8	.9039	+ 4.4	73.0
3.5	12.06	+ 50	43.0	.9060	+ 5.2	83.4

Dwg. 7739A29

TABLE 23—DYNAMIC CHARACTERISTICS OF S3 STRAIGHT SEAL FOR FORWARD WHIRL AND 15 PSIA DOWNSTREAM PRESSURE

$P_1 - P_3$ psi	f Hz	K_c Dial	$\dot{m}$ SCFM	$(X_p/X_d)^2$	E lb/in	K_s lb/in
0.0	13.08	0	0.0	.9193	0.0	+2.1
0.2	13.14	−51	3.6	.9201	−5.4	+6.1
0.5	13.24	−55	6.9	.9214	−5.8	+12.7
0.6	13.28	−58	7.6	.9220	−6.1	+15.2
0.7	13.32	−70	8.2	.9225	−7.4	18.0
0.85	13.40	−73	9.2	.9235	−7.7	23.3
0.9	13.43	−69	9.5	.9239	−7.3	25.5
1.0	13.48	−53	10.0	.9246	−5.6	29.0
1.1	13.50	−48	10.6	.9249	−6.1	30.3
1.2	13.52	−63	11.2	.9251	−6.7	31.8
1.3	13.54	−101	11.7	.9254	−10.7	33.1
1.4	13.56	−148	12.3	.9256	−15.6	34.6
1.5	13.59	−168	12.8	.9260	−17.8	36.5
1.6	13.62	−180	13.3	.9264	−19.0	38.6
1.75	13.67	−192	14.1	.9271	−20.3	42.0
2.0	13.75	−198	15.3	.9281	−21.0	47.5
2.5	13.93	−217	17.7	.9305	−23.1	59.9
3.0	14.11	−238	20.0	.9328	−25.4	71.5
3.5	14.30	−258	22.0	.9353	−27.6	85.0
4.0	14.48	−269	24.0	.9377	−28.8	97.1
4.3	14.59	−278	25.0	.9391	−29.8	104.6
4.5	14.66	−283	25.7	.9400	−30.4	110.0
4.7	14.73	−290	26.3	.9410	−31.2	115.2
5.0	14.84	−298	27.2	.9424	−32.1	124.4
5.5	15.02	−312	28.5	.9448	−33.7	137.2
6.0	15.20	−328	29.7	.9471	−35.5	152.3
6.5	15.37	−345	30.9	.9493	−37.4	166.0
7.0	15.53	−366	32.1	.9514	−39.8	179.8
8.0	15.80	−390	34.4	.9550	−42.5	200.4
9.0	16.03	−413	36.7	.9580	−45.2	219.7
10.0	16.24	−421	38.8	.9607	−46.2	237.5

Dwg. 7739A52

TABLE 24—DYNAMIC CHARACTERISTICS of S3 STRAIGHT SEAL FOR FORWARD WHIRL AND 30 PSIA DOWNSTREAM PRESSURE

$P_1 - P_3$ psi	f Hz	K_c Dial	$\dot{m}$ SCFM	$(X_p/X_d)^2$	E lb/in	K_s lb/in
0.02	13.05	− 10	0.37	.9190	− 1.0	+ 0.0
0.3	13.16	− 81	5.6	.9204	− 8.5	+ 7.4
0.5	13.24	− 83	8.8	.9214	− 8.7	+12.7
0.7	13.32	− 73	11.3	.9225	− 7.7	+18.0
0.85	13.39	−108	13.0	.9234	−11.4	22.8
1.0	13.45	− 153	14.6	.9242	−16.1	26.9
1.2	13.54	− 184	16.6	.9254	−19.4	33.1
1.5	13.67	− 213	19.5	.9271	−22.6	42.0
1.75	13.78	− 235	21.5	.9285	−24.9	49.6
2.0	13.89	− 263	23.5	.9300	−27.9	57.2
2.55	14.14	− 298	27.0	.9332	−31.8	73.8
3.0	14.34	− 320	29.3	.9359	−34.2	87.8
3.5	14.56	− 333	31.5	.9387	−35.7	103.2
4.0	14.78	− 353	33.5	.9416	−38.0	118.8
4.5	15.00	− 373	35.3	.9445	−40.2	135.5
5.0	15.20	− 388	37.2	.9471	−42.0	152.3
6.0	15.55	− 408	40.7	.9517	−44.3	180.8
7.0	15.80	− 433	44.0	.9550	−47.2	200.4

Dwg. 7739A53

TABLE 25—DYNAMIC CHARACTERISTICS OF S3 STRAIGHT SEAL FOR FORWARD WHIRL AND 45 PSIA DOWNSTREAM PRESSURE

$P_1 - P_3$ psi	f Hz	K_c Dial	$\dot{m}$ SCFM	$(X_p/X_d)^2$	E lb/in	K_s lb/in
0.09	13.05	− 7	1.9	.9190	− 0.7	+ 0.0
0.5	13.20	−105	9.3	.9209	−11.0	+10.0
0.75	13.31	−113	13.5	.9224	−11.9	+17.3
1.0	13.43	−152	17.0	.9239	−16.0	+25.5
1.25	13.55	−207	20.0	.9255	−21.9	33.9
1.5	13.67	−242	23.0	.9271	−25.6	42.0
2.0	13.91	−284	27.9	.9302	−30.2	58.5
2.5	14.15	−322	31.5	.9334	−34.3	74.5
3.0	14.38	−357	34.6	.9364	−38.2	90.0
3.5	14.59	−382	37.4	.9391	−41.0	104.6
4.0	14.78	−392	40.0	.9416	−42.2	118.8
5.0	15.09	−409	44.8	.9457	−44.2	142.4
5.8	15.30	−424	48.0	.9484	−45.9	160.0

Dwg. 7739A54

TABLE 26—DYNAMIC CHARACTERISTICS OF S3 STRAIGHT SEAL FOR FORWARD WHIRL AND 60 PSIA DOWNSTREAM PRESSURE

$P_1 - P_3$ psi	f Hz	K_c Dial	$\dot{m}$ SCFM	$(X_p/X_d)^2$	E lb/in	K_s lb/in
0.15	13.05	− 5	2.8	.9190	−0.5	+0.0
0.5	13.15	−113	9.3	.9203	−11.9	+6.8
0.75	13.26	−140	13.8	.9217	−14.7	+14.0
1.0	13.38	−150	18.0	.9233	−15.8	+22.0
1.25	13.50	−200	21.7	.9249	−21.1	30.3
1.4	13.58	−235	23.8	.9259	−24.8	35.9
1.5	13.63	−245	25.2	.9266	−25.9	39.3
1.8	13.78	−290	28.9	.9285	−30.8	49.6
2.0	13.88	−315	31.2	.9298	−33.4	56.4
2.5	14.11	−335	36.0	.9328	−35.7	71.2
3.0	14.34	−370	39.8	.9359	−39.5	87.4
3.5	14.55	−395	43.0	.9386	−42.3	102.6

TABLE 27—EFFECT OF PLATFORM STIFFNESS K_p ON THE WHIRL EXCITATION CONSTANT E OF THE S1 DIVERGING SEAL

Backward Whirl

P_3 psia	$P_1 - P_3$ psi	K_p lb/in	f Hz	K_c Dial	$(X_p/X_d)^2$	E lb/in
15	3	0	10.50	+465.6	.8856	+47.1
15	3	+171.3	12.61	507.6	.829	48.1
15	3	+342.6	14.42	552.9	.775	48.9
15	3	−171.3	7.75	418.9	.938	44.9
30	6	0	11.85	517.5	.9032	53.4
30	6	+171.3	13.85	560.5	.849	54.3
30	6	+342.6	15.55	608.0	.801	55.6
30	6	−171.3	9.50	488.3	.955	53.3
45	3	0	11.15	437.3	.8941	44.7
45	3	+171.3	13.25	473.6	.836	45.2
45	3	+342.6	15.00	505.7	.787	45.4
45	3	−171.3	8.60	423.7	.947	45.8

Forward Whirl

P_3 psia	$P_1 - P_3$ psi	K_p lb/in	f Hz	K_c Dial	$(X_p/X_d)^2$	E lb/in
15	3	0	12.85	−211.9	.9163	−22.2
15	3	+171.3	15.10	−190.9	.856	−18.7
15	3	+342.6	16.90	−172.7	.806	−15.9
15	3	−171.3	10.05	−228.6	.979	−25.6
30	6	0	14.30	−325.7	.9353	−34.8
30	6	+171.3	16.35	−331.6	.880	−33.3
30	6	+342.6	18.10	−333.0	.831	−31.6
30	6	−171.3	11.80	−316.7	.993	−35.9
45	3	0	13.72	−316.0	.9277	−33.5
45	3	+171.3	15.88	−320.2	.868	−31.7
45	3	+342.6	17.62	−300.8	.820	−28.2
45	3	−171.3	11.15	−316.9	.986	−35.7

Dwg. 7739A55

TABLE 28--EFFECT OF PLATFORM STIFFNESS K_p ON THE WHIRL EXCITATION CONSTANT E OF THE S2 CONVERGING SEAL DURING BACKWARD WHIRL

P_3 psia	$P_1 - P_3$ psi	K_p lb/in	f Hz	K_c Dial	$(X_p/X_d)^2$	E lb/in
15	1.5	0	11.95	−138	.9045	−14.3
15	1.5	+171.3	13.90	−180	.852	−17.5
15	1.5	+342.6	15.62	−207	.803	−19.0
15	1.5	−171.3	9.50	−115	.958	−12.6
15	3	0	12.90	−165	.9170	−17.3
15	3	+171.3	14.80	−212	.866	−21.0
15	3	+342.6	16.40	−260	.823	−24.4
15	3	−171.3	10.60	−141	.970	−15.6
30	6	0	14.20	−623	.9340	−66.5
30	6	+171.3	15.99	−736	.886	−74.5
30	6	+342.6	17.53	−831	.842	−79.9
30	6	−171.3	12.09	−509	.983	−57.1
45	3	0	12.70	−496	.9144	−51.8
45	3	+171.3	14.65	−616	.861	−60.6
45	3	+342.6	16.30	−722	.815	−67.2
45	3	−171.3	10.40	−395	.967	−43.6

Dwg. 7739A56

TABLE 29—EFFECT OF PLATFORM STIFFNESS K_p ON THE WHIRL EXCITATION CONSTANT E OF THE S2 CONVERGING SEAL DURING FORWARD WHIRL

P_3 psia	$P_1 - P_3$ psi	K_p lb/in	f Hz	K_c Dial	$(X_p/X_d)^2$	E lb/in
15	1.5	0	14.20	−180	.9340	−19.2
15	1.5	+171.3	16.20	−219	.880	−22.0
15	1.5	+342.6	17.95	−246	.830	−23.3
15	1.5	−171.3	11.70	−131	.990	−14.8
15	3	0	15.10	−279	.9458	−30.1
15	3	+171.3	17.00	−328	.894	−33.5
15	3	+342.6	18.65	−370	.848	−35.8
15	3	−171.3	12.80	−228	.990	−25.8
30	6	0	16.20	−528	.9602	−57.9
30	6	+171.3	18.10	−656	.908	−68.0
30	6	+342.6	19.60	−736	.865	−72.7
30	6	−171.3	14.10	−409	1.000	−46.7
45	3	0	14.85	−437	.9425	−47.0
45	3	+171.3	16.83	−557	.888	−56.5
45	3	+342.6	18.50	−653	.841	−62.7
45	3	−171.3	12.50	−304	.995	−34.5

Dwg. 7709A57

TABLE 30—EFFECT OF PLATFORM STIFFNESS K_p ON THE WHIRL EXCITATION CONSTANT E OF THE S3 STRAIGHT SEAL DURING BACKWARD WHIRL

P_3 psia	$P_1 - P_3$ psi	K_p lb/in	f Hz	K_c Dial	$(X_p/X_d)^2$	E lb/in
15	0.9	0	11.10	0	.8934	0
15	0.9	+342.6	14.95	− 20	.786	− 1.8
15	2	+342.6	15.40	+100	.791	+ 9.0
15	2	0	11.50	+107	.8986	+11.0
15	2	−171.3	9.00	+105	.953	+11.4
15	2	+171.3	13.60	+105	.841	+10.1
15	5	0	12.60	+110	.9131	+11.5
15	5	+342.6	16.25	+102	.812	+ 9.5
15	5	−171.3	10.30	+125	.965	+13.8
15	5	+171.3	14.50	+112	.861	+11.0
30	5	+342.6	16.50	+ 72	.816	+ 6.7
30	5	0	12.82	+107	.9159	+11.2
30	5	−171.3	10.50	+137	.968	+15.1
30	5	+171.3	14.80	+ 89	.863	+ 8.8
45	3	+342.6	15.75	+ 29	.800	+ 2.6
45	3	0	11.95	+ 69	.9045	+ 7.1
45	3	−171.3	9.55	+109	.957	+11.9
45	3	+171.3	13.95	+ 44	.850	+ 4.3

Dwg. 7739A58

TABLE 31—EFFECT OF PLATFORM STIFFNESS K_p ON THE WHIRL EXCITATION CONSTANT E OF THE S3 STRAIGHT SEAL DURING FORWARD WHIRL

P_3 psia	$P_1 - P_3$ psi	K_p lb/in	f Hz	K_c Dial	$(X_p/X_d)^2$	E lb/in
15	0.9	0	13.40	− 73	.9235	− 7.7
15	0.9	+342.6	17.28	− 88	.816	− 8.2
15	2	+342.6	17.70	−231	.821	−21.7
15	2	0	13.75	−193	.9281	−20.5
15	2	−171.3	11.25	−173	.986	−19.5
15	2	+171.3	15.85	−223	.873	−22.2
15	5	0	14.84	−298	.9424	−32.1
15	5	+342.6	18.60	−338	.839	−32.4
15	5	−171.3	12.52	−278	.995	−31.6
15	5	+171.3	16.80	−323	.890	−32.8
30	5	0	15.18	−388	.9469	−42.0
30	5	+342.6	18.88	−463	.845	−44.7
30	5	−171.3	12.80	−343	.998	−39.1
30	5	+171.3	17.10	−430	.894	−43.9
45	3	0	14.38	−357	.9364	−38.2
45	3	+342.6	18.20	−412	.830	−39.1
45	3	−171.3	11.95	−317	.990	−35.8
45	3	+171.3	16.35	−397	.882	−40.0

Dwg. 7739A53

TABLE 32--EXCITATION CONSTANT AND SEAL STIFFNESS CORRESPONDING TO MEASURED PRESSURES IN SEAL ANNULUS. α = ANGLE BY WHICH $P_{21}-P_{22}$ LEADS Y DISPLACEMENT. SEE FIGS. 14 AND 15. R = 4 IN. and a = .5086 IN.

Seal	Whirl Dir.	Whirl Mils. S. P.	P_3 psia	P_1-P_3 psi	$P_{21}-P_{22}$ mpsi	α Deg	E lb/in	K_s lb/in
S1	B	.797	15	3	18.5	10	60.8	−42.6
S1	F	.783	15	3	9	15	−18.4	−31.8
S1	B	.789	30	6	20	29	77.9	−22.3
S1	F	.776	30	6	11	−40	−45.2	− 4.0
S1	B	.796	15	1.5	11	52	43.8	5.4
S1	F	.783	15	1.5	5	225	0	20.4
S2	F	.771	15	3	12	−87	−37.0	33.3
S3	B	.791	15	2	6.3	109	11.2	22.9
S3	F	.778	15	2	7.6	−112	-12.2	28.7
S3	B	.784	30	5	15	136	−1.1	61.2
S3	F	.771	30	5	15	−91	−43.2	44.7

Dwg. 7739A60

TABLE 33—EFFECT OF STATIC OFFSET ON SINUSOIDAL PRESSURES IN S1 DIVERGING SEAL ANNULUS FOR 15 PSIA DOWNSTREAM PRESSURE AND 3 PSI PRESSURE DROP DURING BACKWARD AND FORWARD WHIRL.
α = ANGLE BY WHICH $P_{21}-P_{22}$, P_{21}, or $-P_{22}$ LEADS Y DISPLACEMENT.

SEE FIGS. 14 AND 15

e Mils	θ Deg.	P_{21} mpsi	α_{P21} Deg.	$-P_{22}$ mpsi	α_{-P22} Deg.	$P_{21}-P_{22}$ mpsi	$\alpha_{P21-P22}$ Deg.
		Backward Whirl, .797 Mils Single Peak					
0	—	11	−33	13	47	18.5	10
.72	33.7	4	57	16	5	18	10
.68	−49.1	16.5	− 3	5	65	17	7
.58	219.4	14	−35	13.5	57	17.5	7
.46	139.3	10	−63	17	42	18.5	7
		Forward Whirl, .783 Mils Single Peak					
0	—	9	50	6	−60	9	15
.72	33.7	6	90	9	0	9.5	25
.68	−49.1	13	5	5	175	8.5	5
.58	219.4	11	45	8	−85	9	5
.46	139.3	9	75	10	−40	9	5

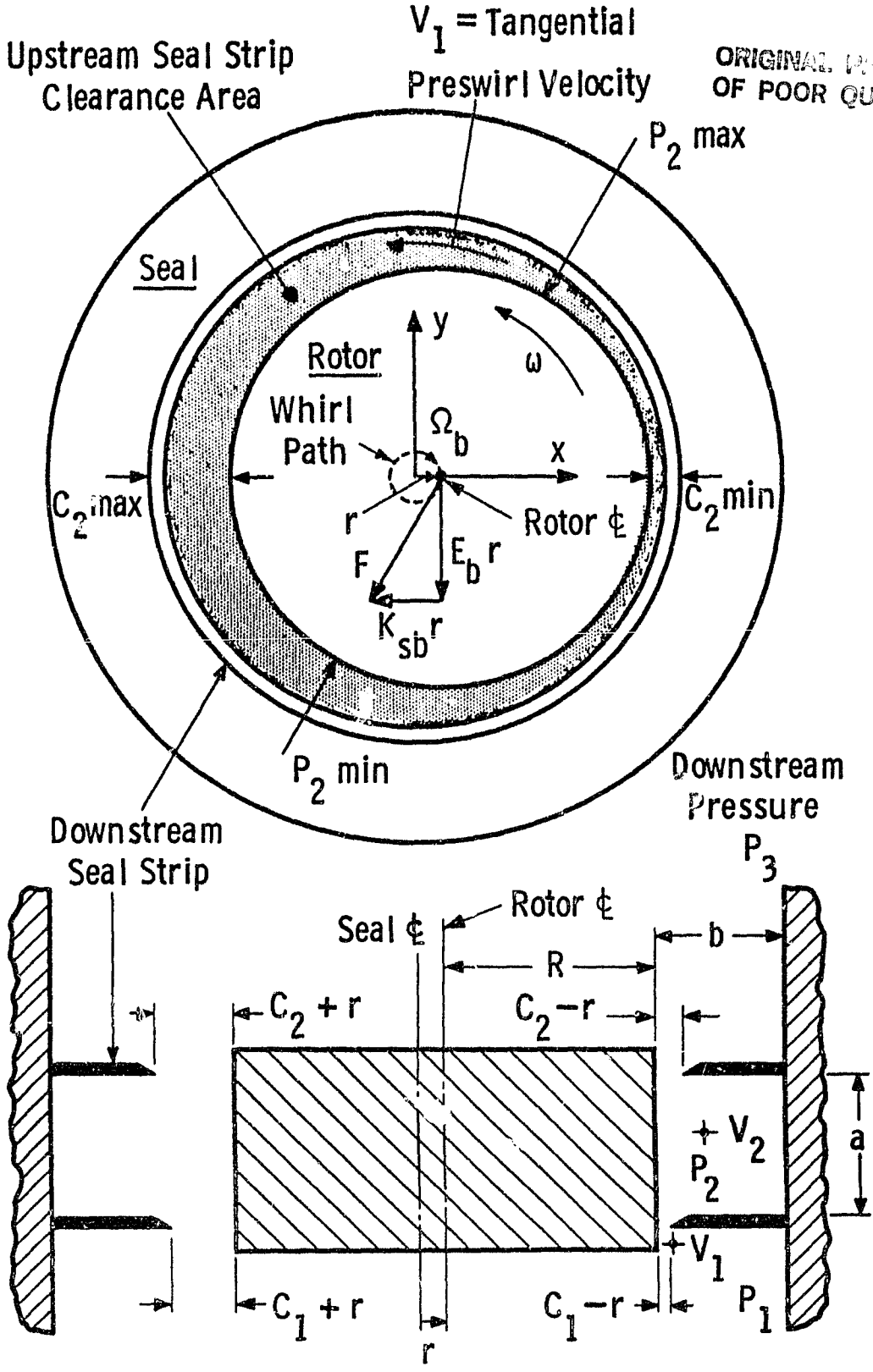

Fig. 1 — Diverging-seal forces on a backward whirling rotor

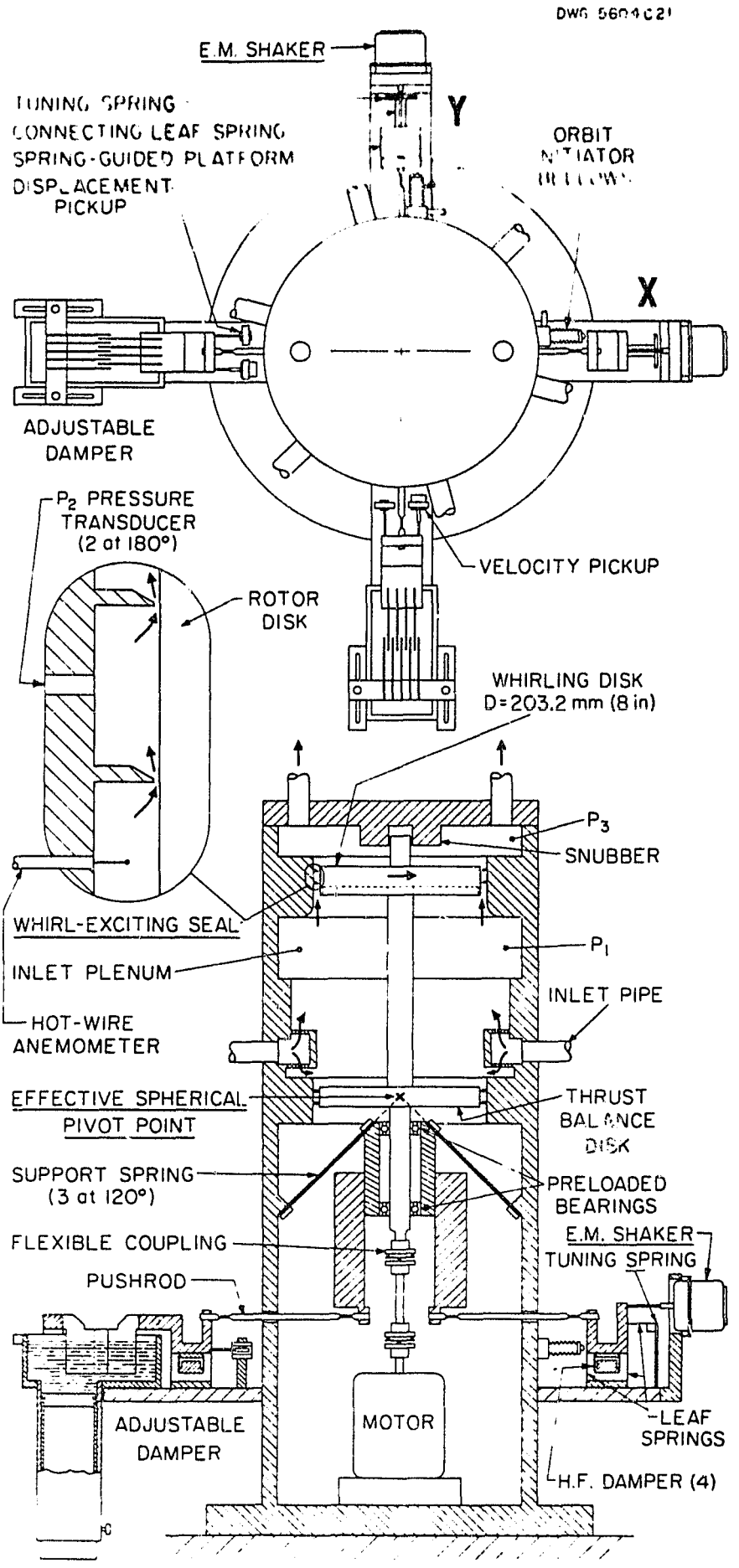

FIG. 2 –SEAL-EXCITED ROTOR WHIRL MODEL

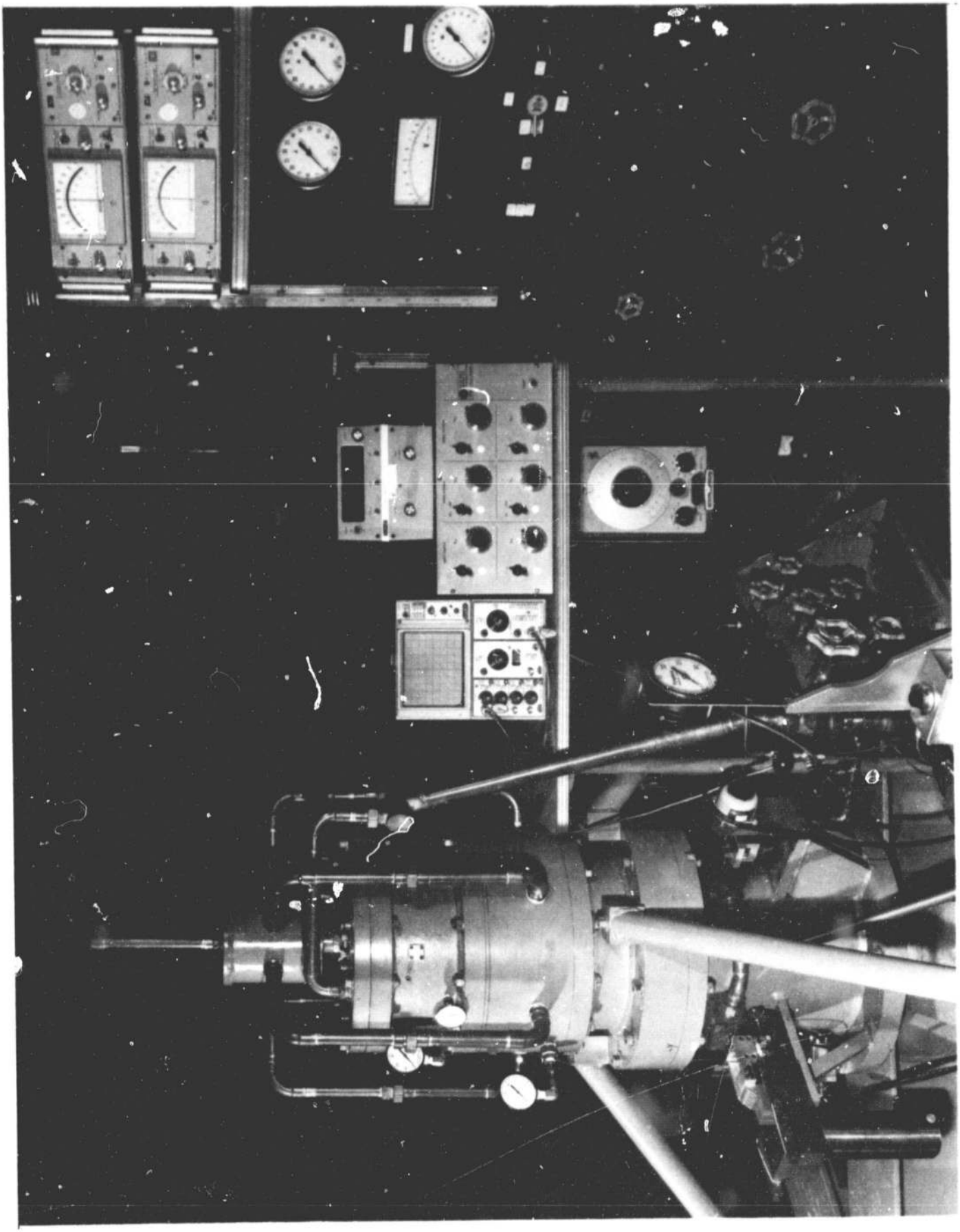

Fig. 3—Seal-excited rotor whirl test rig

Fig. 4—Shaker and spring-guided platform of seal whirl rig

Radial Clearances, mm (mils)			
Seal	C_1	C_2	C_s
S1	.1311 (5.16)	.1963 (7.73)	
S2	.1915 (7.54)	.1272 (5.01)	
S3	.1585 (6.24)	.1585 (6.24)	
Snubber			.0660 (2.60)

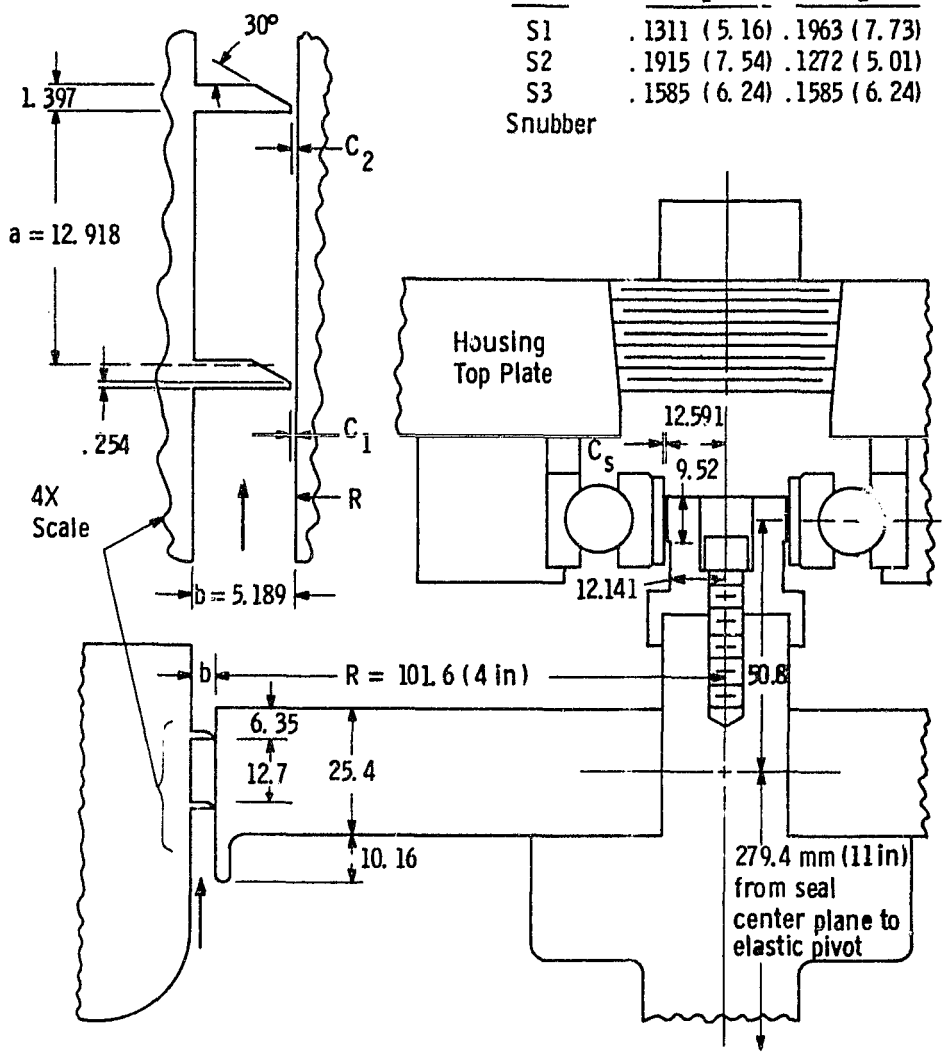

Fig. 5 — Seal, disk, and snubber dimensions

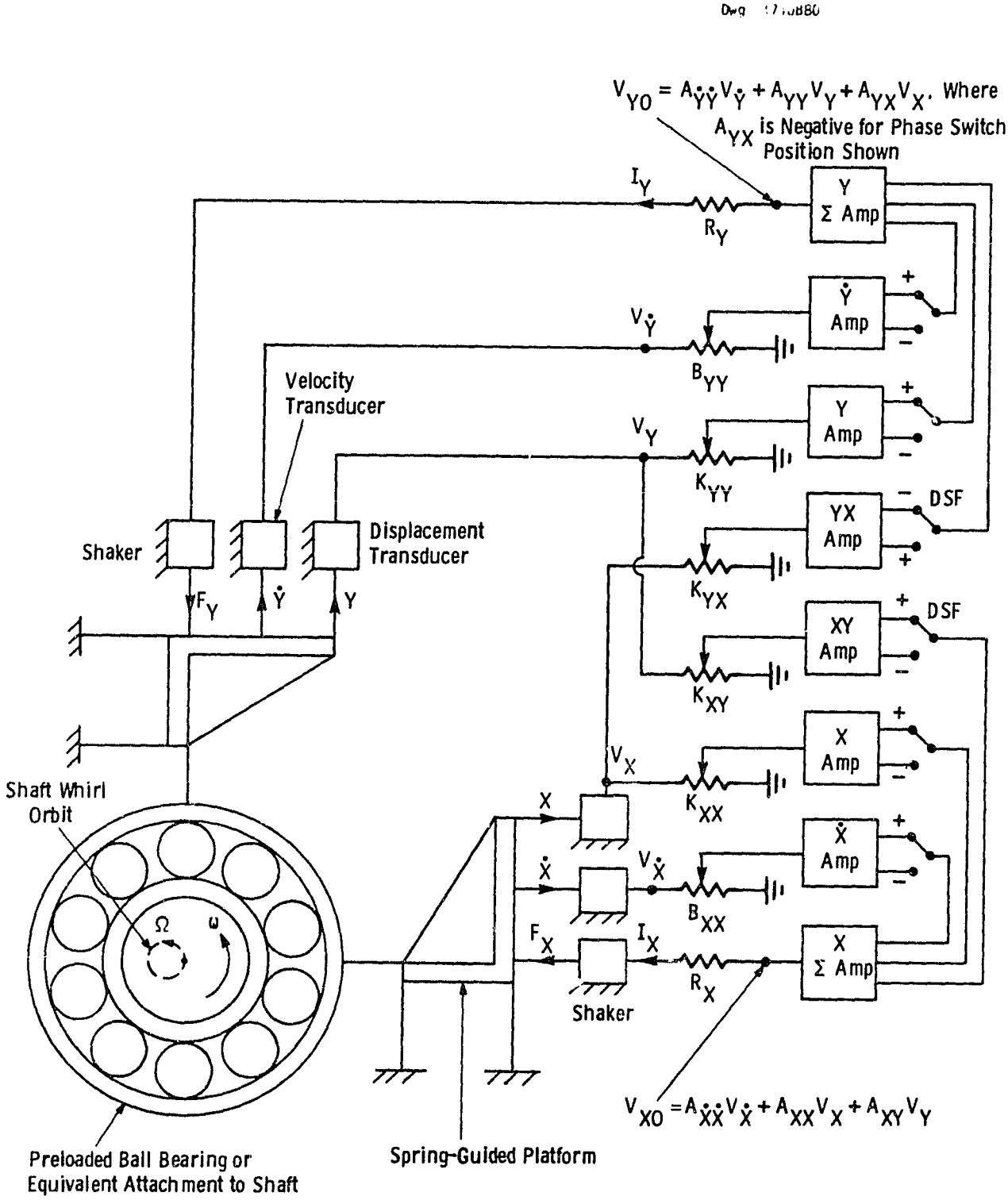

Fig. 6 – Schematic of active rotor whirl damping and stiffness system

Dwg. 2625C08

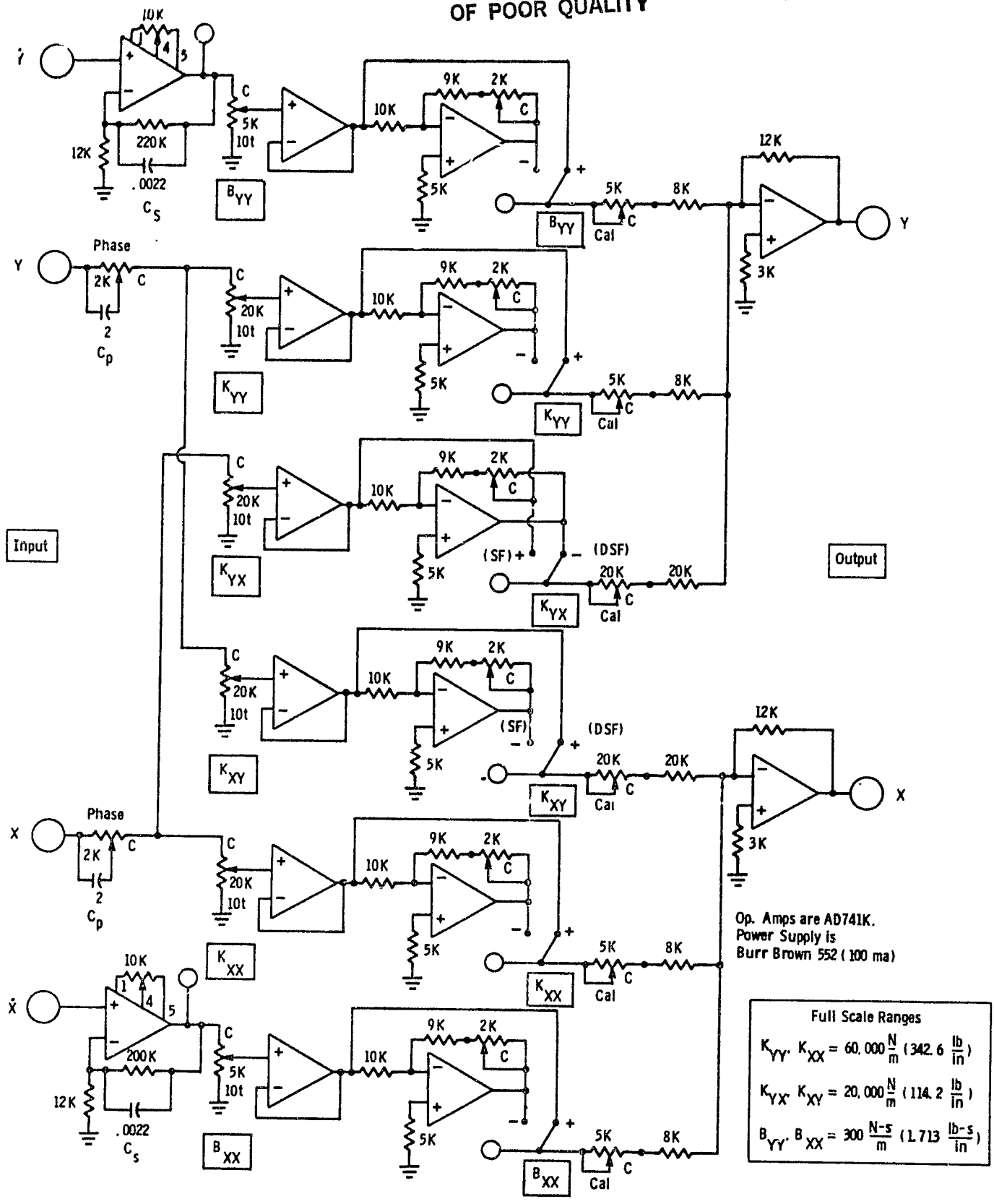

FIG. 7 – CONTROL UNIT OF ACTIVE WHIRL DAMPING AND STIFFNESS SYSTEM, GAINS ARE:
K_{YY} = 1.0116, K_{XX} = 1.0093, K_{YX} = .3372, K_{XY} = .3364, B_{YY} = 23.32, B_{XX} = 22.22

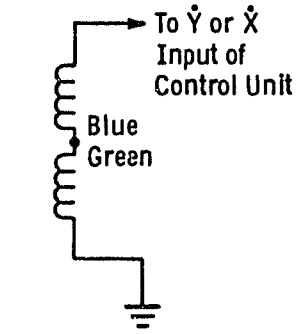

Velocity Transducer
Schaevitz 050 VTA
$\dot{Y}$ = .3995 Volt-sec/in
$\dot{X}$ = .4542 Volt-sec/in
11.2 KΩ, 1.6 h
+ Volts for + $\dot{Y}$ or + $\dot{X}$

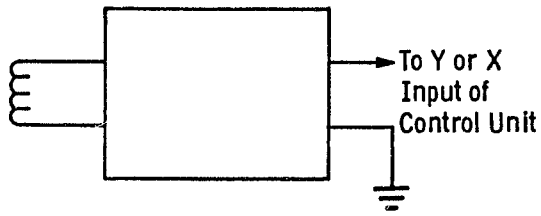

LVDT
Schaevitz
025 M-HR

Daytronic 3000 Transducer Indicator
With Type 71 LVDT Module and
Type V Output Module, ± 5 mils F. S.,
2 Volts/mil, + Volts for + Y or + X

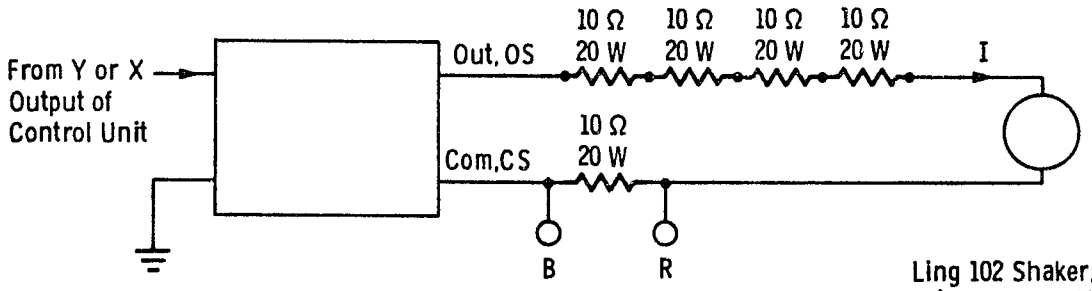

HP 6824 A
DC Amplifier ± 50 V, 1 Amp
Connect A3, A4, & A5 Together
180 deg Phase Shift
Voltage Gain Y = 10.15, X = 10.27

Total Load Ohms
Y = 51.8, X = 52.2

Ling 102 Shaker, 2.5 Ω
lb/amp Y = .8642, X = .8627
+ I Causes Force in
− Y or − X Direction
(prods retract)

Fig. 8 — Input and output units for each channel of active whirl damping and stiffness system

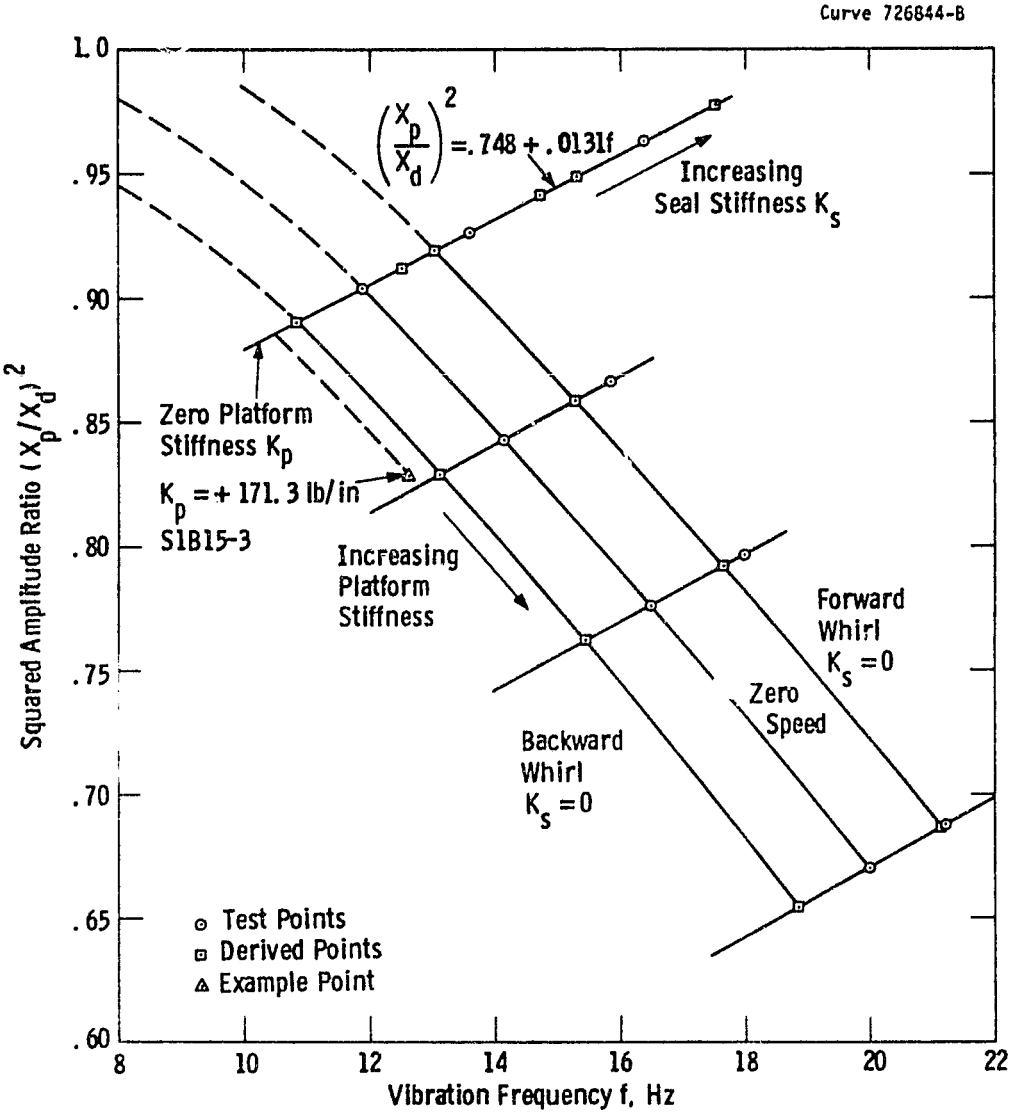

Fig. 9—Squared ratio of platform motion to disk motion at resonance. Also ratio of seal cross stiffness to platform cross stiffness. See table 1

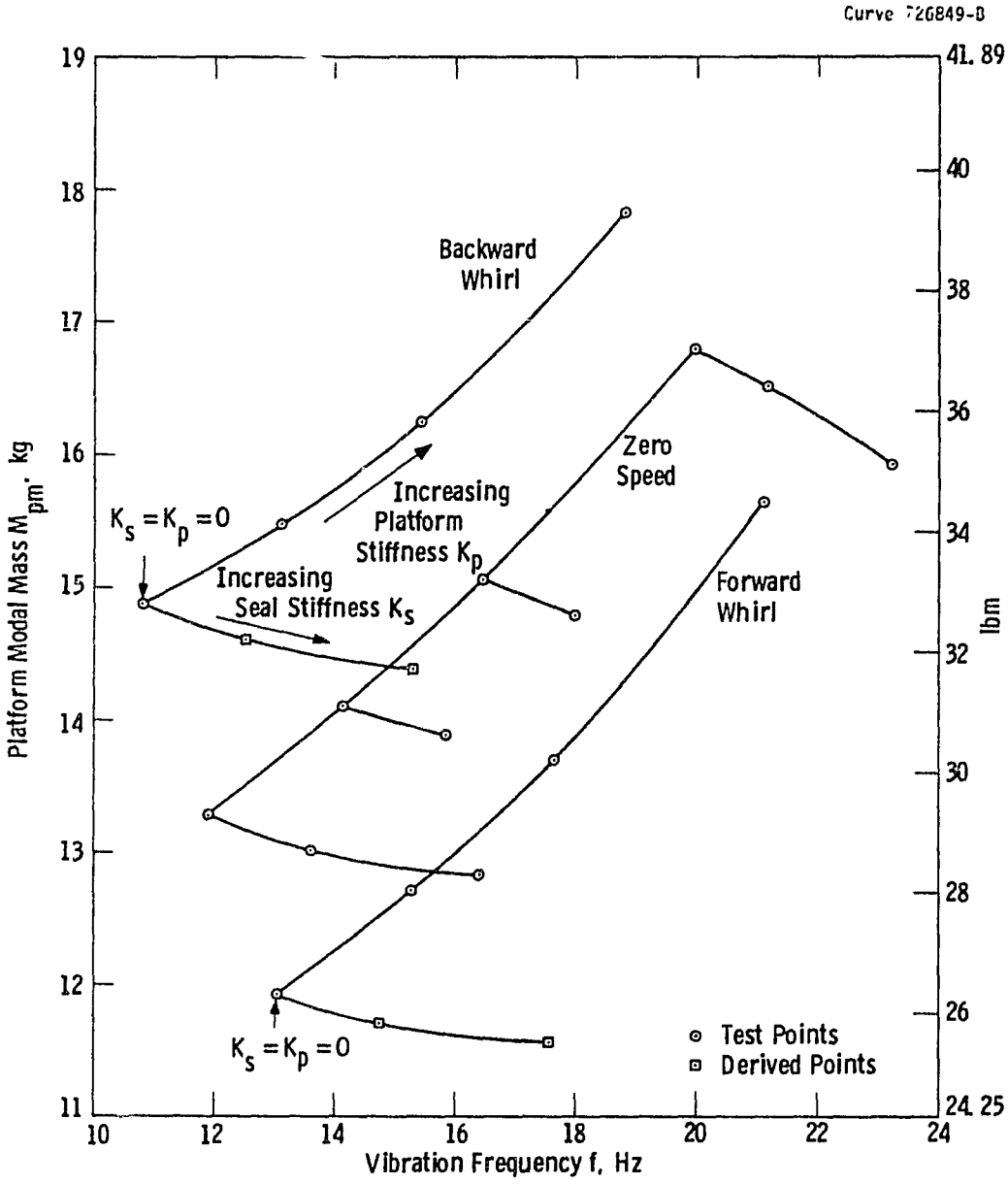

Fig. 10—Platform modal mass. See table 1

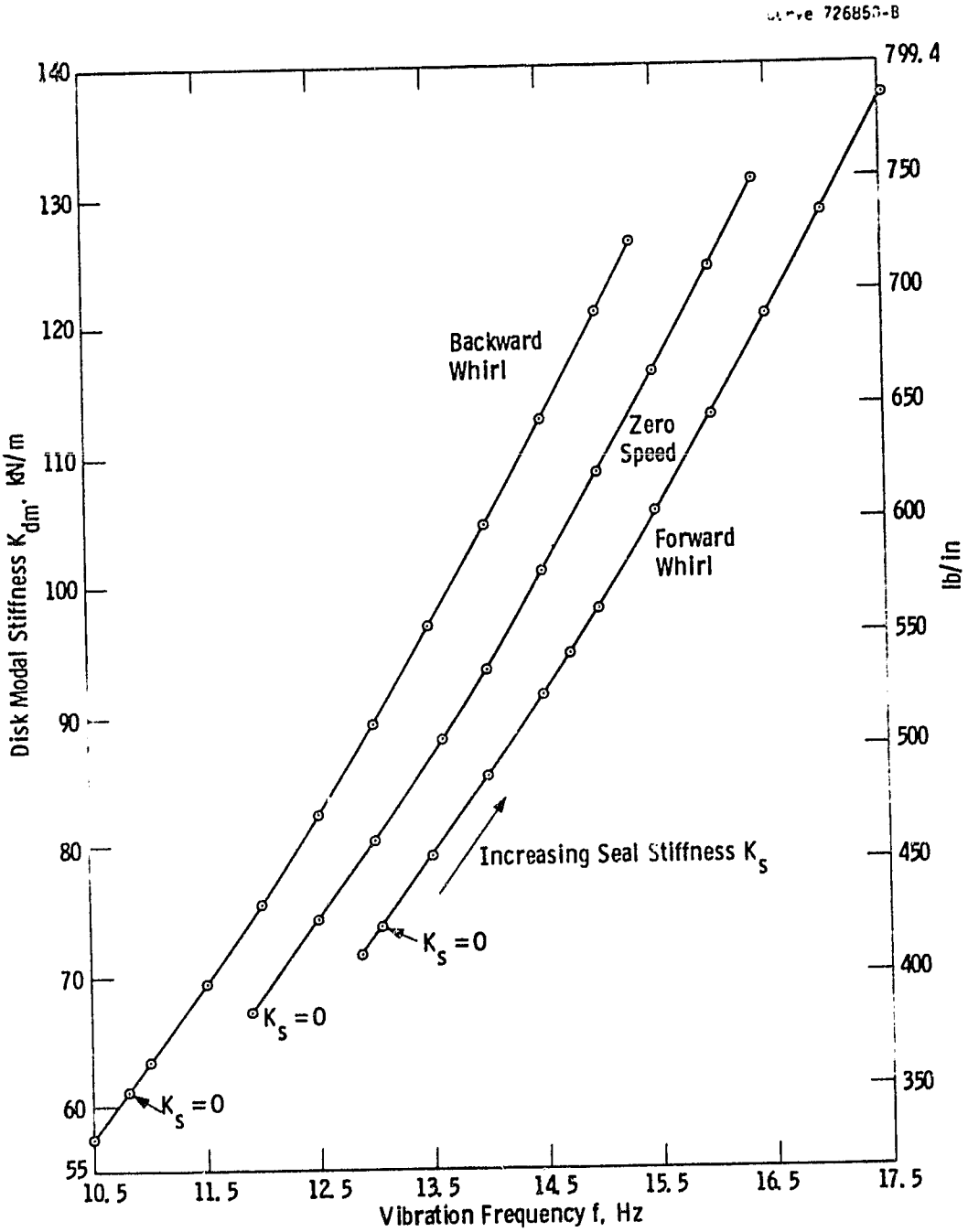

Fig. 11—Disk modal stiffness for varying seal stiffness and zero platform stiffness

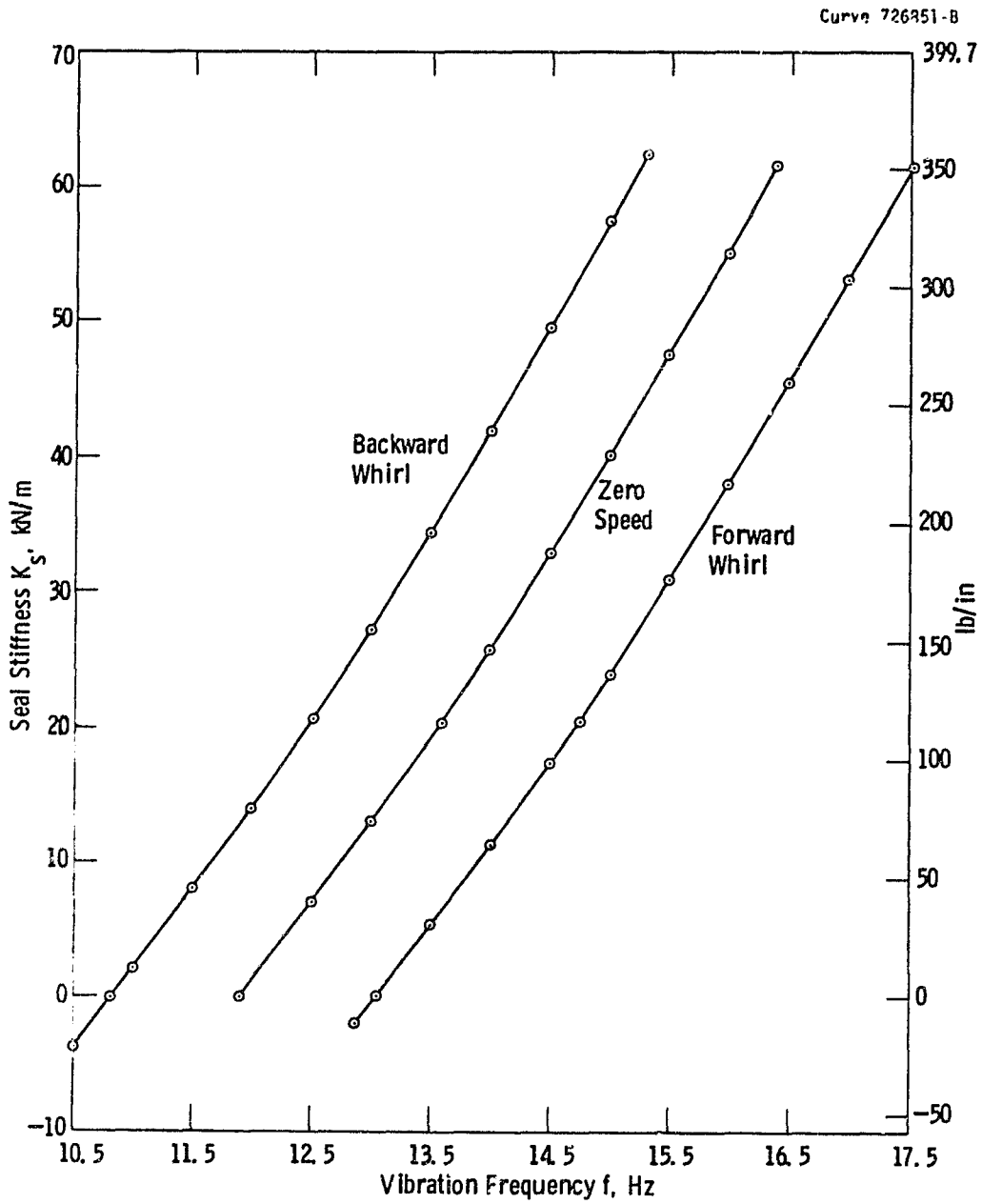

Fig. 12—Effect of seal stiffness on vibration frequency for zero platform stiffness. See table 2

Dwg.7739A62

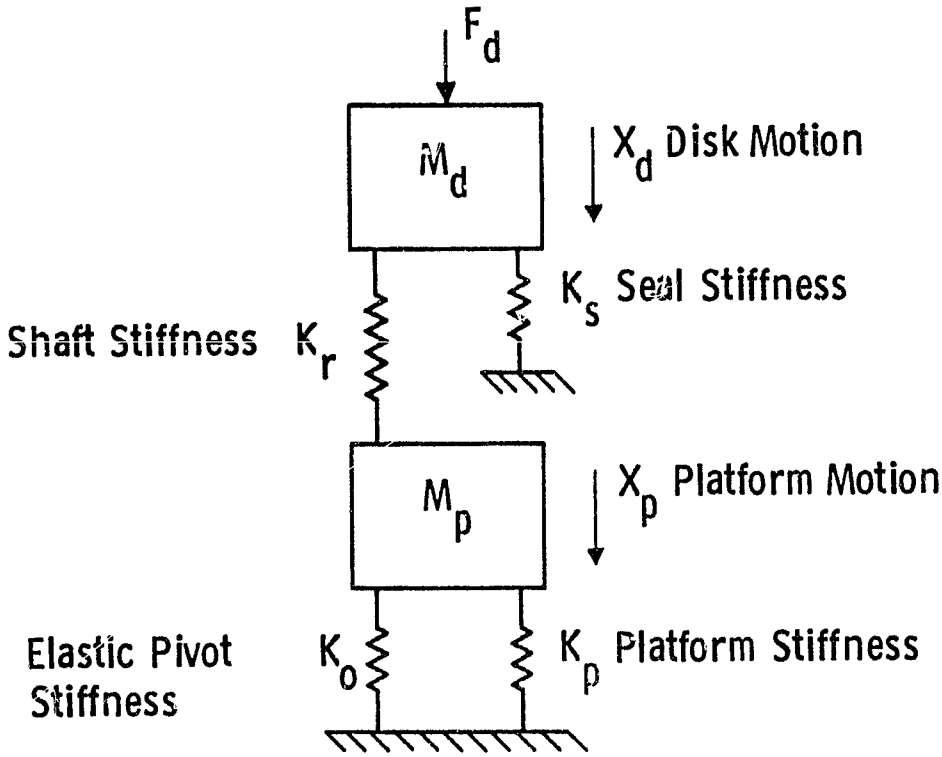

Fig. 13—Mass-spring representation of seal whirl test rig

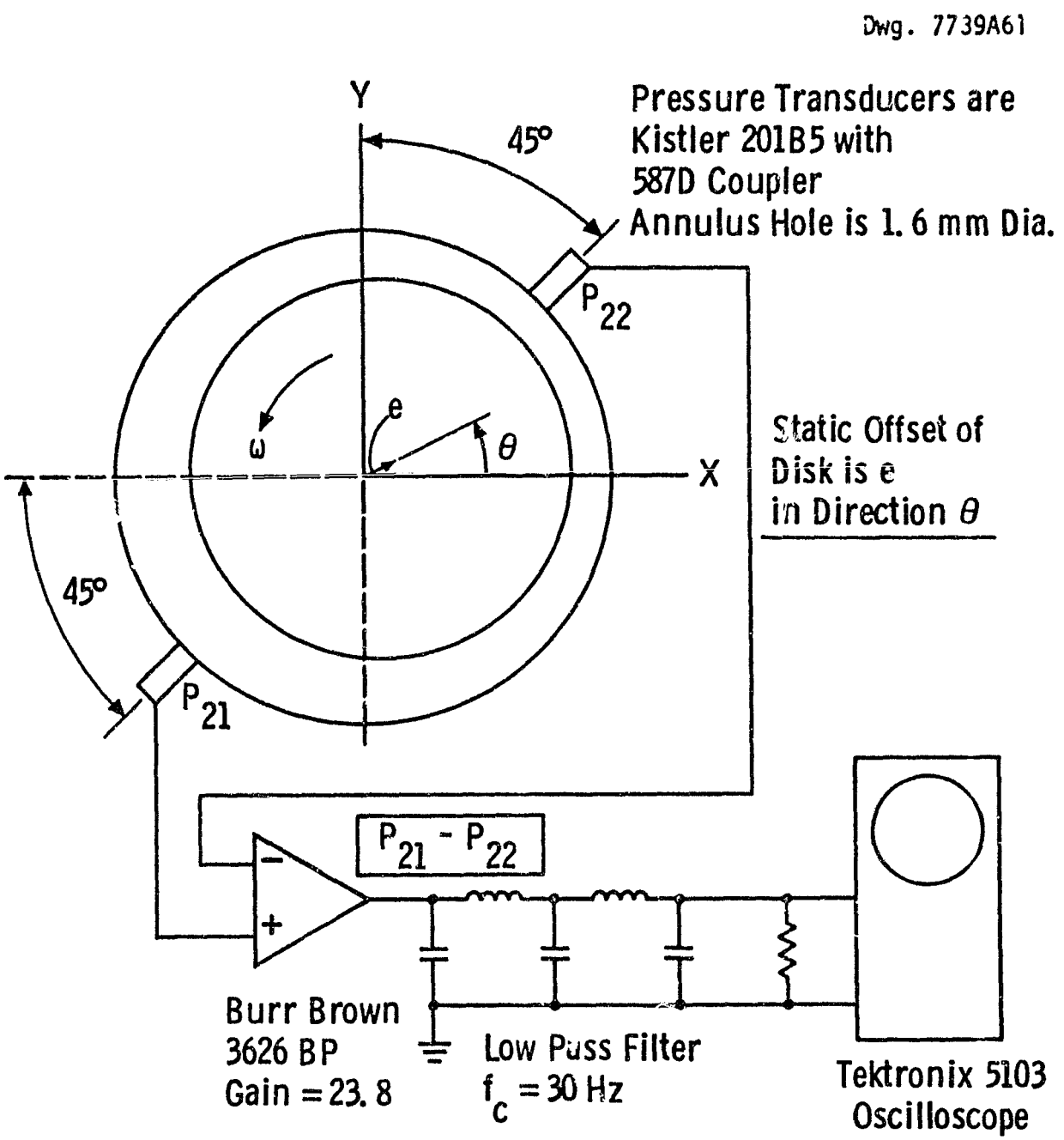

Fig. 14—Seal annulus pressure gage instrumentation

Dwg. 7739A63

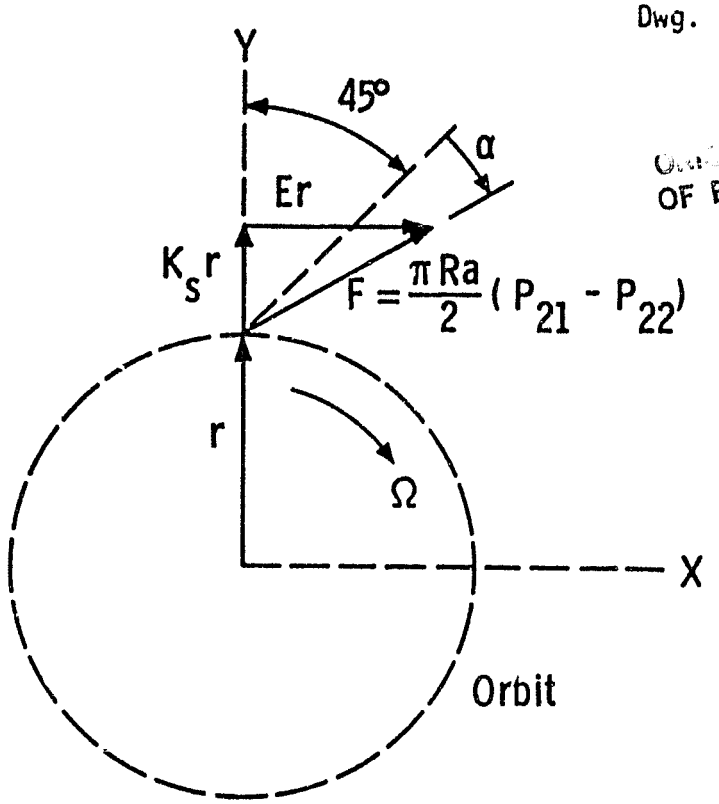

(a) Backward Whirl (E Positive and K_s Negative for α Shown)

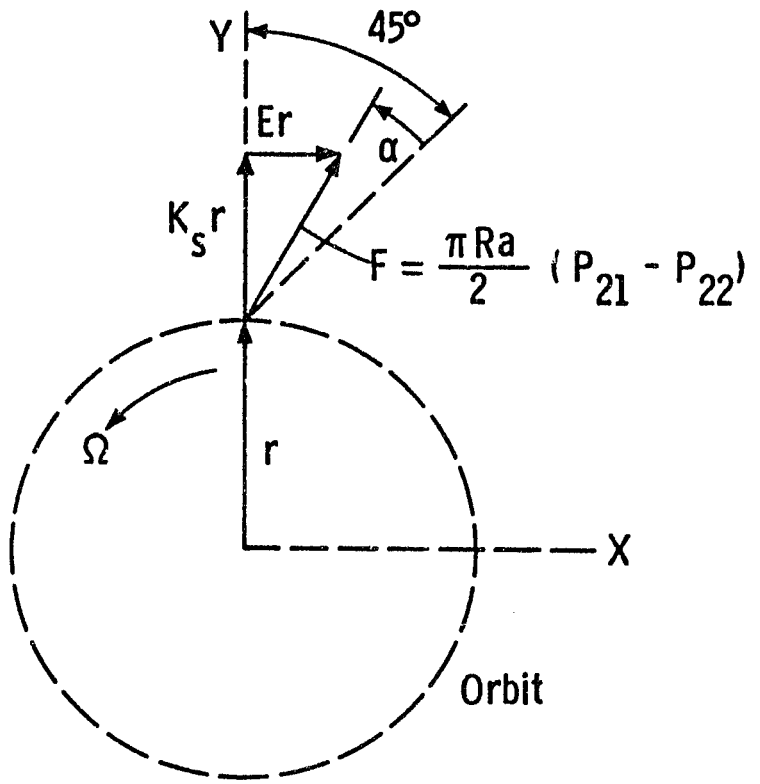

(b) Forward Whirl (E Negative and K_s Negative for α shown)

Fig. 15—Net annulus pressure forces on rotor

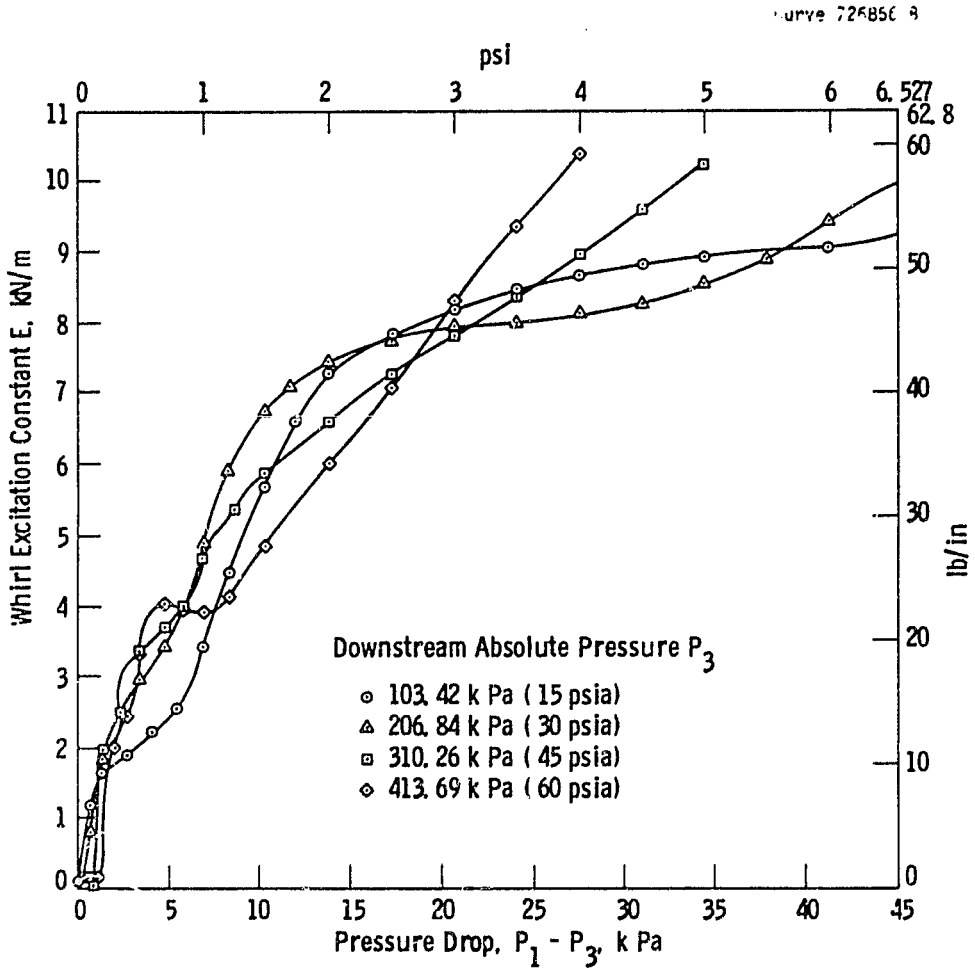

Fig. 16—Whirl excitation constant of S1 diverging seal during backward whirl

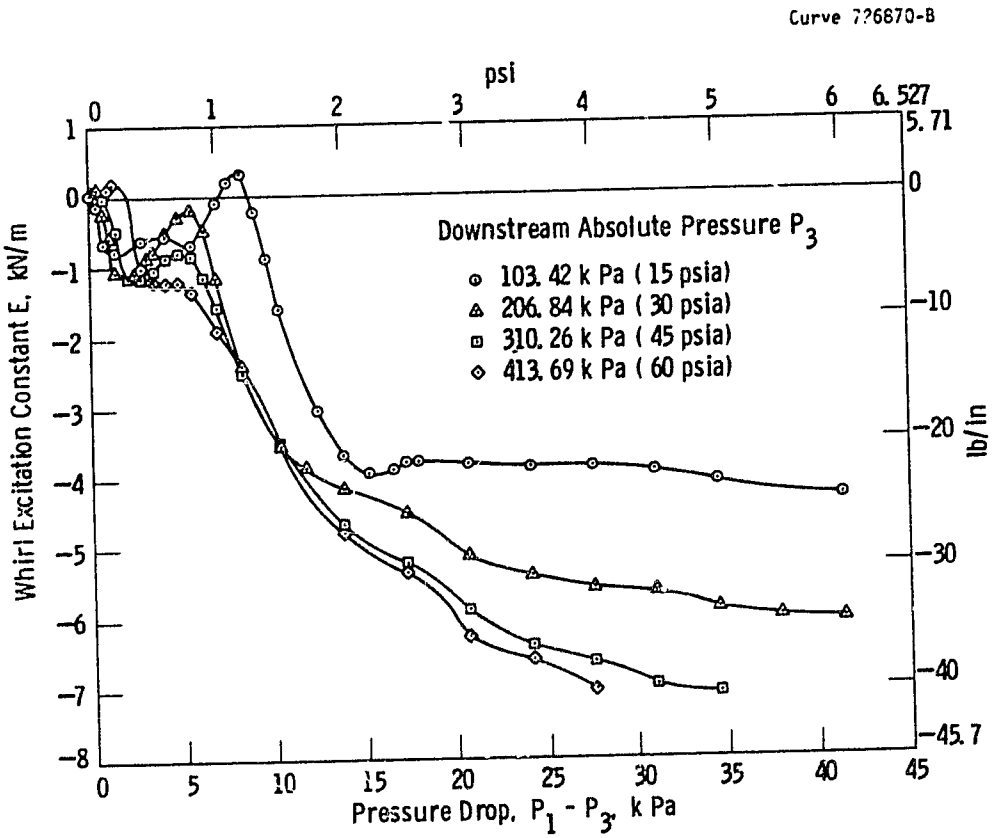

Fig. 17—Whirl excitation constant of S1 diverging seal during forward whirl

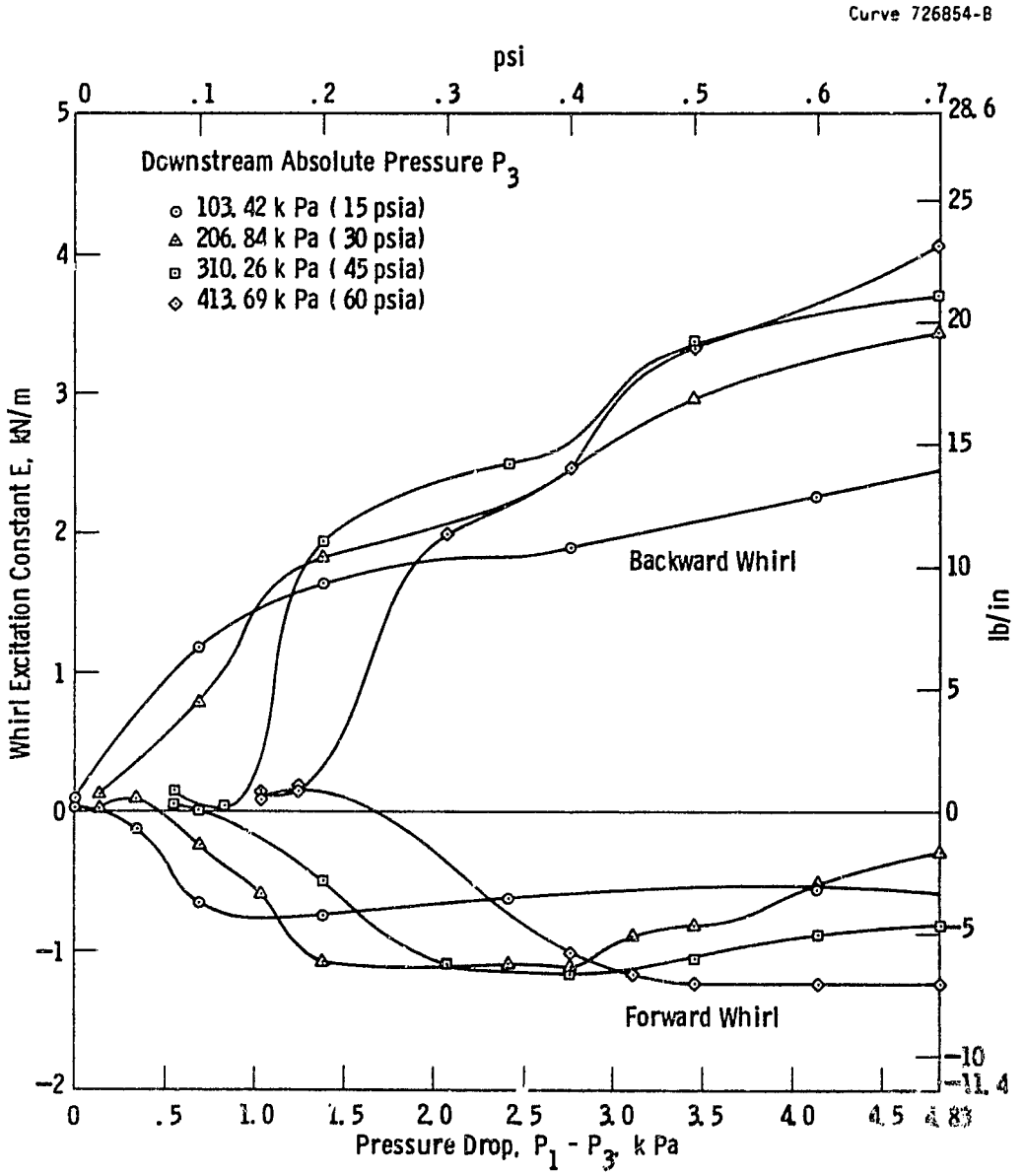

Fig. 18—Whirl excitation constant of S1 diverging seal at low pressure drops

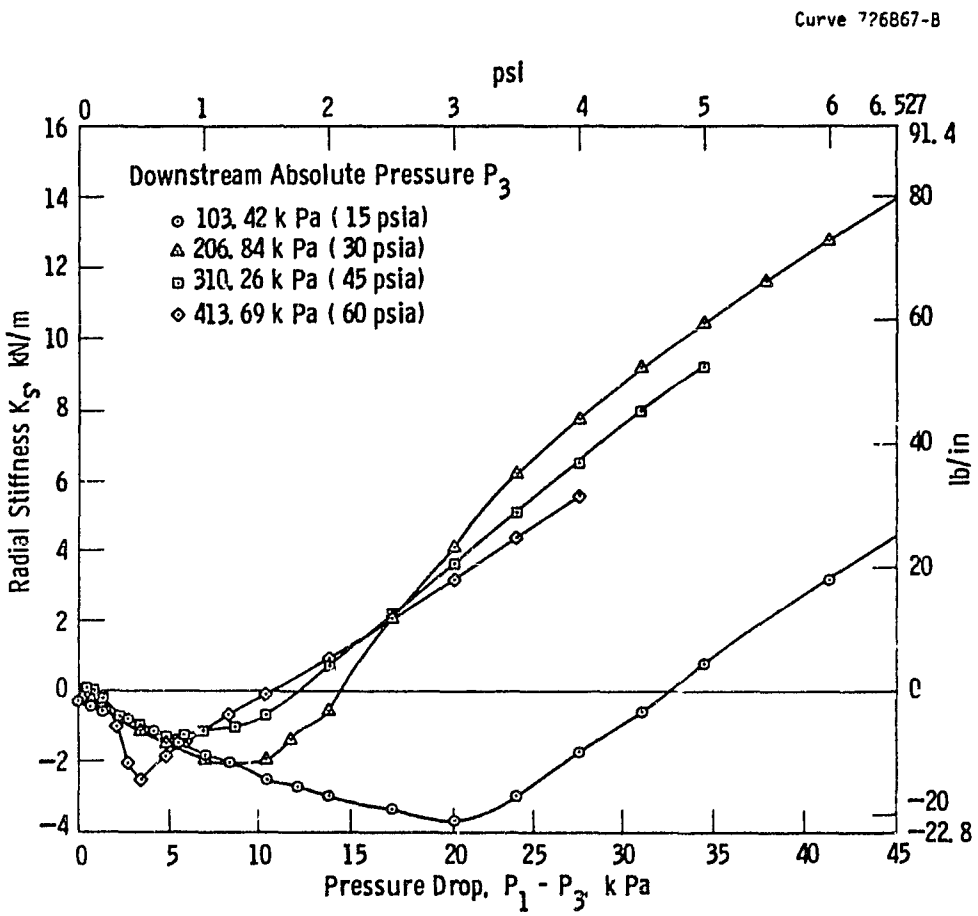

Fig. 19—Radial stiffness of S1 diverging seal during backward whirl

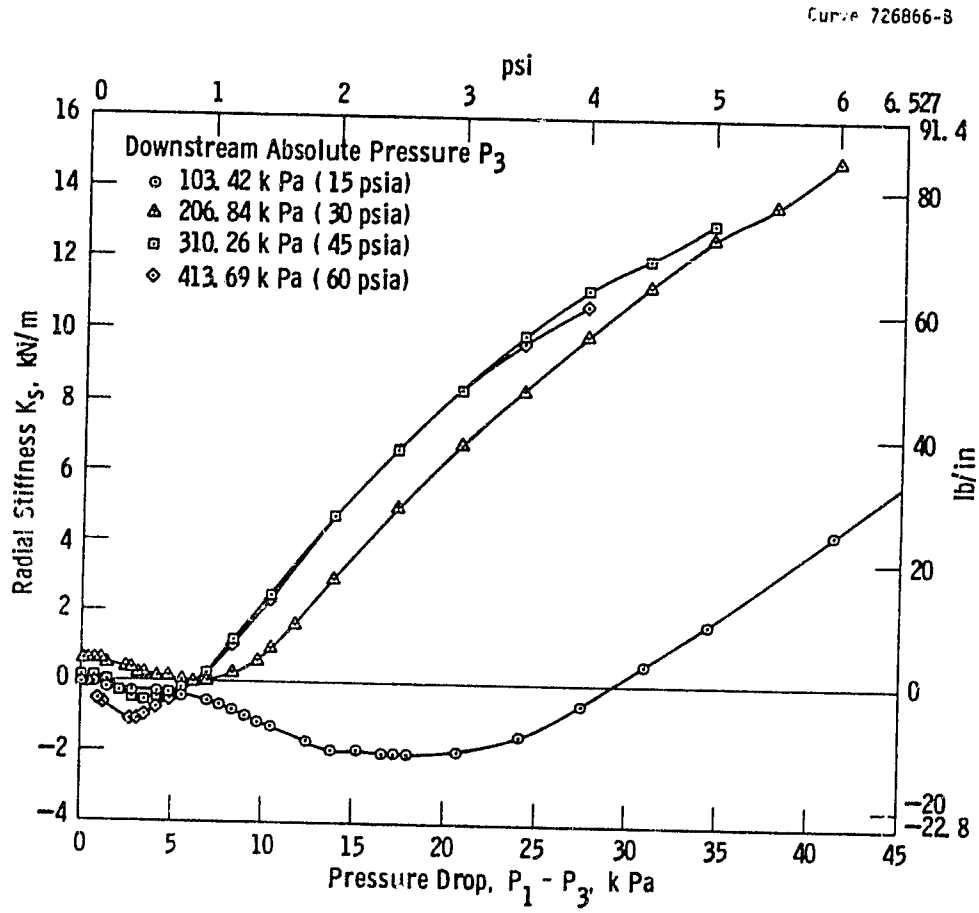

Fig. 20—Radial stiffness of S1 diverging seal during forward whirl

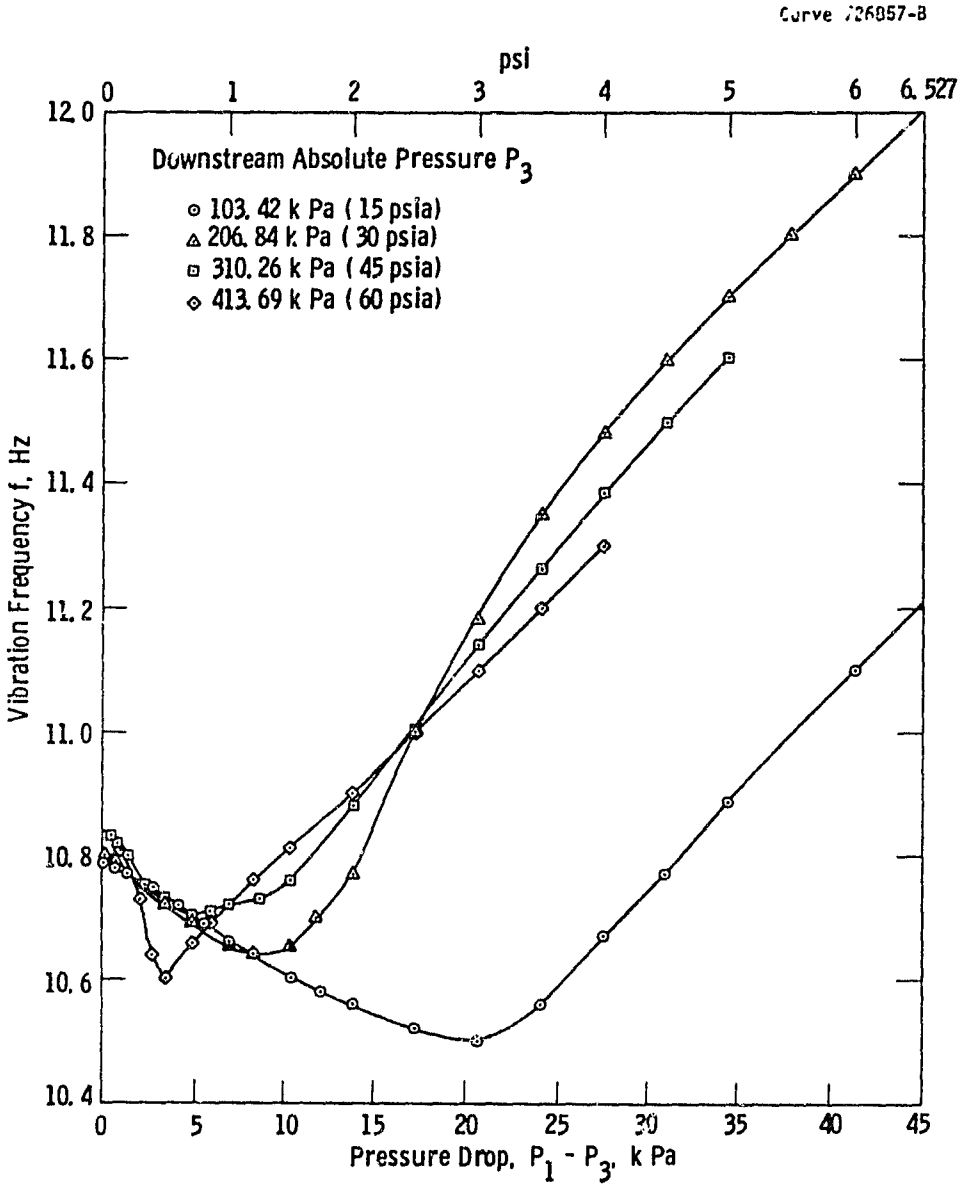

Fig. 21—Vibration frequency of S1 diverging seal during backward whirl

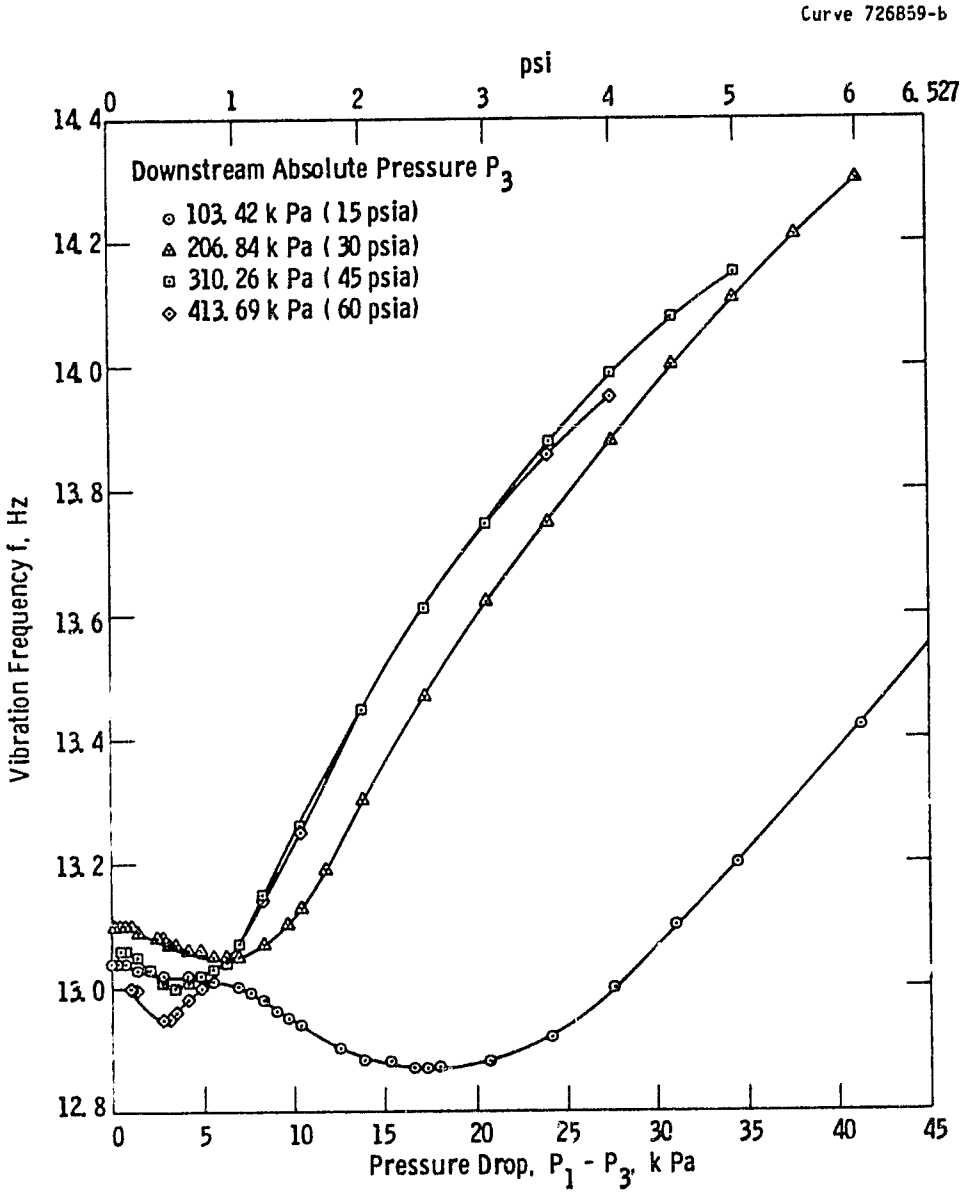

Fig. 22—Vibration frequency of S1 diverging seal during forward whirl

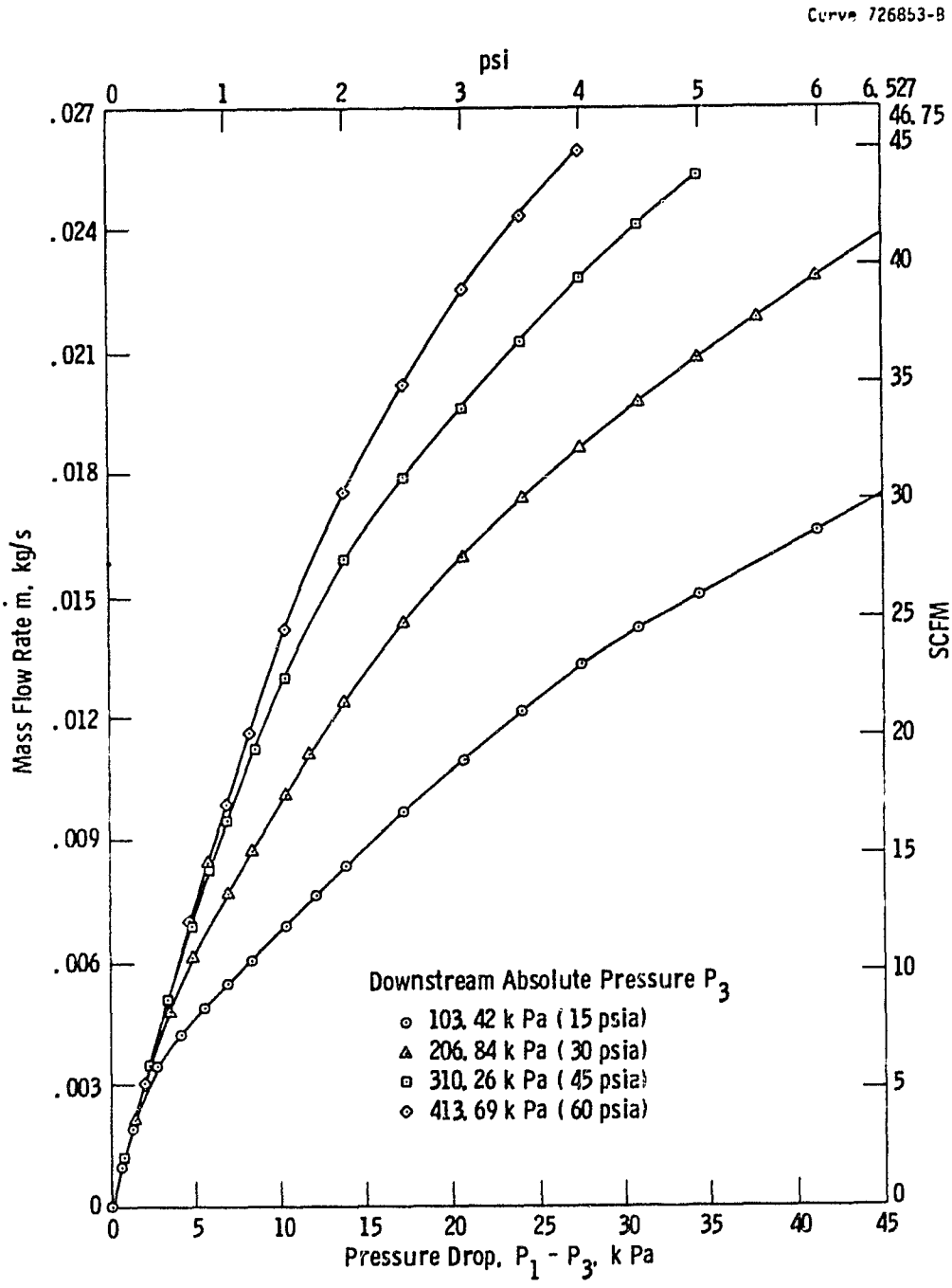

Fig. 23—Mass flow rate of S1 diverging seal

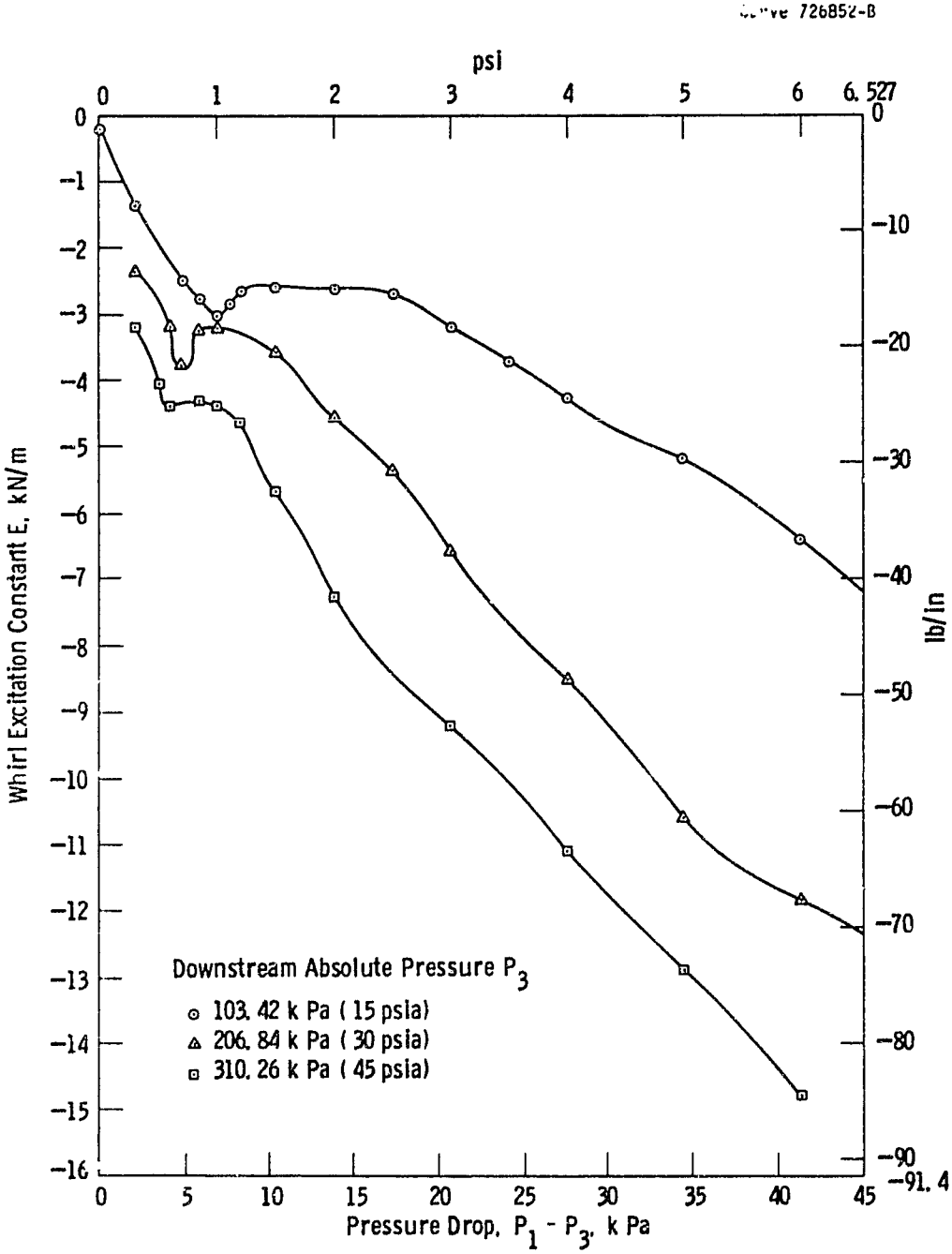

Fig. 24—Whirl excitation constant of S2 converging seal during backward whirl

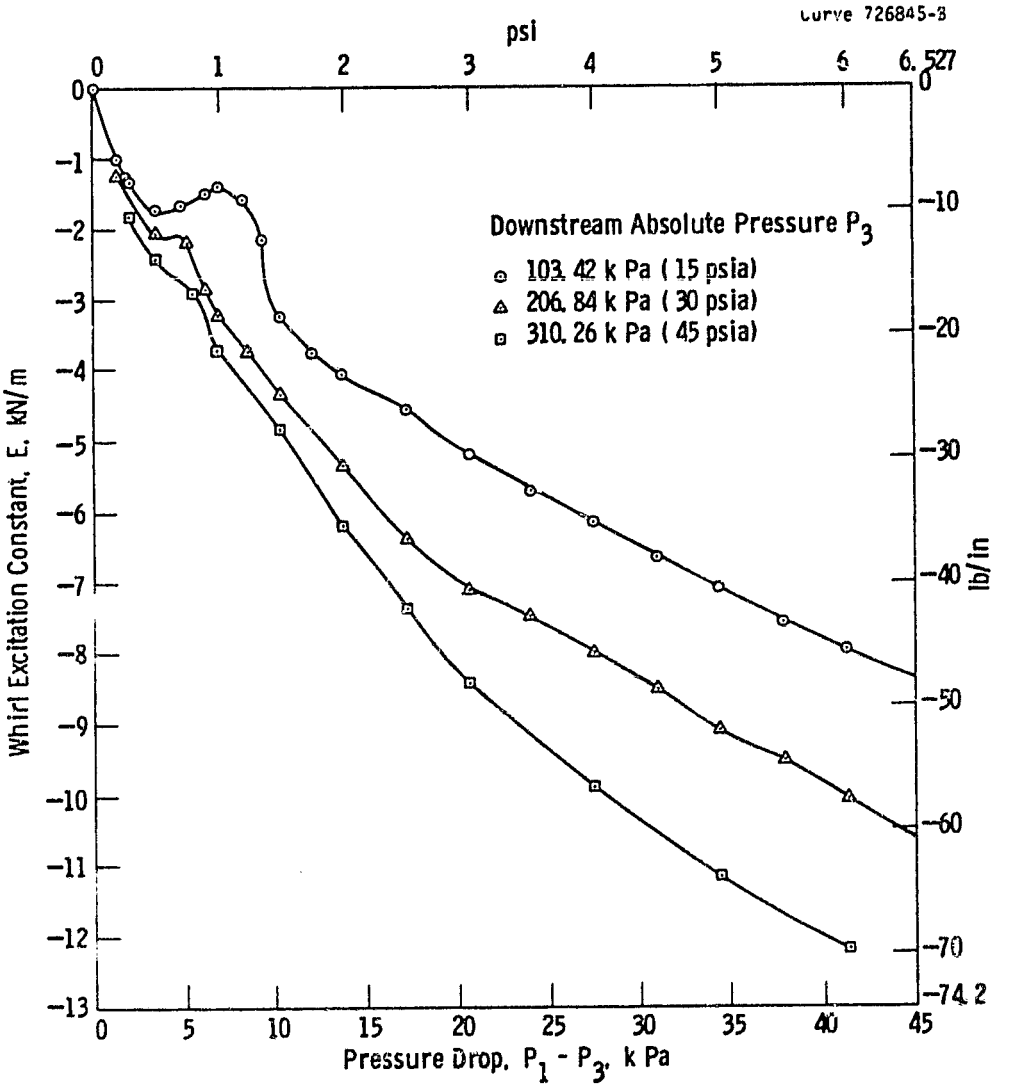

Fig. 25--Whirl excitation constant of S2 converging seal during forward whirl

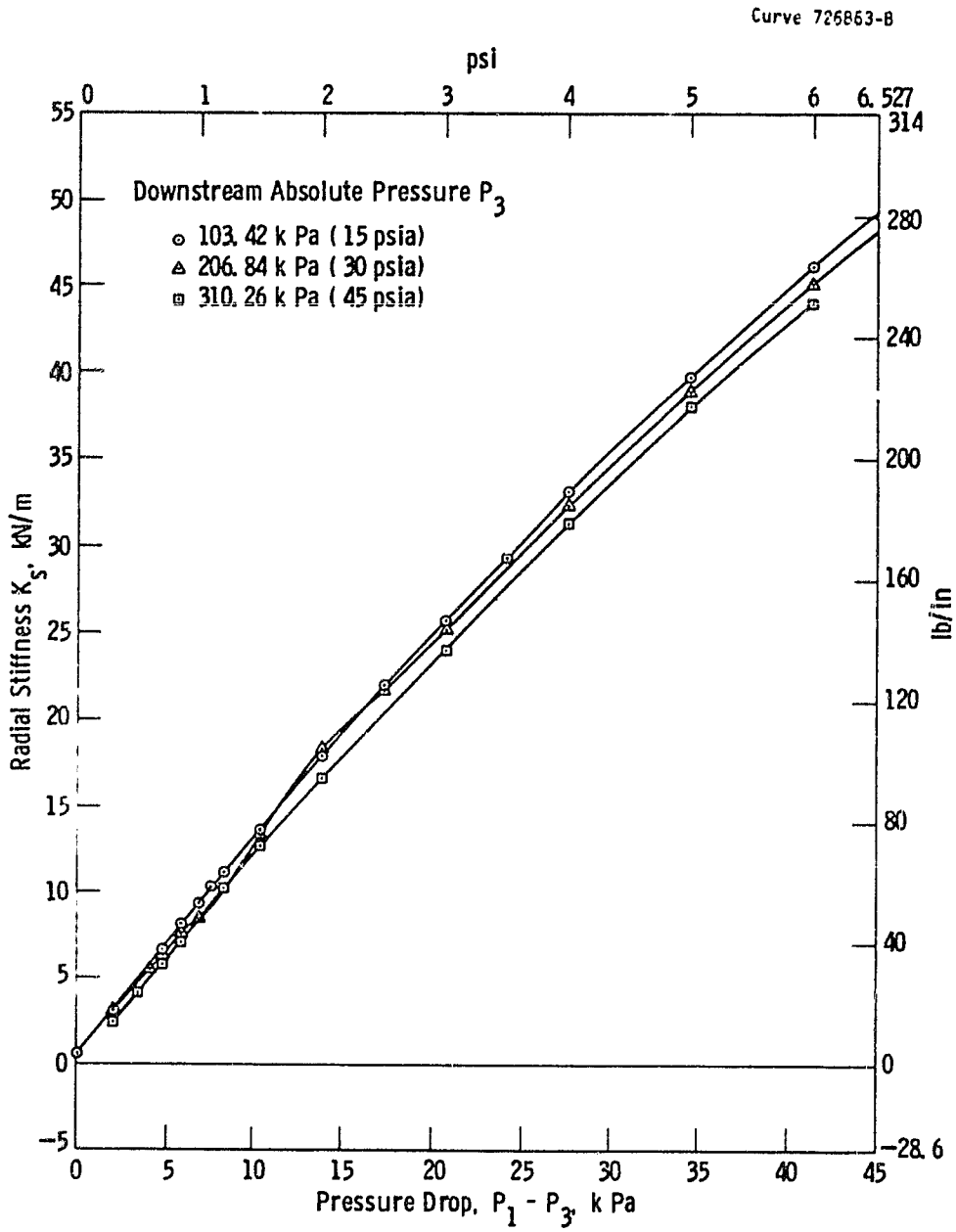

Fig. 26—Radial stiffness of S2 converging seal during backward whirl

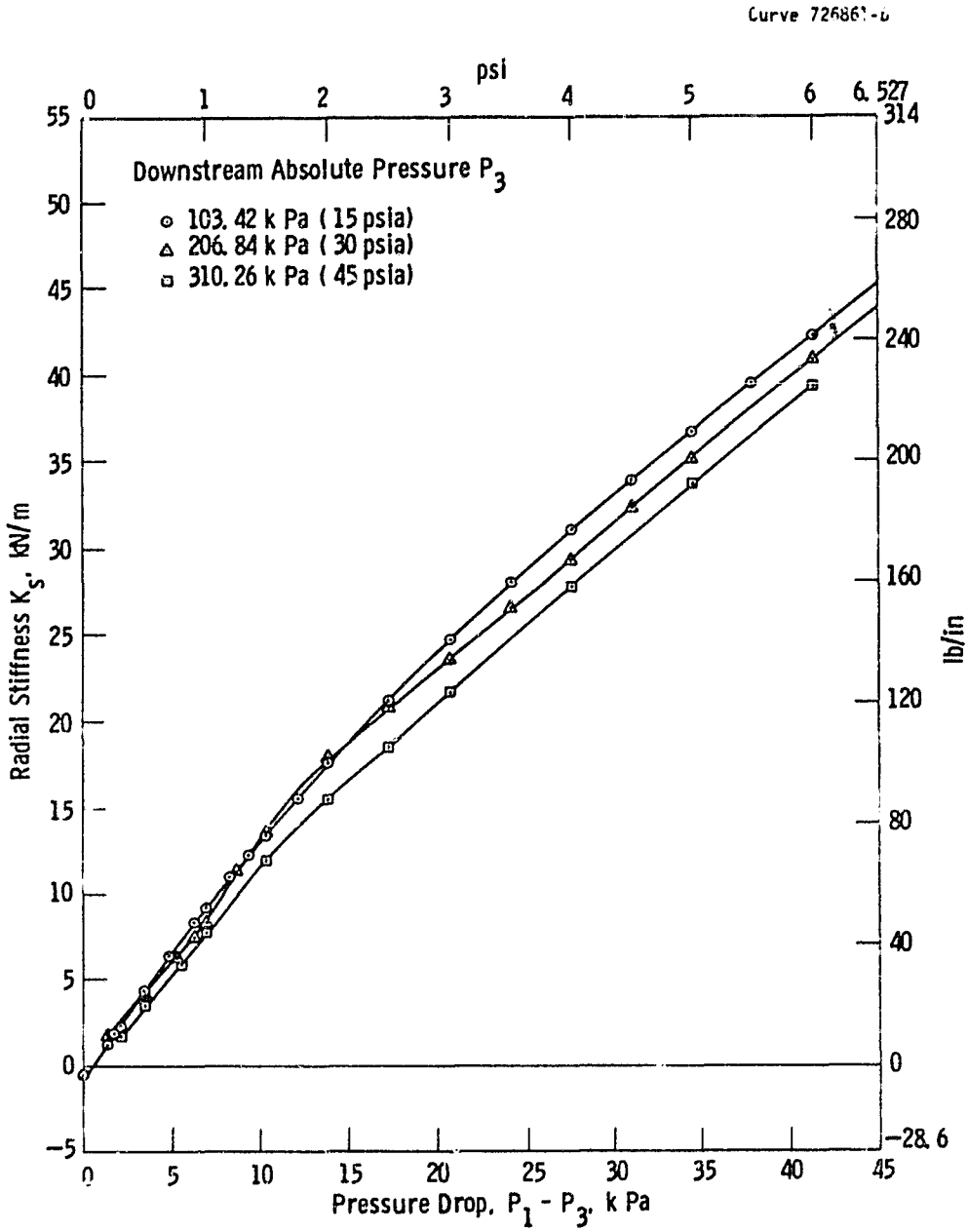

Fig. 27—Radial stiffness of S2 converging seal during forward whirl

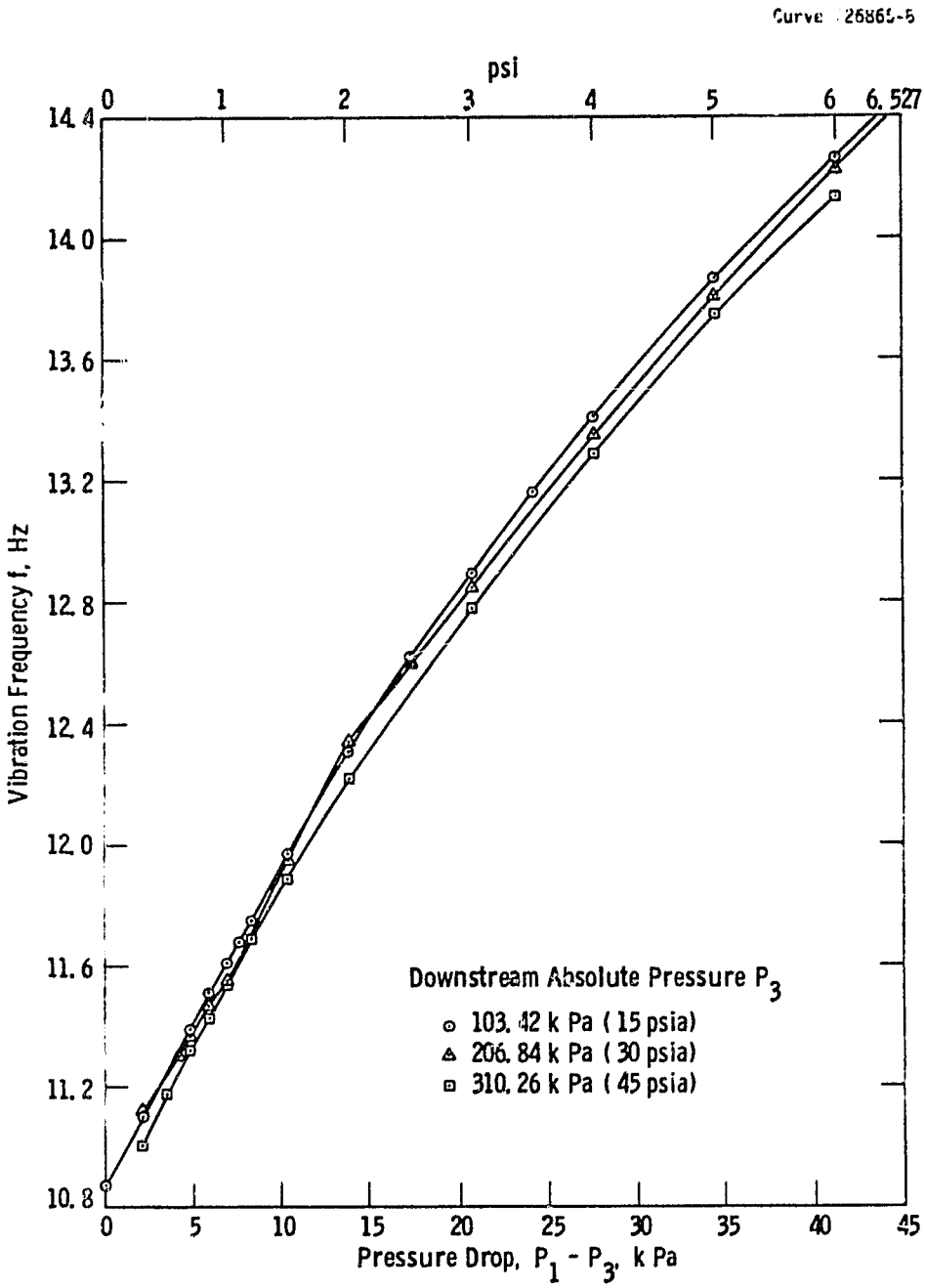

Fig. 28—Vibration frequency of S2 converging seal during backward whirl

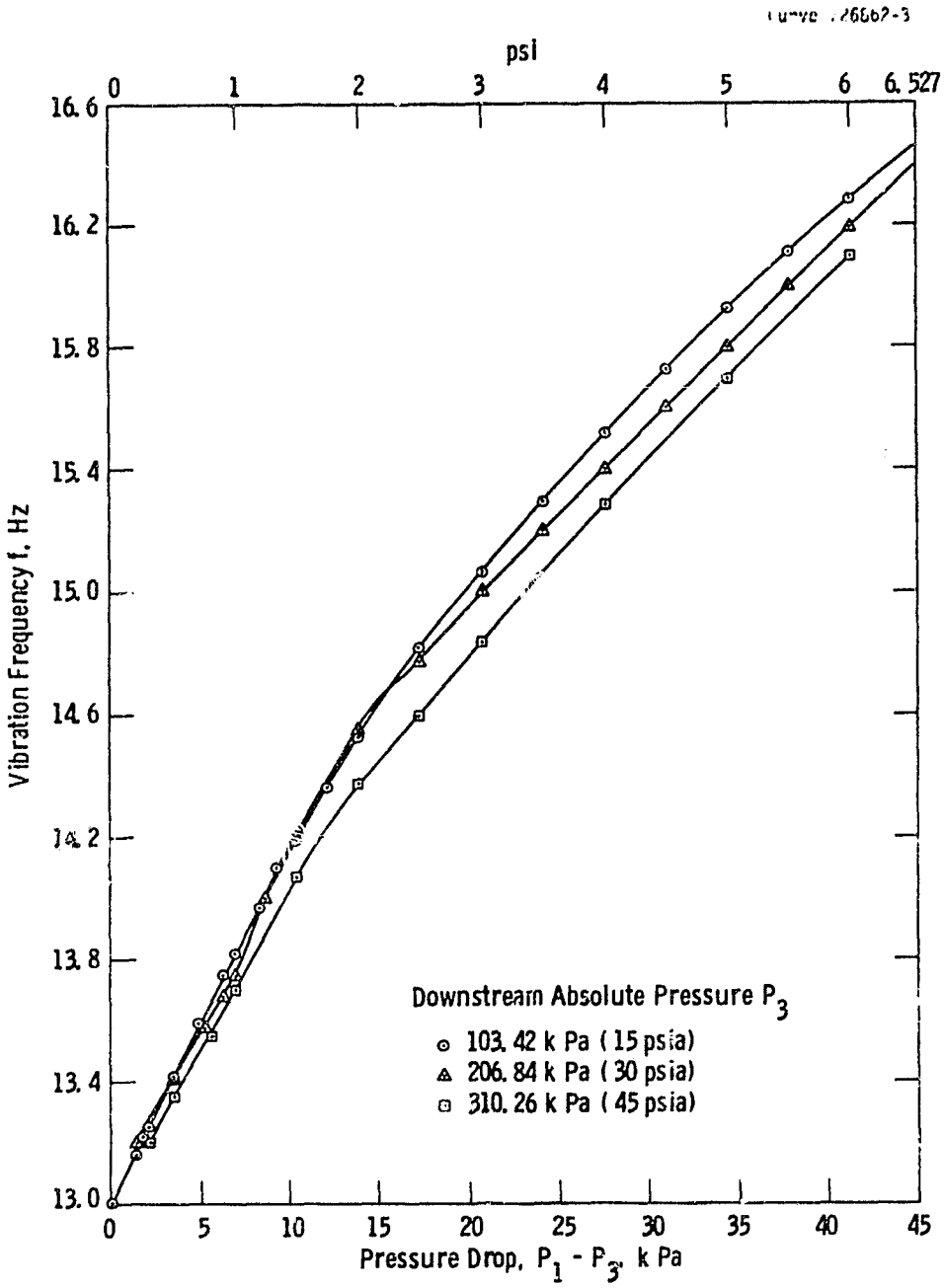

Fig. 29—Vibration frequency of S2 converging seal during forward whirl

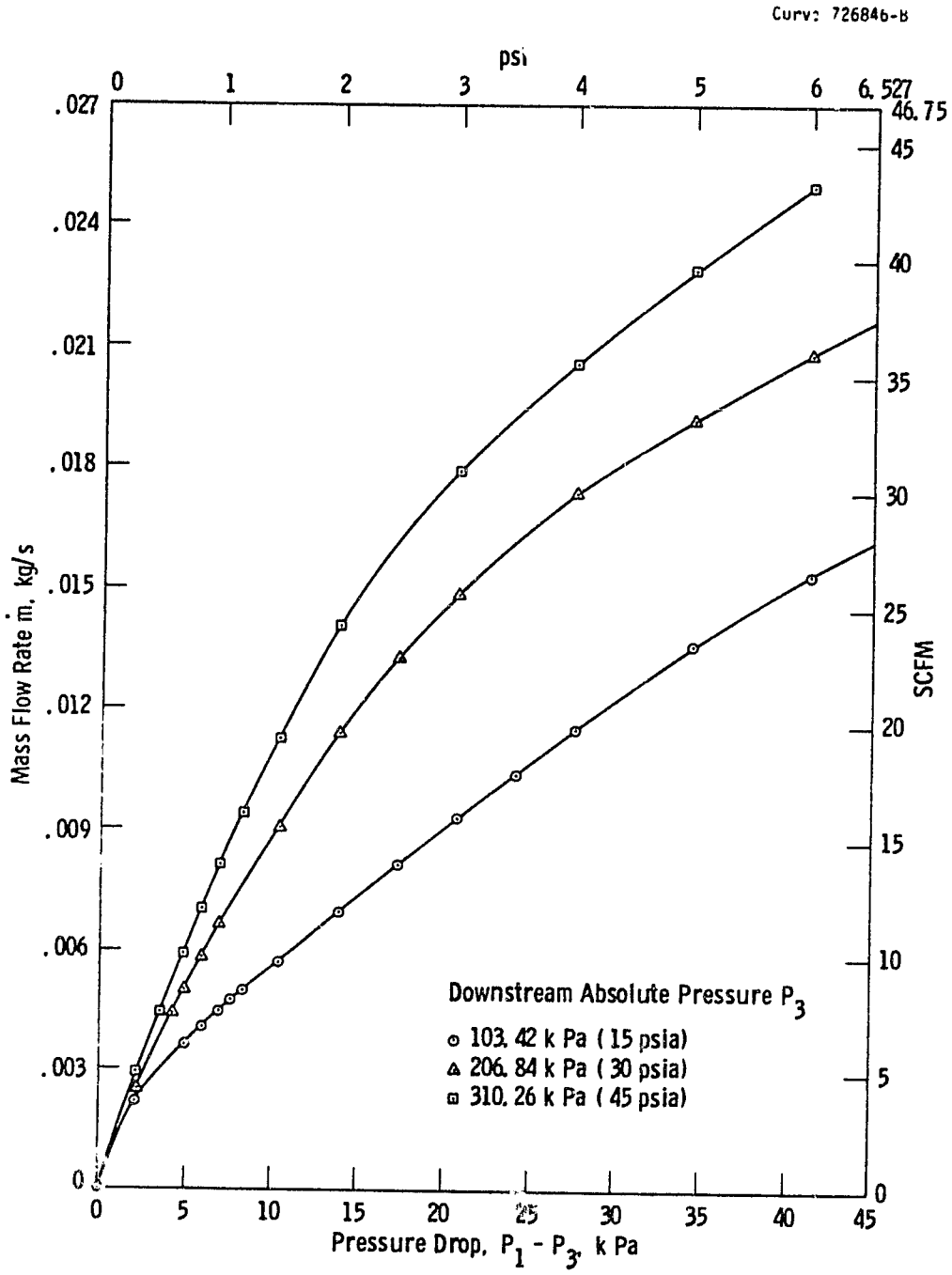

Fig. 30—Mass flow rate of S2 converging seal

C-2

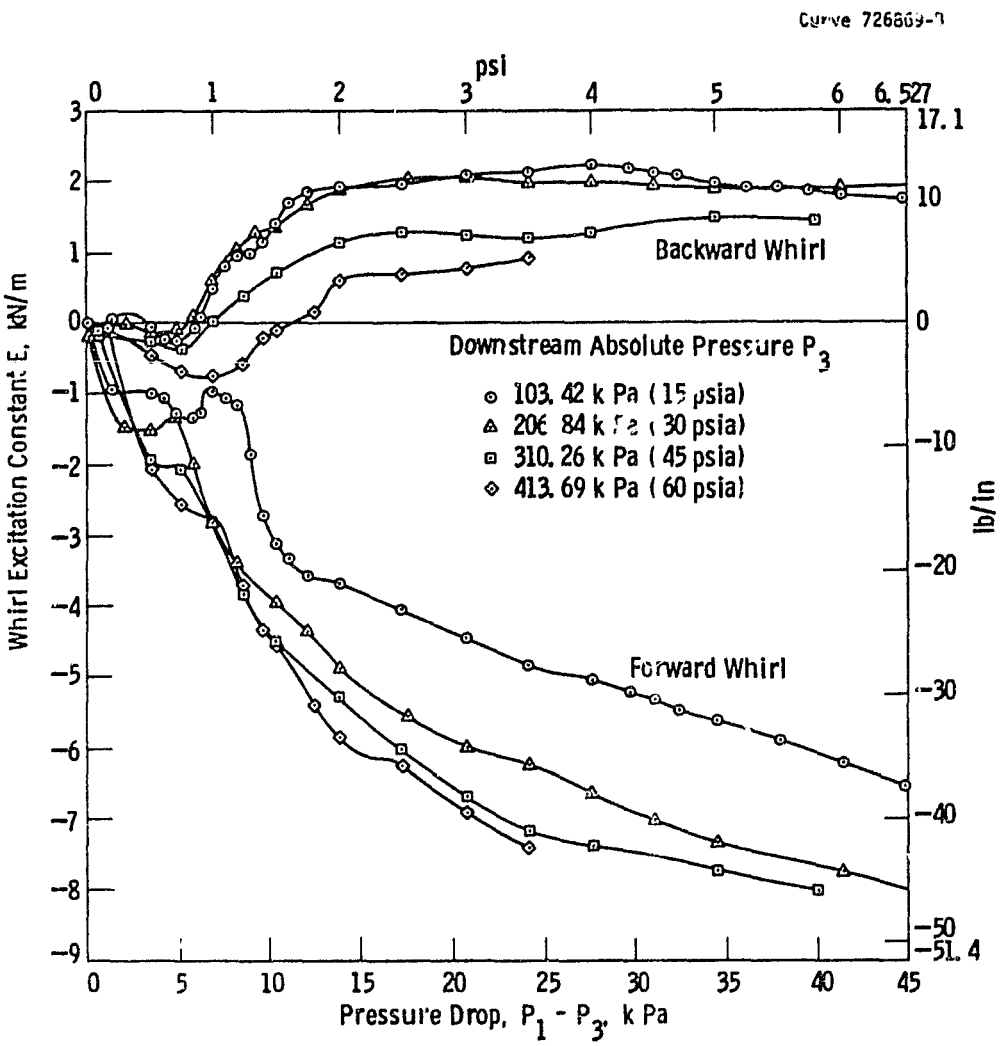

Fig. 31—Whirl excitation constants of S3 straight seal

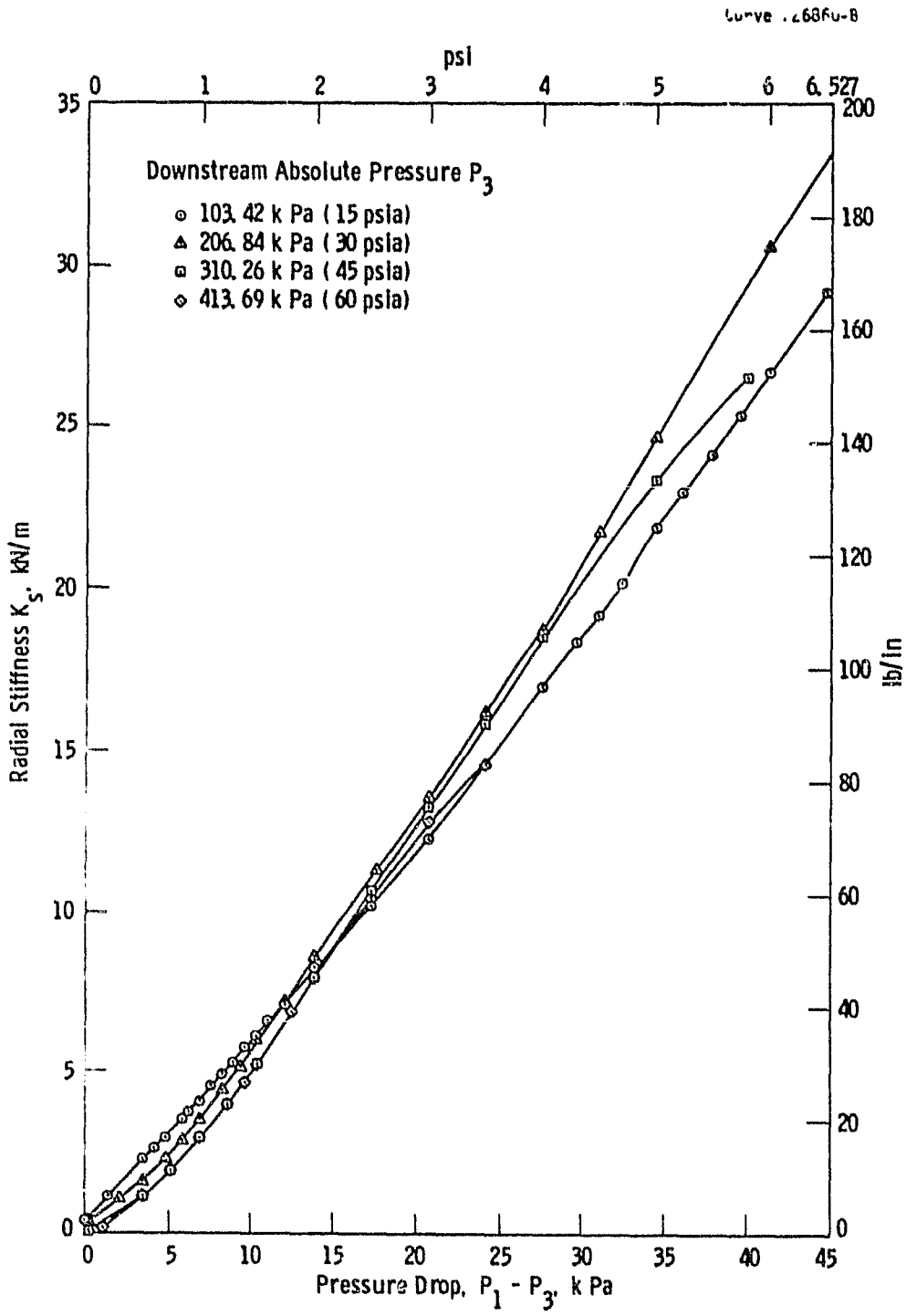

Fig. 32—Radial stiffness of S3 straight seal during backward whirl

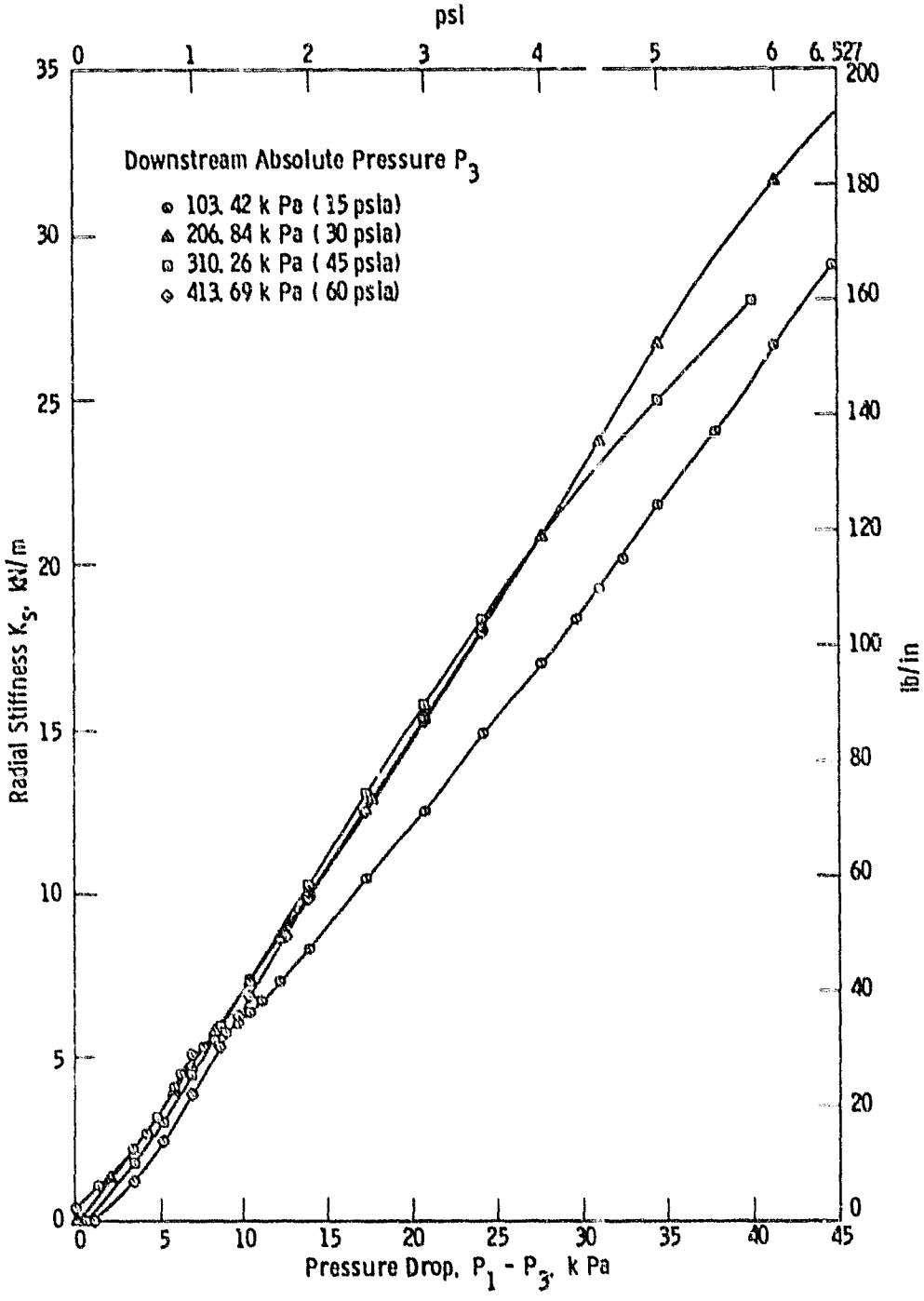

Fig. 33—Radial stiffness of S3 straight seal during forward whirl

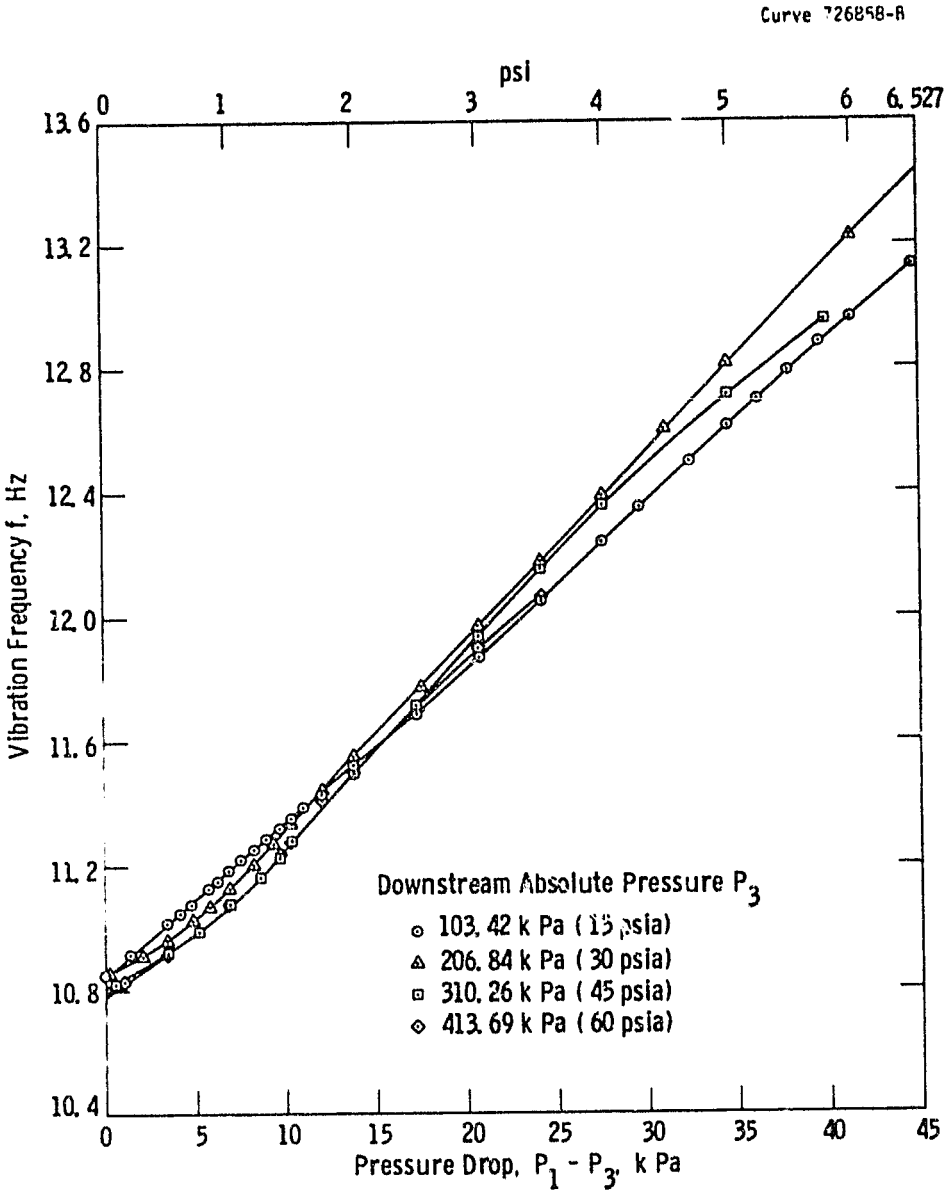

Fig. 34—Vibration frequency of S3 straight seal during backward whirl

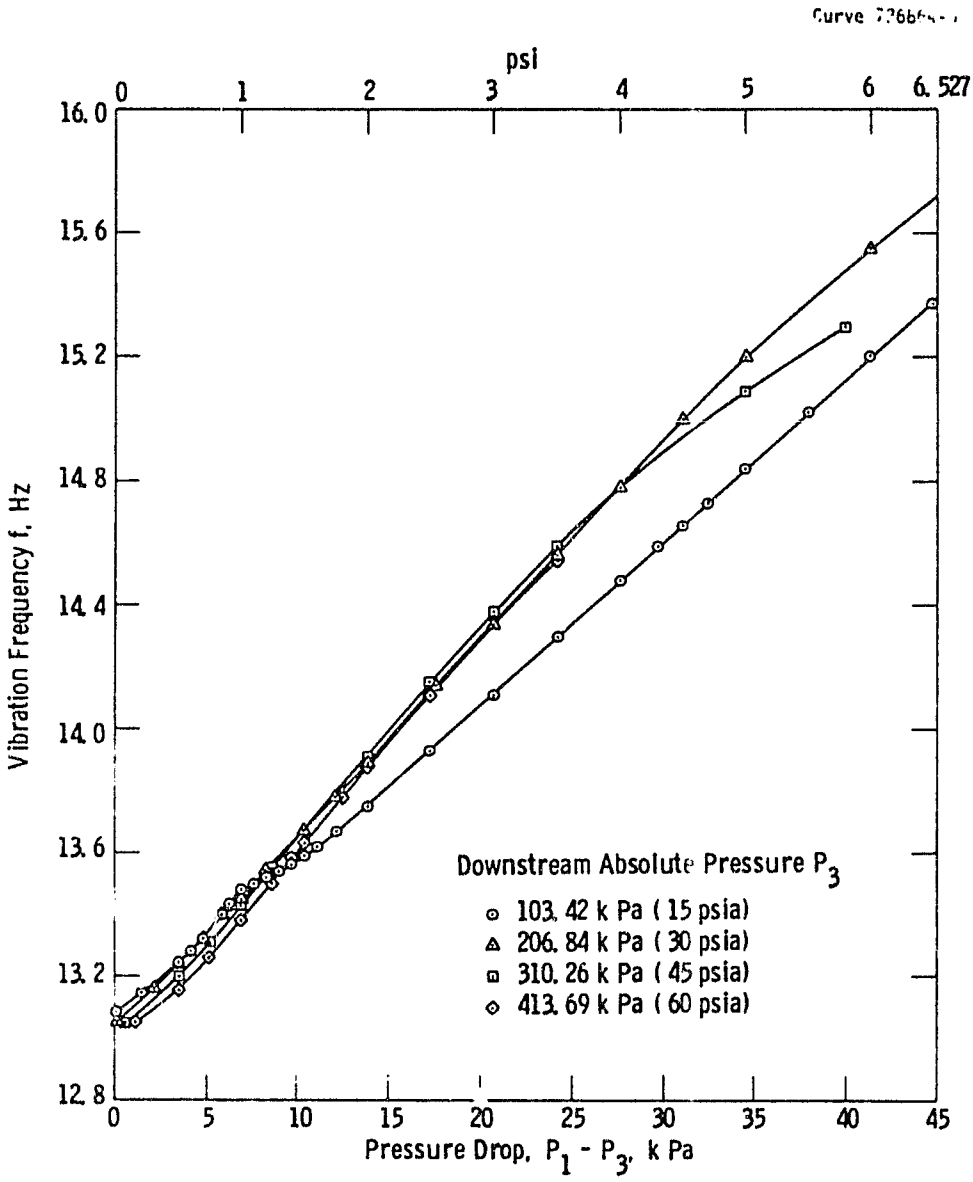

Fig. 35—Vibration frequency of S3 straight seal during forward whirl

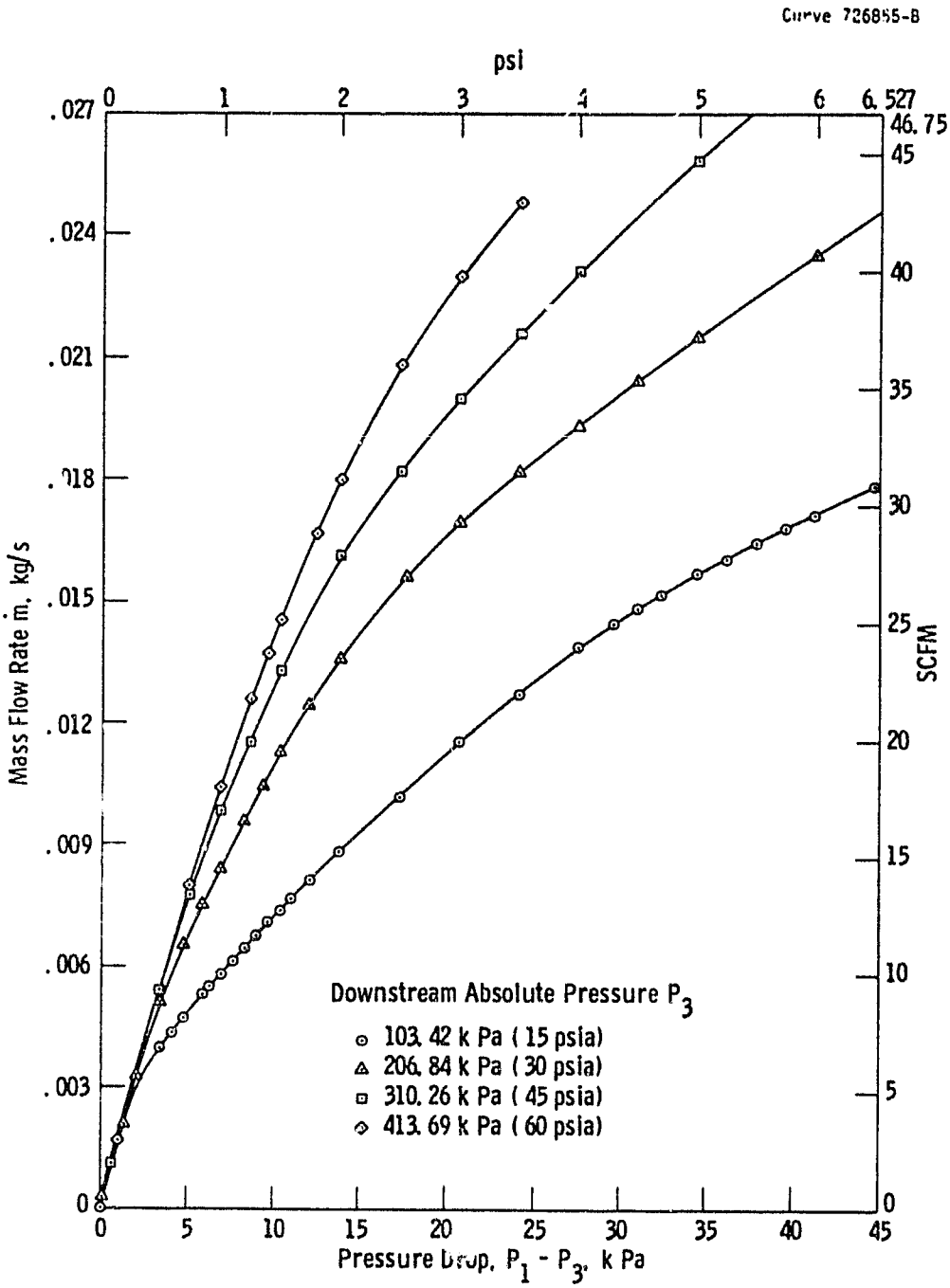

Fig. 36—Mass flow rate of S3 straight seal

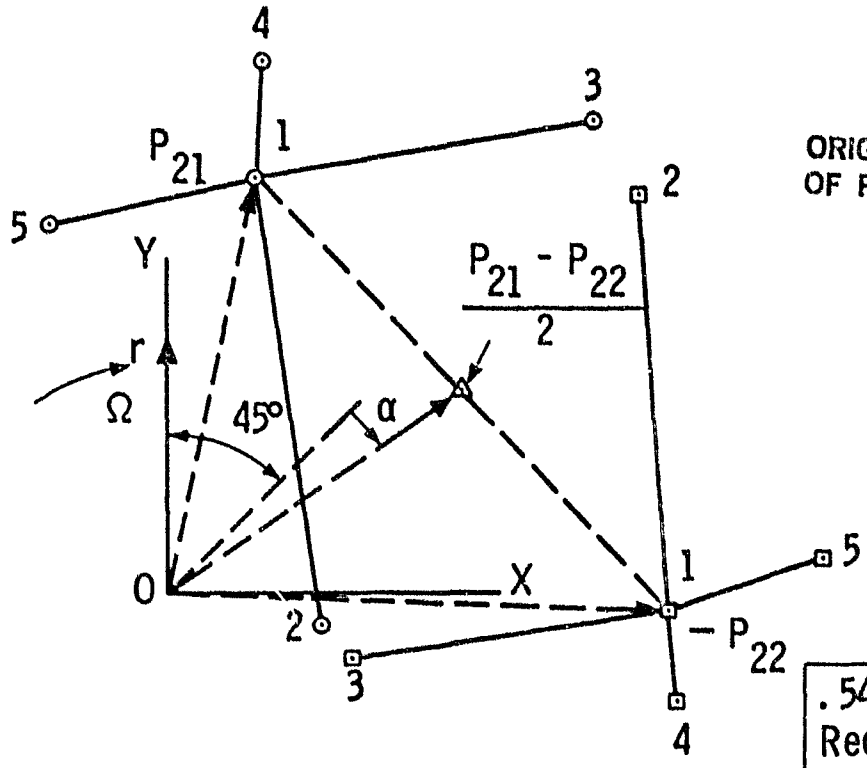

(a) Backward Whirl, .797 Mils Single Peak

.54 ∠0.2° Offset Required for True Zero Offset

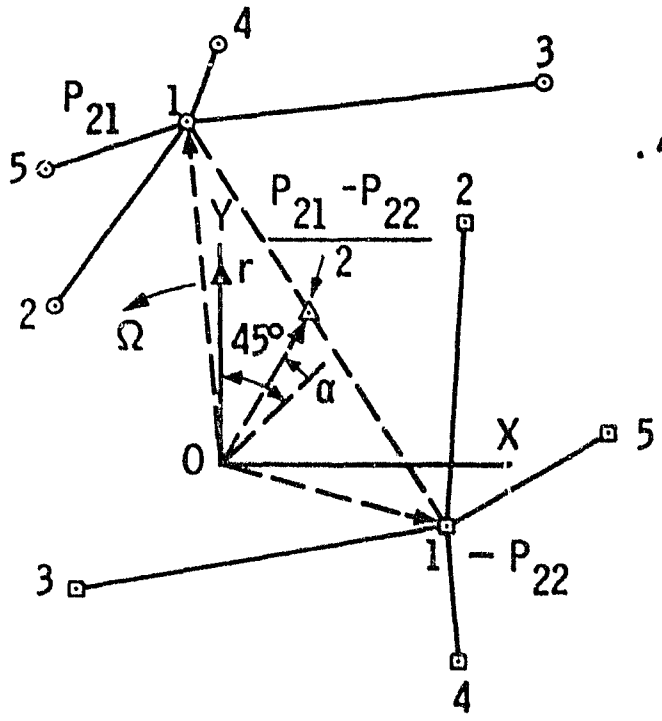

(b) Forward Whirl, .783 Mils Single Peak

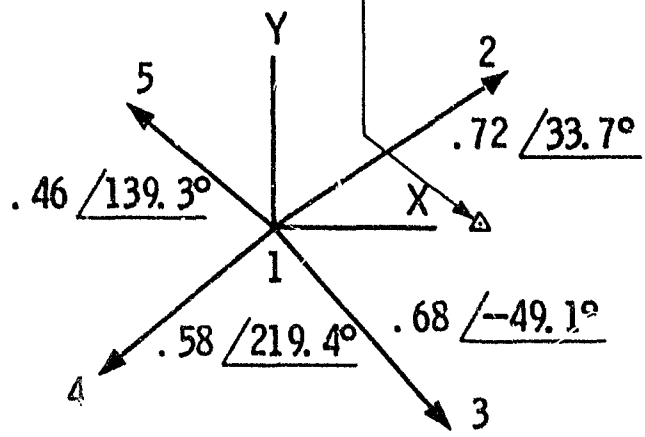

(c) Static Offsets in Mils

Fig. 37—Effect of static offset on the sinusoidal pressures in the annulus of the S1 diverging seal with back pressure $P_3 = 15$ psia and pressure drop $P_1 - P_3 = 3$ psi. Points show ends of pressure vectors for each offset. See table 33 and figs. 14 and 15

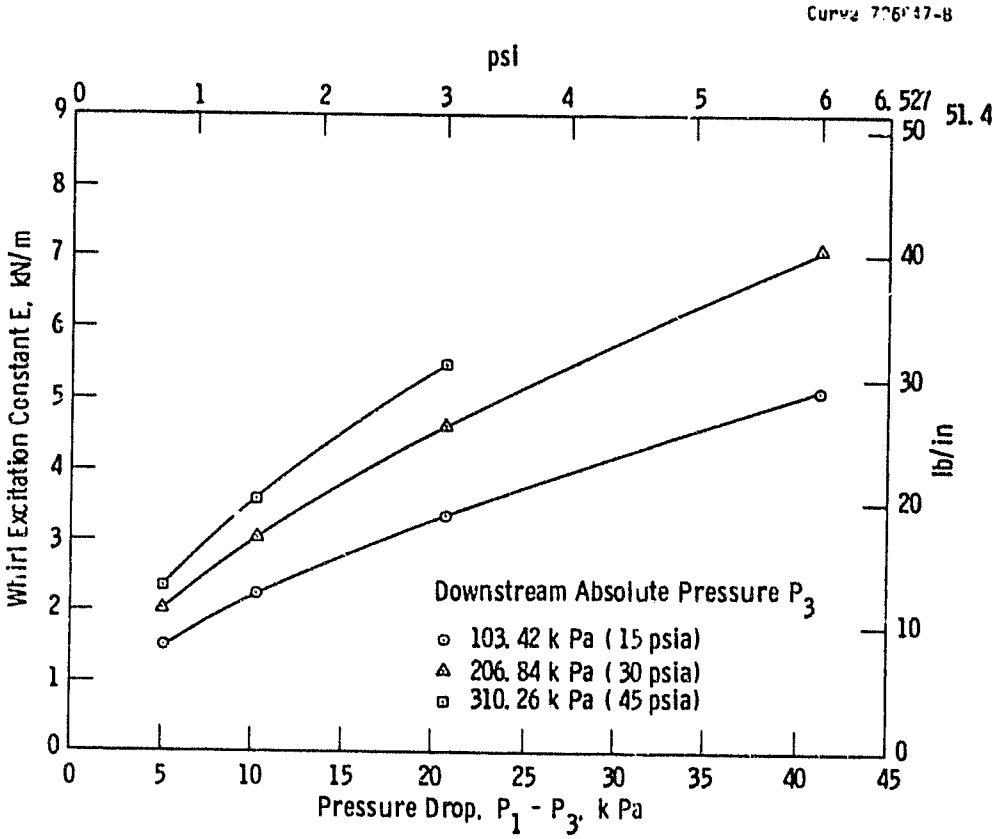

Fig. 38—Calculated whirl excitation constant of S1 diverging seal during backward whirl

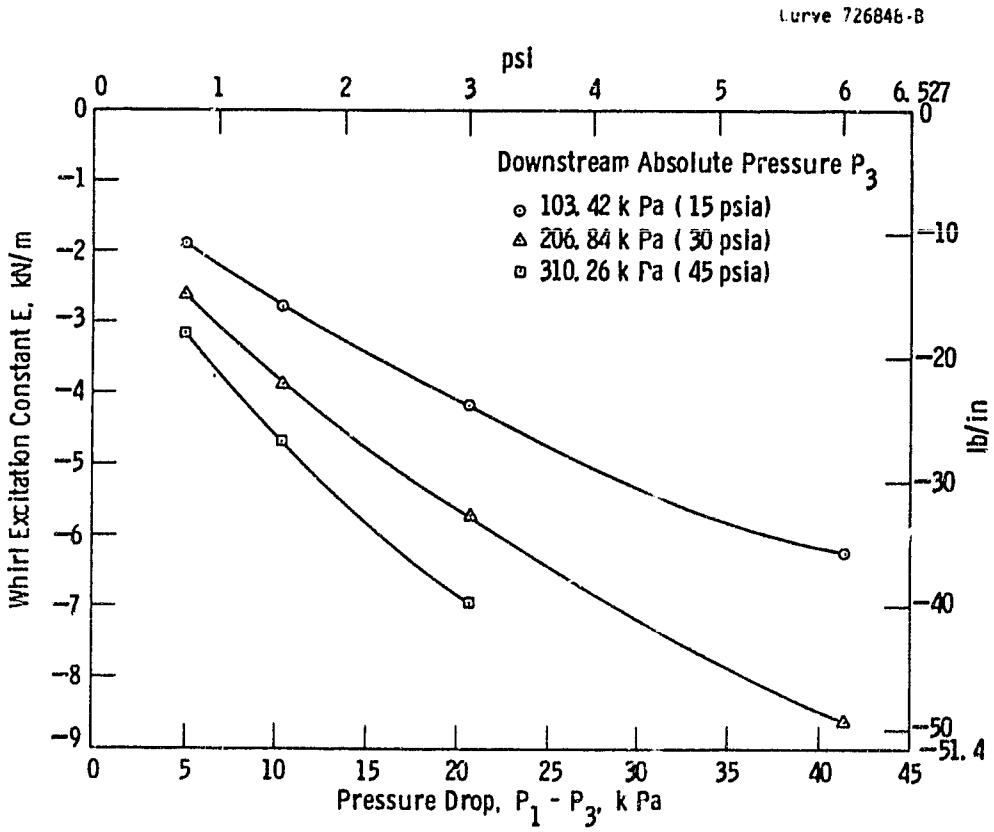

Fig. 39—Calculated whirl excitation constant of S2 converging seal during backward whirl

Dwg. 7772A11

ORIGINAL PAGE IS
OF POOR QUALITY

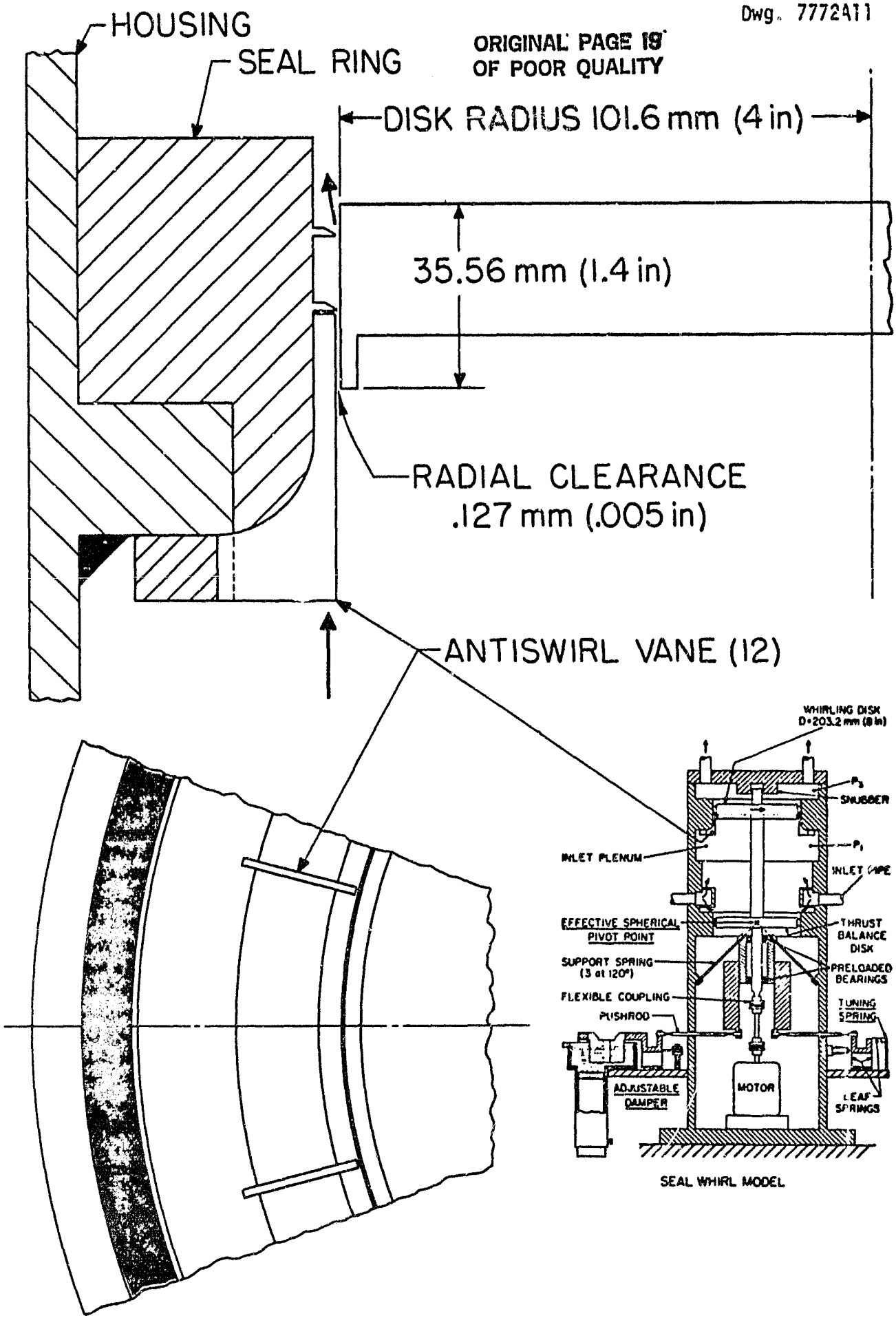

FIG.40-ANTISWIRL VANES FOR SEAL WHIRL MODEL

Dwg. 7739A64

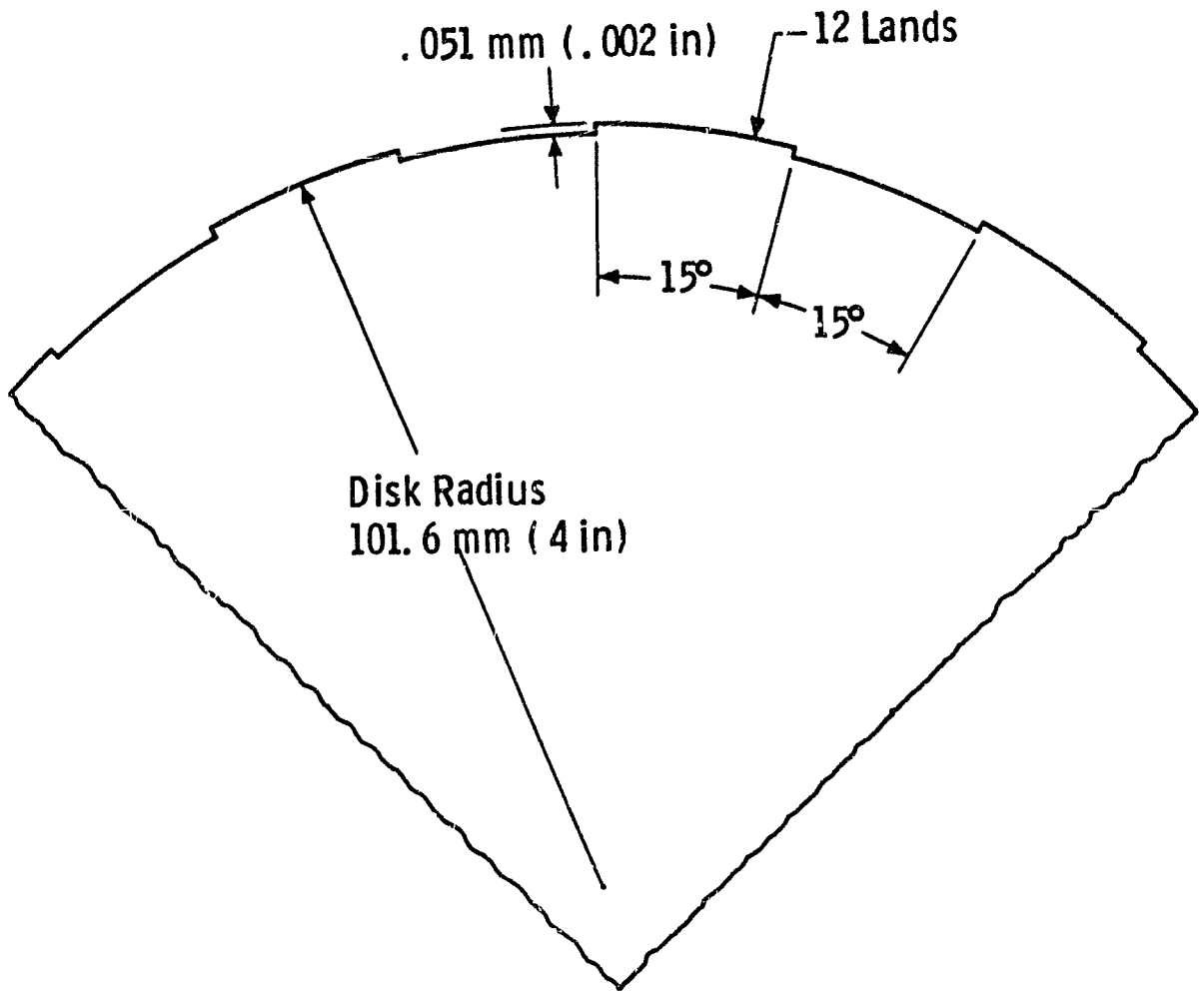

Fig. 41—Stepped rotor for seal whirl model